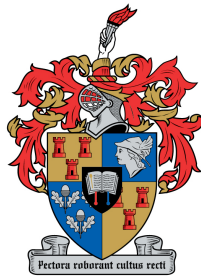


# An Assessment of the Inherent Reliability of SANS 10162-2 for Cold-Formed Steel Columns using the Direct Strength Method

Presented By:

Michael Alexander West-Russell



UNIVERSITEIT  
iYUNIVESITHI  
STELLENBOSCH  
UNIVERSITY

100  
1918 · 2018

*Thesis presented in partial fulfilment of the requirements for the degree of Master of Structural Engineering in the Faculty of Civil Engineering at Stellenbosch University*

Supervisors:

Dr. C. Viljoen

Mr. E. Van der Klashorst

March 2018

# Declaration:

By submitting this thesis electronically, I declare that the entirety of the work contained therein is my own, original work, that I am the sole author thereof (save to the extent explicitly otherwise stated), that reproduction and publication thereof by Stellenbosch University will not infringe any third-party rights and that I have not previously in its entirety or in part submitted it for obtaining any qualification.

Signed: .....

Michael Alexander West-Russell

Date: .....

Copyright © 2017

Stellenbosch University

All Rights Reserved

# Abstract

With their thin and slender nature, Cold formed Steel (CFS) elements can be forged into a large variety of cross sections. It is recommended that the Direct Strength Method (DSM), a modern design method, replaces the effective width method for the design of CFS members.

Research by Bauer (2016) revealed that, using the DSM, there is an insufficient level of safety provided by SANS 10162-2: design guide for Cold-Formed Steel Structures to achieve the target reliability prescribed by SANS 10160-1: the basis of structural design. This is partly due to a relatively high model uncertainty of the structural resistance. The main objective of this study is to determine whether the level of safety provided by SANS 10160-1 is enough to ensure an overall acceptable level of reliability for CFS members.

A prequalified plain lipped C-section is considered for the investigation of the local and global buckling failure modes. A prequalified lipped C-section with a web stiffener is considered for the investigation of the distortional and global buckling failure modes. Various member lengths are considered to ensure that all buckling modes are induced. The Finite Strip Method (FSM) is performed to identify the three buckling modes.

The members are subject to four load cases. Of which, each had different combinations of permanent, imposed and wind loads determined by partial factors and combination factors presented in SANS 10160-1. For the purposes of this study, only the ultimate limit-state was considered.

The considered limit-state is analysed in two parts: the semi- and full probabilistic formulations of the limit-state. The former considers the structural resistance and the load effect according to codified design. The latter considers the structural resistance and the load effect as functions of random variables. The reliability analysis is conducted on the full probabilistic formulation of the limit-state to assess the reliability achieved by using the codified semi-probabilistic formulation of the limit-state.

Model factors are considered for the structural resistance and the load effect. The structural resistance model factor is dependent on the buckling mode (Ganesan and Moen, 2010). A model factor for the permanent load is not considered and the model factor for

wind load had been accounted for in the respective statistical moment parameters. A model factor for the imposed load is described by Holický (2009).

The statistical moment parameters of the permanent and imposed loads are described by Holický (2009) and the statistical moment parameters of the wind load are described by Botha (2016).

The global buckling mode yields the lowest reliability levels, ranging from  $\beta = 1.78$  corresponding to an STR-P load combination to  $\beta = 2.87$  corresponding to an STR load combination. The safety margin present in SANS 10160-1 partially compensates for the low level of reliability when the total load comprises of high proportions of imposed and wind load. The low levels of reliability, especially when there is significant permanent loading, are cause for concern. It is recommended that a different capacity reduction factor be applied to each dominating buckling mode for CFS compression members.

# Acknowledgements

The completion of this thesis would not have been possible if it were not for the encouragement and influence of several people. Their contribution and support have been more than I could have ever expected.

Above all, I would like to express great appreciation to my study supervisors, both of whom provided funding during my postgraduate studies.

Since introducing me to the prospect of continuing my studies to a postgraduate degree, Dr. Celeste Viljoen has kept me excited to learn and motivated to work hard. As a co-supervisor, her deep understanding of reliability theory has truly been an enormous contributor to the basis of this work.

Before his departure from Stellenbosch, Mr. Etienne Van der Klashorst had consistently been supportive of my efforts and patient with my learning as a co-supervisor. His profound knowledge of the behaviour of structural steel members has been imperative to the success of this study.

Furthermore, I would like to thank my family. Throughout my entire academic career, they have never ceased to offer their encouragement. Consistently willing to share in my stresses and successes, the support structure that they offer is never failing.

Lastly, I would like to thank the 2017 MEng Structural Design graduate students. Everyone has been prepared to discuss ideas and share valuable opinions. Continuing our studies to a postgraduate level, they have ensured that my student life will never be forgotten, both in and out of the office.

# Table of Contents

Declaration:.....	i
Abstract .....	ii
Acknowledgements .....	iv
Table of Contents .....	v
List of Figures .....	viii
List of Tables .....	x
Nomenclature .....	xiii
CHAPTER 1: Introduction .....	1
1.1    Background.....	1
1.2    Problem Statement .....	2
1.3    Aim of study.....	2
1.4    Limitations .....	3
CHAPTER 2: Background into Cold-Formed Steel and Reliability Theory .....	4
2.1    Cold-Formed Steel.....	4
2.1.1    Description and Application .....	4
2.1.2    Design Methods of Cold-Formed Steel Members.....	6
2.2    Reliability Theory.....	18
2.2.1    The Ultimate Limit-State Equation.....	18
2.2.2    Reliability Simulation Methods.....	26
2.3    Model Factor.....	33
CHAPTER 3: Assessment of Cold-Formed Steel Columns Designed with the Direct Strength Method .....	37
3.1    Basis of Reliability Analysis .....	37
3.1.1    Semi-Probabilistic Formulation of the Limit-State.....	38

3.1.2	Full Probabilistic Formulation of the Limit-State .....	39
3.1.3	Process of Reliability Analysis.....	40
3.2	Analysis of Cold-Formed Steel Compression Member .....	43
3.2.1	Member Geometric Properties.....	43
3.2.2	Member Material Properties .....	46
3.2.3	Design and Mean Yield Loads .....	47
3.2.4	Signature Curves and Buckling Modes.....	48
3.2.5	Direct Strength Method Design of Members .....	51
3.2.6	Reliability Analyses.....	54
3.3	Semi-Probabilistic Formulation of the Limit-State.....	56
3.3.1	Obtaining Characteristic Values of the Loads.....	56
3.3.2	Load Combination Choice .....	59
3.4	Full Probabilistic Formulation of the Limit-State .....	62
3.4.1	Variables of the Load Effect.....	62
3.4.2	Variables of the Structural Resistance .....	64
3.4.3	Reliability Analysis .....	65
3.4.4	Monte-Carlo Simulation.....	66
3.4.5	Chapter Summary.....	66
CHAPTER 4: Results & Discussion .....		68
4.1	Results of Reliability Analysis.....	68
4.1.1	Global Buckling .....	68
4.1.2	Local Buckling and Local-Global Buckling Interaction .....	81
4.1.3	Distortional Buckling.....	89
4.2	Discussion of Reliability Results .....	94
4.2.1	Overview .....	94
4.2.2	Discussion of Reliability Levels of Buckling Modes .....	94
4.2.3	Detailed Discussion .....	95

CHAPTER 5: Conclusion & Recommendations.....	97
5.1 Conclusion .....	97
5.2 Recommendations .....	99
References .....	101



# List of Figures

Figure 2.1: Various sections of cold-formed steel (Yu & LaBoube, 2010) .....	5
Figure 2.2: Edge loaded simply supported plate (American Iron and Steel Institute et al., 2016) .....	7
Figure 2.3: Change in stress distribution with increasing edge load (Yu and Schafer, 2005) .....	7
Figure 2.4: Representation of the local buckling mode (Bauer, 2016) .....	9
Figure 2.5: Representation of the distortional buckling mode (Bauer, 2016) .....	9
Figure 2.6: Representation of the global buckling mode in the form of (a) flexural buckling, (b) torsional buckling and (c) flexural-torsional buckling (Bauer, 2016) .....	10
Figure 2.7: Typical signature curve showing the three types of buckling modes (Bauer, 2016) .....	12
Figure 2.8: Probability density functions of load effect and structural resistance (Bauer, 2016) .....	21
Figure 2.9: Probability density function of the limit-state G (Bauer, 2016).....	22
Figure 2.10: Two-dimensional space of state variables (Nowak and Collins, 2000) .....	24
Figure 2.11: 3-Dimensional plot of the joint density function (Nowak and Collins, 2000) .....	24
Figure 2.12: Reliability margin and sensitivity factors in a standardised space for a non-linear limit-state equation (Haldar and Mahadevan, 2000).....	25
Figure 2.13: First order reliability method (Holický, 2009) .....	27
Figure 2.14: Graphical representation of the FORM analysis (Lopez and Beck, 2012)...	29
Figure 2.15: Test-to-predicted ratios of CFS columns as a function of global slenderness for the DSM (Ganesan and Moen, 2010).....	34
Figure 2.16: General concept of the model factor (Holický et al, 2015) .....	36
Figure 3.1: Sensitivity factors of structural resistance random variables (Bauer, 2016)	38
Figure 3.2: Flow diagram depicting the general procedure of the reliability analysis ....	42

Figure 3.3: Plain lipped C-section with centreline dimensions .....	44
Figure 3.4: Stiffened lipped C-section with centreline dimensions.....	44
Figure 3.5: Signature curves of plain lipped C-section .....	49
Figure 3.6: Signature curves of stiffened lipped C-section .....	49
Figure 3.7: Direct strength method buckling loads for the plain lipped C-section .....	52
Figure 3.8: Direct strength method buckling loads for the stiffened lipped C-section ....	53

# List of Tables

Table 2.1: Pre-qualified geometric limits for compression members (SANS 10162-2, 2011) .....	14
Table 2.2: Categorisation of the model factor (Holicky, et al., 2015) .....	34
Table 3.1: Geometrical properties of compression elements .....	45
Table 3.2: Sectional properties obtained from CUFSM .....	46
Table 3.3: Material properties of Grade G550 high strength steel .....	47
Table 3.4: Yield stresses and yield capacities for the plain and stiffened lipped C-sections .....	48
Table 3.5: Load factors of $N_d$ and $N_r$ signature curves for plain lipped-C section .....	50
Table 3.6: Load factors of $N_d$ and $N_r$ signature curves for stiffened lipped-C section .....	50
Table 3.7: Test summary of reliability analysis .....	55
Table 3.8: Summary of considered load combinations .....	57
Table 3.9: Values of partial and combination factors .....	57
Table 3.10: Dominating load combinations for different values of $\chi_Q$ and $\chi_W$ .....	61
Table 3.11: Statistical moment parameters of the considered loads (Holický, 2009) .....	62
Table 3.12: Updated Eurocode full probabilistic wind load model of the FORM analysis (Botha, 2016) .....	63
Table 3.13: Statistical moment parameters of the structural resistance model factors for different buckling modes (Ganesan & Moen, 2010) .....	65
Table 3.14: MC analyses of dominating load combinations.....	66
Table 4.1: Reliability levels for test one.....	69
Table 4.2: $\alpha_{dR}$ for test one.....	70
Table 4.3: $\alpha_{dQ}$ for test one .....	70
Table 4.4: $\alpha_G$ for test one.....	71

Table 4.5: $\alpha_Q$ for test one.....	71
Table 4.6: $\alpha_W$ for test one .....	72
Table 4.7: Reliability levels for test two .....	73
Table 4.8: $\alpha_{\partial R}$ for test two .....	74
Table 4.9: $\alpha_{\partial Q}$ for test two .....	74
Table 4.10: $\alpha_G$ for test two .....	75
Table 4.11: $\alpha_Q$ for test two .....	75
Table 4.12: $\alpha_W$ for test two .....	76
Table 4.13: Reliability levels for test three.....	77
Table 4.14: $\alpha_{\partial R}$ for test three.....	77
Table 4.15: $\alpha_{\partial Q}$ for test three .....	78
Table 4.16: $\alpha_G$ for test three.....	78
Table 4.17: $\alpha_Q$ for test three.....	79
Table 4.18: $\alpha_W$ for test three .....	79
Table 4.19: Reliability levels achieved through FORM and MCS for each load combination .....	81
Table 4.20: Reliability levels for test four.....	82
Table 4.21: $\alpha_{\partial R}$ for test four.....	82
Table 4.22: $\alpha_{\partial Q}$ for test four .....	83
Table 4.23: $\alpha_G$ for test four.....	83
Table 4.24: $\alpha_Q$ for test four.....	84
Table 4.25: $\alpha_W$ for test four .....	84
Table 4.26: Reliability levels for test five .....	85
Table 4.27: $\alpha_{\partial R}$ for test five .....	86
Table 4.28: $\alpha_{\partial Q}$ for test five .....	86
Table 4.29: $\alpha_G$ for test five .....	87
Table 4.30: $\alpha_Q$ for test five .....	87

Table 4.31: $\alpha_W$ for test five .....	88
Table 4.32: Reliability levels for test six.....	90
Table 4.33: $\alpha_{\partial R}$ for test six.....	90
Table 4.34: $\alpha_{\partial Q}$ for test six .....	91
Table 4.35: $\alpha_G$ for test six.....	91
Table 4.36: $\alpha_Q$ for test six.....	92
Table 4.37: $\alpha_W$ for test six .....	92

# Nomenclature

## Acronyms

AISI	American Iron and Steel Institute
CFS	Cold-Formed Steel
cFSM	Constrained Finite Strip Method
DSM	Direct Strength Method
FORM	First Order Reliability Method
FSM	Finite Strip Method
MCS	Monte Carlo Simulation
SANS	South African National Standard
VaP	Variable Processor

## Symbols

$[A]$	Load factor matrix
$\{\alpha\}$	Sensitivity factor vector
$\{D\}$	Vector of partial derivatives
$\{N_k\}$	Characteristic load vector
$\{N_d\}$	Design load vector
$\{U\}$	Vector of standardised random variables
$\{u^*\}$	Vector of standardised random variable realisations
$\{X\}$	Vector of random variables
$\{x^*\}$	Vector of random variable realisations
$\alpha$	Sensitivity factor

$\alpha_{\partial}$	Sensitivity factor of the model uncertainty
$\alpha_{\partial Q}$	Sensitivity factor of the imposed load model factor
$\alpha_{\partial R}$	Sensitivity factor of the structural resistance model factor
$\alpha_E$	Sensitivity factor of the load effect
$\alpha_G$	Skewness of the limit state probability density distribution
$\alpha_R$	Sensitivity factor of the structural resistance
$\beta$	Reliability index
$\beta_f$	Stress coefficient
$\beta_t$	Target reliability index
$\gamma_G$	Partial factor of the permanent load
$\gamma_Q$	Partial factor of the imposed load
$\gamma_W$	Partial factor of the wind load
$\partial$	Model factor
$\partial_E$	Model factor of the load effect
$\partial_R$	Model factor of the structural resistance
$\partial_{R(d)}$	Model factor for the distortional buckling mode
$\partial_{R(g)}$	Model factor for the global buckling mode
$\partial_{R(lg)}$	Model factor for the local-global interaction buckling mode
$\theta$	Lip angle
$\lambda_c$	Non-dimensional slenderness for global buckling of a column
$\lambda_d$	Non-dimensional slenderness for distortional buckling of a column
$\lambda_l$	Non-dimensional slenderness for local buckling of a column
$\sigma$	Standard deviation
$\sigma_E$	Standard deviation of the load effect
$\sigma^e$	Standard deviation of the equivalent normal distribution

$\sigma_R$	Standard deviation of the structural resistance
$\sigma_X$	Standard deviation of a random variable
$\mu$	Mean value
$\mu_E$	Mean value of the load effect
$\mu^e$	Mean value of the equivalent normal distribution
$\mu_R$	Mean value of the structural resistance
$\mu_X$	Mean value of a random variable
$\rho_{RE}$	Correlation coefficient of structural resistance and load effect
$\Phi_G$	Probability distribution function of the limit-state
$\Phi_U$	Probability distribution function of a standardised random variable
$\varphi$	Probability density function
$\phi_c$	Capacity reduction factor for compression elements
$\chi_Q$	Imposed load ratio
$\chi_W$	Wind load ratio
$A$	Cross-sectional area
$t$	Thickness
$E$	Modulus of elasticity (Young's Modulus)
$E$	Load effect
$E_d$	Codified design value of the load effect.
$f_{oc}$	Elastic flexural, torsional, and flexural-torsional buckling stress
$f_{od}$	Elastic distortional buckling stress
$f_{ol}$	Elastic local buckling stress
$f_{ox}$	Elastic buckling stress in a compressive element for flexural buckling about the x-axis
$f_{oxz}$	Elastic buckling stress in a compressive element for flexural-torsional buckling about the x-axis



$f_{oy}$	Elastic buckling stress in a compressive element for flexural buckling about the y-axis
$f_{oz}$	Elastic buckling stress in a compressive element for torsional buckling
$f_y$	Yield stress
$G$	Limit-state
$G$	Shear modulus
$G_d$	Design value of the permanent load
$G_k$	Characteristic value of the permanent load
$h$	Web height
$I_w$	Warping constant for a cross-section
$J$	Torsion constant for a cross-section
$L$	Member length
$l$	Lip height
$l_e$	Effective member length
$l_{ex}$	Effective member length for buckling about the x-axis
$l_{ey}$	Effective member length for buckling about the y-axis
$l_{ez}$	Effective member length for twisting
$l_d$	Distortional buckling half-wavelength
$l_l$	Local buckling half-wavelength
$l_{l-g}$	Local-Global interaction buckling half-wavelength
$N_{\mu}$	Mean compressive critical buckling load
$N_{cl}$	Nominal compressive local buckling capacity
$N_{cd}$	Nominal compressive distortional buckling capacity
$N_{ce}$	Nominal compressive global buckling capacity
$N_{cr,d}$	Distortional buckling based compressive capacity of a column

$N_{cr,e}$	Least of the elastic flexural, torsional, and flexural-torsional buckling compressive load
$N_{cr,l}$	Local buckling based compressive capacity of a column
$N_d$	Design compressive critical buckling load
$N_y$	Compressive yield load
$N_{y,\mu}$	Yield capacity based on the design values of material properties
$N_{y,d}$	Yield capacity based on the mean values of material properties
$p_f$	Probability of failure
$R$	Structural resistance
$R_d$	Codified design value of the structural resistance.
$r$	Lip radius <i>or</i> radius of gyration
$r_{ol}$	Polar radius of gyration of the cross section about the shear centre
$r_x, r_y$	Radius of gyration about the x- and y-axes
$U$	Standardised random variable
$u$	Realisation of a standardised random variable
$u^*$	Standardised design point
$V$	Coefficient of Variation
$\nu$	Poisson's Ratio
$w$	Flange width
$X$	Random variable
$X_E$	Random variable associated with the load effect
$X_G$	Random variable of the permanent load
$X_Q$	Random variable of the imposed load
$X_R$	Random variable associated with the load effect
$X_W$	random variable of the wind load

$x$	Realisation of a random variable
$x^*$	Design point
$x_{cg}, y_{cg}$	Coordinates of the centre of gravity of a cross-section
$x_o, y_o$	Coordinates of the shear centre of a cross-section

# CHAPTER 1: Introduction

---

## 1.1 Background

When a design method is introduced to codified design standards, the reliability level of the method needs to be investigated. Various probability analyses are required to determine the level of inherent reliability of a newly developed design method. Considering the variables involved in structural design, the influence that the variables have on the reliability also needs to be investigated. The target level of reliability depends on direct and indirect costs of failure such as loss of human life, economic, social, and environmental consequences (Holický, 2009).

As a construction material, thin-walled steel has been used in a range of structures. Failure of the thin-walled steel members in these structures may result in the loss of human life, pollution, or damage to property. The use of thin-walled elements as a construction material is increasing, as design methods are becoming more simplified and the use of steel is further optimised. With the growing application of thin-walled steel members, it is becoming more important to ensure the safety of the material in structural design.

Proposed by Schafer (2006a), a design method called the Direct Strength Method (from here on referred to as DSM) has been introduced to thin-walled steel design over the last two decades. The method was officially adopted as an appendix to the American Iron and Steel Institute (from here on referred to as AISI) design code for Cold-Formed Steel (from here on referred to as CFS) structural members in 2004 and as an additional chapter to SANS 10162-2: Cold-formed steel structures (from here on referred to as SANS 10162-2). The method incorporates the unique structural behaviour of the thin-walled steel elements with existing codified design procedures.

## 1.2 Problem Statement

SANS 10162-2 (2011) uses partial factors to provide a safety margin. The code is an adaption of the Australian/New Zealand standard (AS/NZS 4600) for CFS members in structural design. The target reliability level presented in the South African National Standard 10160-1: Basis of structural design (from here on referred to as SANS 10160-1) for reliability class 2 structures is a factor of  $\beta_t = 3$ . Reliability verification procedures are generally specified as reliability class 2 structures as a reference classification.

The work conducted by Bauer (2016) examined the inherent reliability of the DSM in a South African design context, particularly for the structural resistance of CFS elements. Amongst the findings of the study, two points are to be noted. Firstly, it was found that the level of model uncertainty for the structural resistance had a dominating effect on the level of reliability. Secondly, the safety margin of the structural resistance provided by SANS 10162-2 (2011) proved insufficient to achieve the target reliability level. The study, however, did not consider the effect the load effect had on the reliability level.

## 1.3 Aim of study

The primary goal of this study is to determine whether there is a sufficient safety margin supplied by SANS 10160-1 (2011) to achieve an overall acceptable level of reliability for CFS compression members. The compression members are to be designed in accordance to the DSM. The reliability levels of each dominating buckling mode presented by the DSM are to be determined.

The reliability analysis needs to be conducted on the full probabilistic formulation of the limit-state to assess the inherent reliability of the codified semi-probabilistic formulation of the limit-state. The structural resistance and the load effect of the full probabilistic formulation of the limit state are to be expressed as functions of random variables.

The reliability analysis needs to consider various dominating load combinations. The total load needs to be comprised of the permanent, imposed and the wind load. In the analysis, load combinations of SANS 10160-1 (2011) are to be considered over a full range of ratios of characteristic imposed loads and wind loads to the characteristic total load.

Once the above is achieved, the reliability levels produced from the full probabilistic analysis of the limit state must be assessed and scrutinised for all buckling modes by varying member lengths. Additionally, the sensitivity factors for each of the associated

random variables must be evaluated to assess their respective influences on the level of reliability.

## 1.4 Limitations

Innate to the use of the DSM are certain limitations. Only prequalified members may be used to adhere to the conventional capacity reduction factor presented in SANS 10162-2 (2011). This is due to the limits of available research and development (Schafer, 2006a). This includes a limitation on the ratio of the Elastic modulus to the yield strength of the steel, as well as cross-sectional geometric limitations.

The DSM does not make provision for cross sections that vary along the length of the member. This includes members with holes and elements that are tapered. Additionally, the applied load must be consistent throughout the length of the member.

The DSM makes provision for compression and bending CFS elements. For the purposes of this study, only compression members were considered.

Four load combinations were considered. Of each, only the permanent, imposed and wind loads were included.

# CHAPTER 2:

## Background into Cold-Formed Steel and Reliability Theory

---

The following chapter covers the fundamental information required to understand the behaviour of cold-formed steel sections and how design methods incorporate this into design equations. Relevant reliability theory is discussed for the purposes of this investigation and how it is applied to cold-formed steel members.

### 2.1 Cold-Formed Steel

#### 2.1.1 Description and Application

CFS is a light-weight and slender building material. According to Yu and LaBoube (2010), the manufacturing processes of cold-formed sections begin from rolls, plates, or strips of steel. The steel makes its way through roll-forming machines at room temperature. The manufacturing process of CFS members enables it to be formed into a variety of cross sections. The typical cross-sections that are widely used in the South African construction industry are C-, Z, and hat-sections. Each of these sections can be stiffened or lipped. Examples of CFS cross-section are shown in Figure 2.1 from Yu and LaBoube (2010). The plate thickness of the members typically ranges between 0.378mm to 6.35mm, depending on the required application. With a relatively high width-to-thickness ratio, CFS members are considered as thin-walled slender members.

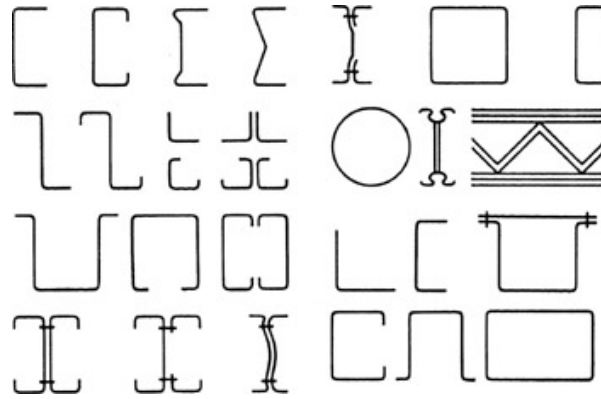


*Figure 2.1: Various sections of cold-formed steel (Yu & LaBoube, 2010)*

Due to their slender nature, the behaviour of thin-walled members under loads are different from conventional hot-rolled steel members. As the thickness of a member decreases, the elements of the member begin to buckle in a similar manner to plate buckling. Therefore, one cannot use the same design principles of thin-walled members using the limit-states design method presented in South African National Standard 10162-1: Limit-states design of hot-rolled steelwork (from here on referred to as SANS 10162-1).

Although cold-formed steel is not as familiar as hot-rolled steel, cold-formed steel is growing in application, importance, and innovation in the construction industry. When CFS was first introduced as a building material in the 1930's, the acceptance of it in the construction industry was limited, since there were no adequate design standards or methods (Yu and LaBoube, 2010). Their use ranged from truss and wall panel systems to structural bracing and roof purlins. However, these types of elements were rarely used as primary load-bearing elements such as columns and beams (Allen, 2006).

The application of this type of steel has since evolved and buildings up to six storeys consisting of primarily cold-formed steel framing elements have been constructed (Yu and LaBoube, 2010). This type of steel is not only more cost-effective and lighter than hot rolled steel, but requires less labour to erect structures. Thus, it is an attractive construction material.

However, the conventional CFS design method may dissuade designers from optimising the cross-section of elements, as the design procedure is complex and iterative. This limits the potentially broad application of the steel. Thus, a new design method called the Direct Strength Method has been developed to address these design issues (Schafer, 2006b).



In the design context of South Africa, the reliability level achieved when using the DSM for CFS members needs to be assessed. Freitas *et al.* (2013) conducted a study that reviewed the calibration procedure of the capacity reduction factor for CFS compression members using the DSM in order to achieve a target reliability. The target reliability was achieved by using a capacity reduction factor of 0.88; higher than that of 0.85 suggested by SANS 10162-2 (2011). However, the target reliability used in the study was of  $\beta_t = 2.5$  and not of  $\beta_t = 3$ . Therefore, the current capacity reduction factors suggested by SANS 10162-2 (2011) may not be sufficient to achieve a target reliability of  $\beta_t = 3$ . Additionally, Freitas *et al.* (2013) only considered two load combinations; both of which exclude the effect of the wind load.

## 2.1.2 Design Methods of Cold-Formed Steel Members

Presented in SANS 10162-2 (2011) are two options for CFS compression member design. The main design specification for CFS compression members is the Effective Width Method (from here on referred to as EWM). Accompanying this method as a separate chapter of SANS 10162-2 (2011) is the DSM. Both methods are subsequently discussed. This is to highlight the differences in design approaches of these methods. With both methods having strengths and limitations, motivation is given for the Direct Strength Method to be the preferred method of CFS member design.

### 2.1.2.1 Effective Width Method

The conventional method used to design CFS compression members in SANS 10162-2 (2011) is the EWM, developed by the AISI (Ziemain, 2010). Simply put, the design equations of the EWM incorporates plate buckling theory. As a compressive stress increases on the edge of a simply supported plate, the plate begins to buckle before the yield stress is reached. Additionally, it is said that an edge of an element is restrained if the element is joined to another element. Due to the restrained edges of CFS members, there is still some post-buckling strength to account for.

Consider a simply supported plate that is edge loaded with a compressive stress shown in Figure 2.2 from American Iron and Steel Institute *et al.* (2016). Initially, the stress distribution across the edge of the plate is uniform through the width of the plate before buckling occurs. As the stress increases, the plate begins to buckle. At this point, the stress begins to redistribute towards the restrained edges of the plate, causing a non-uniform stress distribution. If the edges of the plate were not restrained, then the capacity

of the plate would be determined by the idealised elastic critical buckling stress of the plate (American Iron and Steel Institute *et al.*, 2016).

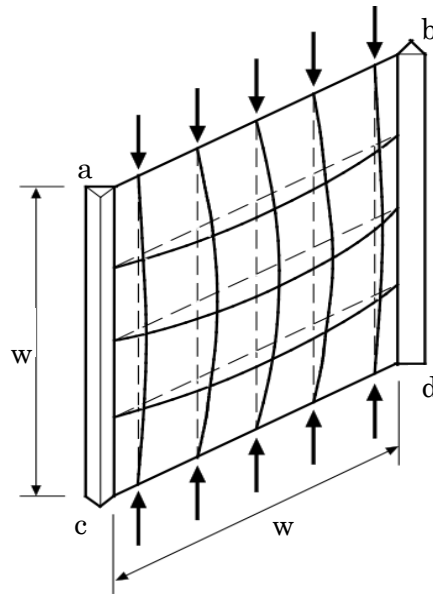


*Figure 2.2: Edge loaded simply supported plate (American Iron and Steel Institute et al., 2016)*

As the applied stress along the loaded edge increases, the stress at the corners of the plate also continue to increase with further stress distribution. Finally, failure occurs when the stress at the edges of the plate reach the material yield stress. The development of the stress distribution along the loaded edge of the plate is shown in Figure 2.3 by Yu and Schafer (2005). The phenomenon of the non-linear stress distribution towards the edges is known as the post-buckling strength (Yu and LaBoube, 2010).

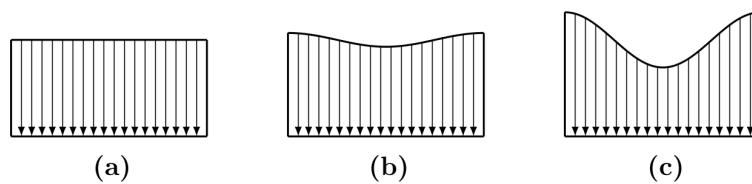


*Figure 2.3: Change in stress distribution with increasing edge load (Yu and Schafer, 2005)*

Observing the stages of the stress distribution in Figure 2.3, part (a) is where the applied uniform stress is less than the critical buckling load. Part (b) is where the redistribution of the stress towards the edges begins. Part (c) is where the most stress distribution has occurred, as the outer edges begin to yield.

This method suggests that the resistance of the entire plate is represented by a part of the width of the plate only; the effective width of the section. The effective width comprises

of edge parts, where fully plastic stresses can occur. As CFS members can consist of many such elements, the overall resistance is calculated as the sum of all resistances of the individual compressed plate elements within the section of the member.

Although the Effective Width Method has been successfully used for CFS design since the 1940's, the method does have drawbacks. With complex CFS sections, this method becomes a tedious procedure with cumbersome iterations. Furthermore, the EWM idealises elastic buckling as individual elements, which ignores the interaction between plate elements (Schafer, 2002).

### **2.1.2.2 Direct Strength Method**

Schafer (2006a) states that the Direct Strength Method was formally adopted as an Appendix in the North American Specification for the Design of Cold-Formed Steel Structural Members in 2004. This newly adopted method attempts to meet current design needs of simple and complex CFS sections through simplified means. SANS 10162-2 (2011) includes the method as an alternative procedure to design thin-walled columns and beams.

Incorporated within the DSM is the Finite Strip Method (from here on referred to as FSM). This method is closely linked to plate buckling theory. The method identifies the buckling modes, as well as the capacity of each buckling mode of any thin-walled element to be assessed. One should not confuse the DSM with the FSM, as the FSM is presented as a procedural calculation step within the DSM.

#### *2.1.2.2.1 Buckling Modes*

Through the development of the DSM, three main stability modes were defined, namely local, distortional, and global buckling modes. The definitions of each are subsequently given by Schafer (2006a).

**Local Buckling** – This buckling mode induces rotational distortion of the cross section at the corners of the member. This is to say that the angles between the elements do not change whilst the elements within the section buckle. There is no translational distortion of the section for this buckling mode. Under a compressive load, the buckling half-wavelength of this buckling mode is no greater than the largest dimension of the member. An illustration of this buckling mode for a lipped channel section is shown in Figure 2.4 by Bauer (2016).

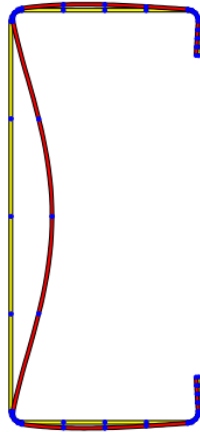


*Figure 2.4: Representation of the local buckling mode (Bauer, 2016)*

**Distortional Buckling** – The distortional buckling mode induces rotational and translational distortion at one or more of the corners of the member. This means that the angle between the elements change as the elements rotate about their intersections. Although this buckling mode is load and geometry dependant, the buckling half-wavelength is larger than that of local buckling but smaller than that of global buckling. This buckling mode is illustrated from Bauer (2016) in Figure 2.5 of a lipped channel section.

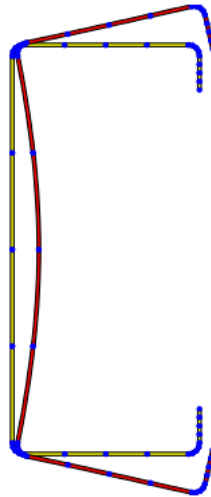


*Figure 2.5: Representation of the distortional buckling mode (Bauer, 2016)*

**Global Buckling** – Associated with flexural, torsional, or flexural-torsional buckling, the global buckling mode for columns induces translation out of plane and/or rotation about the shear centre of the cross section for axially loaded members. Unlike the local and distortional buckling modes, there is no deformation of the cross-sectional shape. The buckling half-wavelength of this buckling mode depends on the end fixities of the member.

When pin-ended, the half-wavelength is at a maximum of the physical length of the member (Schafer, 2006b). From Bauer (2016), Figure 2.6 shows the global buckling mode of a lipped channel section, demonstrating translation and rotation of the section.

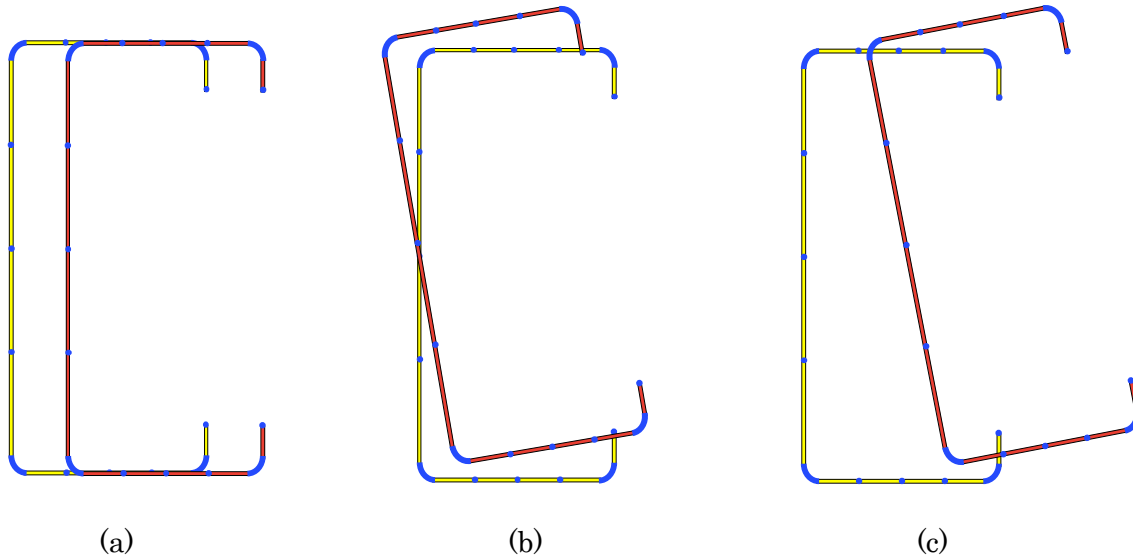


*Figure 2.6: Representation of the global buckling mode in the form of (a) flexural buckling, (b) torsional buckling and (c) flexural-torsional buckling (Bauer, 2016)*

**Buckling Mode Interactions** – At certain member lengths, an interaction between buckling modes can occur (Ungermann *et al.*, 2014). The interaction of the buckling modes depends on the section geometry and profile. If an interaction between buckling modes occur, the capacity of the member can be reduced. For the purposes of this study, only the local-global buckling interaction was considered. This is because the test database that this research is based on only considered the local-global buckling interaction (Ganesan & Moen, 2010).

#### *2.1.2.2.2 Finite Strip Method*

As part of the DSM, the FSM must be used to determine unknown variables in the DSM design procedure. Published in 1974 by Plank and Wittrick, the procedure of the Finite Strip Method allows for elastic behavioural prediction, requiring little effort (Ziemain, 2010). Without getting too detailed about the methodology of the Finite Strip Method, it uses equations to approximate displacements along discrete strips along the length of the member.

To implement this method, the CUFMSM v4.03 computer program was used. The program is based in a MATLAB programming environment and has been made freely available

online by Prof. Benjamin Schafer at Johns Hopkins University in Baltimore, USA (Li and Schafer, 2010). The program requires certain input information about a specific section that is to be analysed. The required input information of CUFSM includes geometrical and material properties. The material properties required for input include the modulus of elasticity ( $E$ ), the Poisson's ratio ( $\nu$ ), the Yield stress ( $f_y$ ) and the shear modulus ( $G$ ).

The section geometry is described using nodes and elements. This allows the user to input any shape of section described using as many elements and nodes as desired, with an option to alter the thicknesses of the elements individually. To simplify the input procedure, templates for lipped C- and lipped Z-sections are supplied. The input values for these templates are the centreline member height, flange widths, lip heights, lip radii and sectional thickness. The program then determines the sectional properties of the section to be analysed.

The end-fixities and the length of the member must also be chosen. With the length of the member, the half-wavelengths to be analysed should also be chosen. These half-wavelengths are typically chosen to follow a logarithmic scale.

As explained in the Direct Strength Method Design Guide (Schafer, 2006a), the program produces two results through the Finite Strip Method; the buckling half-wavelength and corresponding load factor, as well as the buckling mode shape of the cross section. The buckling half-wavelength is an indication of how a given cross-sectional shape varies along the length of the member in the buckled state. The load factor is the ratio of the critical design buckling load to the design yield load of the member in bending or in compression and is shown in Equation 2.1.

$$\text{Load Factor} = \frac{N_{cr}}{N_y} \quad (2.1)$$

The results are displayed graphically in what is known as a signature curve. The shape of the signature curves differ for each CFS section of alternate geometric and material properties analysed by the CUFSM program. The full member deformation signature curve is comprised of three pure buckling mode signature curves of local, distortional, and global buckling.

These individual buckling mode signature curves are generated through the process called the constrained finite strip method (cFSM) which CUFSM implements. An important aspect of the cFSM process is that it identifies the contribution of each buckling

mode at each buckling half-wavelength. From Bauer (2016), a typical signature curve of a lipped C section under axial load is shown in Figure 2.7.

The curve shows that the local buckling region occurs at low buckling half-wavelengths. The global buckling region occurs at high buckling half-wavelengths. The distortional buckling zone occurs at buckling half-wavelengths between that of the local and global buckling zones.

The minima on the signature curve indicate the lowest load level at which each of the buckling modes occur. Typically, there is a minimum point at the local and distortional buckling zones of the curve. Here, the critical buckling load factors for the respective buckling modes may be found. Obtaining the load factors at the curve minima, the critical buckling loads of  $N_{cr,l}$  and  $N_{cr,d}$  for local and distortional buckling respectively may then be calculated from Equation 2.1. This is on the condition that the compression yield load  $N_y$  is known.

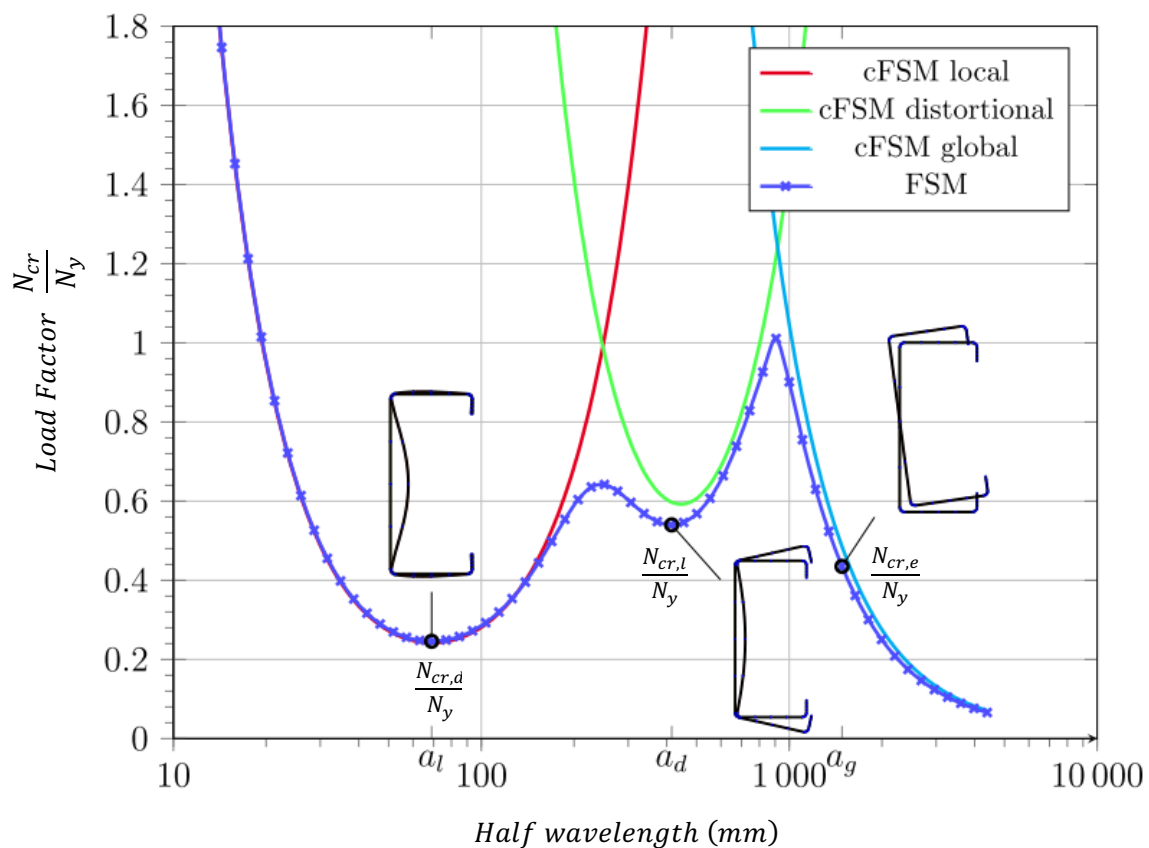


Figure 2.7: Typical signature curve showing the three types of buckling modes (Bauer, 2016)

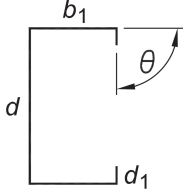
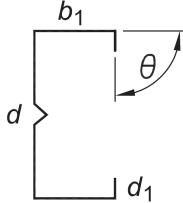
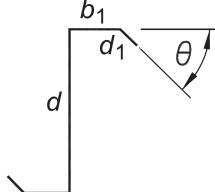
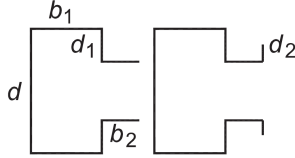
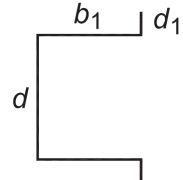
### *2.1.2.2.3 Design Procedure of Compression Members*

Column design according to the DSM is formulated in Section 7 of SANS 10162-2 (2011). It states that the nominal capacity of a compression member ( $N_d$ ) is taken as the minimum of the capacity for local buckling ( $N_{cl}$ ), distortional buckling ( $N_{cd}$ ) and global buckling ( $N_{ce}$ ).

The codified design procedure includes a pre-qualification check. The member must fall within the geometric limitations of the DSM to be designed using the corresponding capacity reduction factor for compression members  $\phi_c$  of 0.85 in the design calculation procedure. A reduced capacity reduction factor for compression members  $\phi_c$  of 0.80 is to be used if the geometric limitations are not met. The pre-qualification requirements of compression members for the DSM are listed in Table 2.1.



Table 2.1: Pre-qualified geometric limits for compression members (SANS 10162-2, 2011)

Section	Geometric Limitation
Lipped Channel 	$d/t < 472$ $b_1/t < 159$ $4 < d_1/t < 33$ $0.7 < d/b_1 < 5.0$ $0.05 < d_1/b_1 < 0.41$ $\theta = 90^\circ$ $E/f_y > 340$
Lipped Channel with Web Stiffener(s) 	$d/t < 489$ $b_1/t < 160$ $6 < d_1/t < 33$ $1.3 < d/b_1 < 2.7$ $0.05 < d_1/b_1 < 0.41$ One or two intermediate stiffeners $E/f_y > 340$
Z-Section 	$d/t < 137$ $b_1/t < 56$ $0 < d_1/t < 36$ $1.5 < d/b_1 < 2.7$ $0 < d_1/b_1 < 0.73$ $\theta = 50^\circ$ $E/f_y > 590$
Rack Upright 	$d/t < 51$ $b_1/t < 22$ $5 < d_1/t < 8$ $2.1 < d/b_1 < 2.9$ $1.6 < b_2/d_1 < 2.0$ ( $b_2$ = small outstand parallel to $b_1$ ) $d_2/d = 0.3$ ( $d_2$ = second lip parallel to $d_1$ ) $E/f_y > 340$
Hat 	$d/t < 50$ $b_1/t < 20$ $4 < d_1/t < 6$ $1.0 < d/b_1 < 1.2$ $d_1/b_1 = 0.13$ $E/f_y > 428$

 $r/t < 10$ , where  $r$  is the centre-line radius

**Global Buckling Capacity**

As per SANS 10162-2 (2011), the nominal global buckling capacity  $N_{ce}$  of a member in compression is calculated as follows:

$$N_{ce} = (0.658\lambda_c^2) \cdot N_y \quad \text{for } \lambda_c \leq 1.5 \quad (2.2)$$

$$N_{ce} = \left(\frac{0.877}{\lambda_c^2}\right) \cdot N_y \quad \text{for } \lambda_c > 1.5 \quad (2.3)$$

where

$$\lambda_c = \sqrt{\frac{N_y}{N_{cr,e}}} \quad (2.4)$$

$$N_y = A \cdot f_y \quad (2.5)$$

$$N_{cr,e} = A \cdot f_{oc} \quad (2.6)$$

$\lambda_c$  is the non-dimensional slenderness for global buckling of the column.  $N_{cr,e}$  is the elastic buckling load obtained from the lesser of the flexural, torsional, and flexural-torsional elastic buckling loads.  $A$  is the area of the full cross section. In the case for compression members,  $f_{oc}$  is the least of the elastic flexural, torsional, and flexural-torsional buckling stress. The procedure to determine  $f_{oc}$  is based on the calculation to determine the characteristic load of a concentrically loaded compression member.

For sections such as closed cross-sections that are not subject to torsional or flexural-torsional buckling,  $f_{oc}$  is determined through Equation 2.7 from SANS 10162-2 (2011).

$$f_{oc} = \frac{\pi^2 \cdot E}{\left(l_e/r\right)^2} \quad (2.7)$$

$E$  is the Young's Modulus of Elasticity.  $l_e$  is effective length of the member.  $r$  is the radius of gyration of the full, unreduced cross-section

For doubly- or singly-symmetric sections that are subject to torsional or flexural-torsional buckling, SANS 10162-2 (2011) states that  $f_{oc}$  is taken as the smaller of  $f_{oc}$  calculated using Equation 2.7 with  $r$  as the radius of gyration about the weak axis and  $f_{oxz}$  calculated in Equation 2.8.

$$f_{oxz} = \frac{1}{2 \cdot \beta_f} \cdot \left[ (f_{ox} + f_{oz}) - \sqrt{(f_{ox} + f_{oz})^2 - 4 \cdot \beta_f \cdot f_{ox} \cdot f_{oz}} \right] \quad (2.8)$$

where

$$\beta_f = 1 - \left(\frac{x_o}{r_{o1}}\right)^2 \quad (2.9)$$

$$r_{o1} = \sqrt{r_x^2 + r_y^2 + x_o^2 + y_o^2} \quad (2.10)$$

$\beta_f$  is the stress coefficient,  $r_{o1}$  is the polar radius of gyration of the cross-section about the shear centre.  $r_x$  and  $r_y$  are the radii of gyration of the cross section about the x- and y-axes respectively.  $x_o$  and  $y_o$  are coordinates of the shear centre of the cross section.

$$f_{ox} = \frac{\pi^2 \cdot E}{\left(l_{ex}/r_x\right)^2} \quad (2.11)$$

$$f_{oz} = \frac{G \cdot J}{A \cdot r_{o1}^2} \cdot \left(1 + \frac{\pi^2 \cdot E \cdot I_w}{G \cdot J \cdot l_{ez}^2}\right) \quad (2.12)$$

$l_{ex}$  and  $l_{ez}$  are the effective lengths for buckling about the x-axis and for twisting respectively.  $G$  is the shear modulus of elasticity.  $J$  is the torsion constant for the cross-section.  $I_w$  is the warping constant for the cross section.

For point-symmetric sections that are subject to flexural- or torsional buckling, SANS 10162-2 (2011) states that  $f_{oc}$  is taken as the lesser of  $f_{ox}$  as calculated in Equation 2.7 and  $f_{oz}$  as calculated in Equation 2.12.

### Local Buckling Capacity

The nominal local buckling capacity  $N_{cl}$  of a member in compression is calculated as follows, from SANS 10162-2 (2011):

$$N_{cl} = N_{ce} \quad \text{for } \lambda_l \leq 0.776 \quad (2.13)$$

$$N_{cl} = \left[1 - 0.15 \cdot \left(\frac{N_{cr,l}}{N_{ce}}\right)^{0.4}\right] \cdot \left(\frac{N_{cr,l}}{N_{ce}}\right)^{0.4} \cdot N_{ce} \quad \text{for } \lambda_l > 0.776 \quad (2.14)$$

where

$$\lambda_l = \sqrt{\frac{N_{ce}}{N_{cr,l}}} \quad (2.15)$$

$\lambda_l$  is the non-dimensional slenderness for local buckling of the column and  $N_{cr,l}$  is the elastic local buckling load. The procedure to determine  $N_{cr,l}$  is explained in Section 2.1.2.2.2.

**Distortional Buckling Capacity**

SANS 10162-2 (2011) states that the nominal distortional buckling capacity  $N_{cd}$  of a member in compression is calculated as follows:

$$N_{cd} = N_y \quad \text{for } \lambda_d \leq 0.561 \quad (2.16)$$

$$N_{cd} = \left[ 1 - 0.25 \cdot \left( \frac{N_{cr,d}}{N_y} \right)^{0.6} \right] \cdot \left( \frac{N_{cr,d}}{N_y} \right)^{0.6} \cdot N_y \quad \text{for } \lambda_d > 0.561 \quad (2.17)$$

where

$$\lambda_d = \sqrt{\frac{N_y}{N_{cr,d}}} \quad (2.18)$$

$\lambda_d$  is the non-dimensional slenderness for distortional buckling of the column and  $N_{cr,d}$  is the elastic distortional buckling load. The procedure to determine  $N_{cr,d}$  is explained in Section 2.1.2.2.2.

## 2.2 Reliability Theory

The fundamental condition that all design methods are required to adhere to are certain limit-states. Holický (2009) states that limit-states are distinct conditions that separate satisfactory and unsatisfactory states of a structure under certain conditions. Therefore, if exceeded, the structure no longer satisfies specific design requirements.

Each limit-state is associated with specific performance criteria. It can become complex to quantify the performance criteria of the limit states. To simplify the design procedure, two fundamental limit states for the design of structures are recognised: the ultimate and serviceability limit-states.

The ultimate limit-state is a representation of the overall stability and safety of the structure. If the ultimate limit-state is exceeded, there is a loss of static equilibrium or stability of the structure. These potential failure mechanisms need to be considered when specifying the reliability parameters.

The serviceability limit-state corresponds to the result of normal use conditions such as a change in structural appearance and human comfort. It is important to take the time-dependency of loads when considering the serviceability limit-state. If exceeded, cracks, large deflections and noticeable vibrations may occur in a structure. Although it is important to consider both limit-states in design, this research focuses on the ultimate limit-state design of CFS members.

### 2.2.1 The Ultimate Limit-State Equation

Equation 2.19 represents a favourable ultimate limit-state. This is where the structural resistance  $R$  exceeds the load effect  $E$ .

$$E < R \quad (2.19)$$

If the limit state represented by Equation 2.19 is not satisfied, it is assumed that structural failure occurs. An unambiguous distinction is made between a desirable and undesirable state by representing Equation 2.19 in the form expressed as the fundamental form of the limit-state equation in Equation 2.20.

$$R - E = 0 \quad (2.20)$$

The ultimate limit-state is represented by  $G$ . The safe-state of the limit-state is where the mathematical difference between the structural resistance and the load effect must be greater or equal to zero. This is expressed in Equation 2.21.

$$G = R - E \geq 0 \quad (2.21)$$

The structural resistance and the load effect can be represented by functions of  $i$  and  $j$  number of  $X$  variables respectively. Randomness of the limit-state equation is the effect of these  $X$  variables. The variables  $R$  and  $E$  are expressed in the form of Equation 2.22 and 2.23 respectively.

$$R = f(X_{R1}, X_{R2}, X_{R3}, \dots, X_{Ri}) \quad (2.22)$$

$$E = f(X_{E1}, X_{E2}, X_{E3}, \dots, X_{Ej}) \quad (2.23)$$

Uncertainties in the load effect and the structural resistance implies that they are both random variables. To get a definitive mathematical difference between the two is therefore problematic. Variability in the load effect and structural resistance are important things to consider when applying a structural reliability analysis (Nowak and Collins, 2000).

The load effect generally consists of long and short-term loads. Although the prediction methods of permanent loads and other long-term loads are fairly accurate, there is still an underlying level of uncertainty that needs to be accounted for. For example, the density of a material cannot be exactly predicted or consistent throughout the structure. Moreover, finding the exact force of imposed loads, wind loads, and other temporary loads are near to impossible to predict at any given time.

Structural resistance generally depends on the yield stress of the material and member geometry. It is unrealistic to suggest that these two properties are consistent along the length of a member. The yield stress of a material is highly dependent on a consistent chemical composition. The resulting thickness of the member is as accurate as the method of manufacture.

### 2.2.1.1 Probability of Failure

Because the load effect and the structural resistance are both random variables in most cases, the validity of Equation 2.21 is not absolutely guaranteed. Thus, it can be said that the limit-state equation expressed in Equation 2.21 can be exceeded and that there exists a probability of failure. In terms of Equation 2.19, the probability of failure denoted by  $p_f$  of the limit-state is expressed in Equation 2.24.

$$p_f = P(E > R) \quad (2.24)$$

As the load effect and the structural resistance are random variables in most cases, they can be expressed as probability distribution functions. The probability distributions for the load effect and the structural resistance can be obtained once their respective random variables have been defined. Each probability distribution function can be described by a mean  $\mu$ , a standard deviation  $\sigma$ , a skewness  $\alpha$ , and a kurtosis  $\varepsilon$ . These statistical parameters, referred to as statistical moment parameters, are important characteristics in determining the probability of failure. They influence the relative positioning, dispersion, and shape of the two probability density functions, as well as their relative distances from one another.

Generally, the statistical moment parameters of each probability distribution function describe how the probability of failure will be affected. The relative position of the two curves is affected by the means of each curve. The probability of failure increases as the distance between the two curves decrease. The dispersion of the two curves is affected by the standard deviation of each curve. The probability of failure decreases the narrower the curves become. If any of the probability distribution functions take on an un-symmetrical shape, the skewness of the curve effects the shape of the curves. Although not exclusively descriptive of a curve shape, the skewness of a probability distribution function is still significant in determining the probability of failure. The shape of the probability distribution function may affect the overlapping area between the two probability distribution functions, thus increasing or decreasing the probability of failure.

The probability density functions are shown graphically in Figure 2.8 by Bauer (2016). Observing Figure 2.8, it is evident that, depending on the variability of their respective random variables, a broad range of realisations can be observed by either the load effect or the structural resistance. Additionally, there exist certain realisation combinations where the limit-state equation is not satisfied.

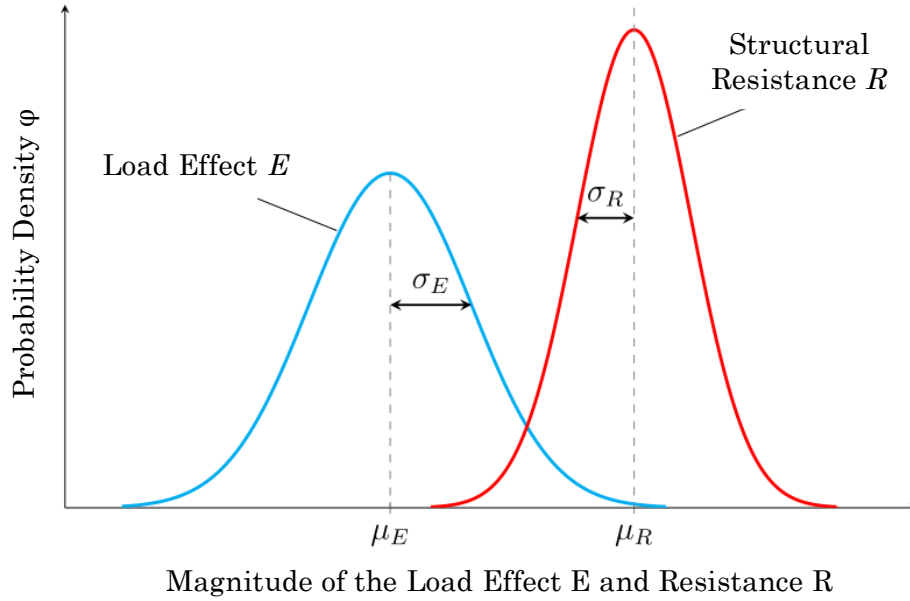


Figure 2.8: Probability density functions of load effect and structural resistance (Bauer, 2016)

### 2.2.1.2 Measure of Structural Reliability

To help describe the procedure, an initial assumption is made for simplicity. It is assumed that the probability density functions of the structural resistance and the load effect both have symmetrical normal distributions with different statistical moment parameters. It is noted that this is unlikely in application and this assumption is being made purely for the purposes of description.

From, Equation 2.21, the safe-state of the limit-state equation represented by  $G$  can be defined as its own random variable. For the normally distributed functions  $E$  and  $R$ , statistical moment parameters of  $\mu_G$ ,  $\sigma_G$  and  $\alpha_G$  of the random variable  $G$  are given in Equation 2.25, 2.26 and 2.27 respectively (Holický, 2009).

$$\mu_G = \mu_R - \mu_E \quad (2.25)$$

$$\sigma_G = \sqrt{\sigma_R^2 + \sigma_E^2 + 2 \cdot \rho_{RE} \cdot \sigma_R \cdot \sigma_E} \quad (2.26)$$

$$\alpha_G = \frac{\sigma_R^3 \cdot \alpha_R - \sigma_E^3 \cdot \alpha_E}{(\sigma_R^2 + \sigma_E^2)^{3/2}} \quad (2.27)$$

$\rho_{RE}$  is the correlation coefficient of the structural resistance and the load effect. Often the structural resistance and the load effect are independent of one another, so that  $\rho_{RE} = 0$  (Holický, 2009).



Figure 2.9 shows the probability density function of the limit-state represented by  $G$ . In this figure by Bauer (2016), it is observed that a portion of the curve extends below zero. With the curve encapsulating all possible realisations of  $G$ , the realisations of the limit-state that extend below zero are the realisations that do not satisfy Equation 2.21. Therefore, it can be said that the area under this part of the curve is the probability of failure, represented by the shaded area in Figure 2.9.

With reference to Equation 2.24, the probability of failure can be statistically expressed in the form of Equation 2.28. This equation expresses  $G$  as a statistical function of  $R$  and  $E$ . The symbol  $\Phi_G$  is the cumulative probability distribution function of the limit-state  $G$ . The probability of failure is therefore the area under the limit-state probability distribution function where the limit-state  $G$  is below zero.

$$p_f = P[(R - E) < 0] \quad (2.28a)$$

$$= P[G(R, E) < 0] \quad (2.28b)$$

$$= \Phi_G(0) \quad (2.28c)$$

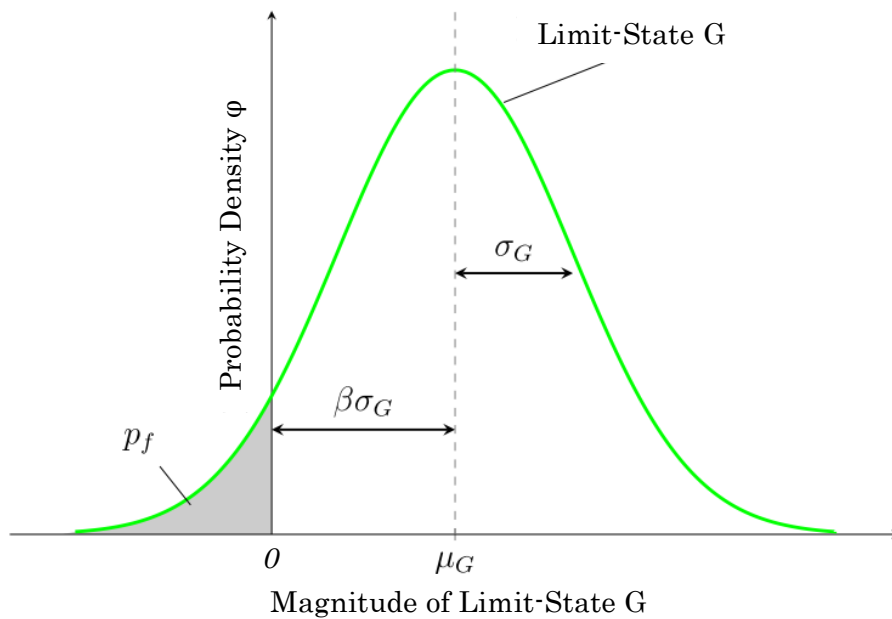


Figure 2.9: Probability density function of the limit-state  $G$  (Bauer, 2016)

The reliability margin, denoted by the symbol  $\beta$ , can be defined as the number of standard deviations the mean of the limit-state function  $G$  is from zero, given that  $G$  is a normally distributed function (Holický, 2009). This implies that  $\beta$  is dimensionless. The reliability margin and the probability of failure are therefore related, as the reliability margin

increases with a decrease of probability of failure. The relation is expressed in Equation 2.29 (Nowak & Collins, 2000).

$$p_f = \Phi_U(-\beta) \quad \text{or} \quad \beta = -\Phi_U^{-1}(p_f) \quad (2.29)$$

$\Phi_U$  is the standardised normal distribution function.

The value of  $\beta$  can be calculated with the moment statistical parameters of the load effect and the structural resistance.  $\beta$  is the ratio of the mean of the limit-state function to the standard deviation of the limit-state function. With reference to Equation 2.25 and 2.26,  $\beta$  is expressed in Equation 2.30.

$$\beta = \frac{\mu_G}{\sigma_G} = \frac{\mu_R - \mu_E}{\sqrt{\sigma_R^2 + \sigma_E^2 + 2 \cdot \rho_{RE} \cdot \sigma_R \cdot \sigma_E}} \quad (2.30)$$

For general reliability verification procedures, SANS 10160-1 (2011) suggests a reliability class 2 to be used. The minimum level of reliability for a reliability class 2 structure is  $\beta_t = 3$ . The basis of this thesis assesses whether the inherent reliability of the DSM equations for compression members formulated in SANS 10162-2 (2011) achieve the minimum level of reliability prescribed by SANS 10160-1 (2011).

### 2.2.1.3 Space of State Variables

Supplementary to the reliability analysis, the space of state variables may be described. The state variables considered are the structural resistance and the load effect. The space of state variables is a two-dimensional space where the limit-state function separates the safe domain and the failure domain. This is depicted in Figure 2.10 by Nowak and Collins (2000). The load effect is plotted on the x-axis and the structural resistance is plotted on the y-axis.

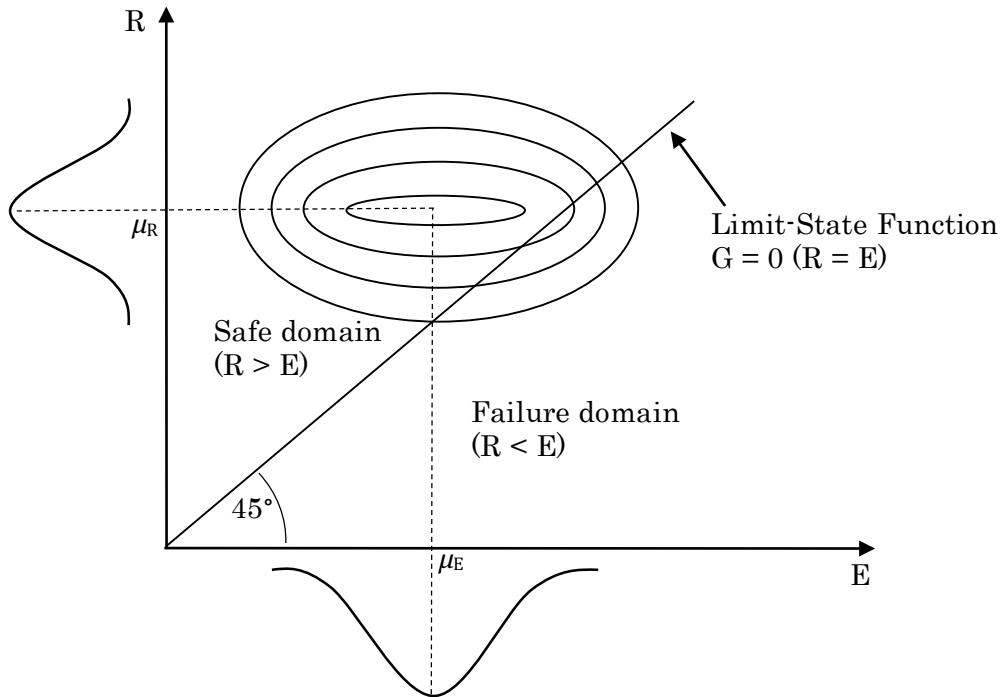


Figure 2.10: Two-dimensional space of state variables (Nowak and Collins, 2000)

Since the load effect and the structural resistance are random variables, a joint density function can be defined. As in Figure 2.10, the joint density function is separated into the safe domain and the failure domain, separated by the limit-state function. This is depicted as a 3-dimensional plot in Figure 2.11 (Nowak and Collins, 2000).

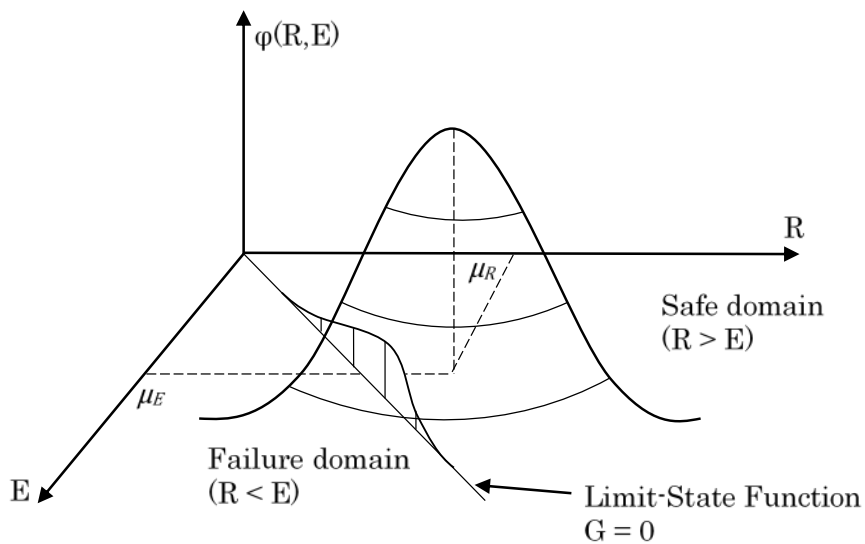


Figure 2.11: 3-Dimensional plot of the joint density function (Nowak and Collins, 2000)

Further, the space of state variables can be visualised in a standardised space to show the reliability margin. This is depicted in Figure 2.12 by Haldar and Mahadevan (2000). As the limit-state equation  $G$  is not necessarily linear, the design point  $(r_{0d}, e_{0d})$  must be determined. The design point is a point on the limit-state equation that is closest to the origin of a standardised space. The distance that the design point is from the origin of the standardised space is measured as the reliability margin  $\beta$ . It is possible for multiple design points to exist if the limit-state equation is non-linear. Figure 2.12 shows an example of the reliability margin for a non-linear limit-state function

Additional to the reliability analysis is the directional vector  $\alpha$  of the reliability margin  $\beta$ . Sharing the same symbol as the skewness of a distribution function, one must not confuse these two as they have completely different meanings. Also referred to as the sensitivity factors, the directional vector is split into two components relating to the load effect  $\alpha_E$  and the structural resistance  $\alpha_R$ . Shown in Equation 2.31 and 2.32, it is evident that the sensitivity factors for the load effect and the structural resistance are directional cosines of the reliability margin from the transformation to a standardised space. These are normal to the failure boundary (Holický, 2009).

$$\alpha_E = -\frac{\sigma_E}{\sqrt{\sigma_E^2 + \sigma_R^2}} \quad (2.31)$$

$$\alpha_R = \frac{\sigma_R}{\sqrt{\sigma_E^2 + \sigma_R^2}} \quad (2.32)$$

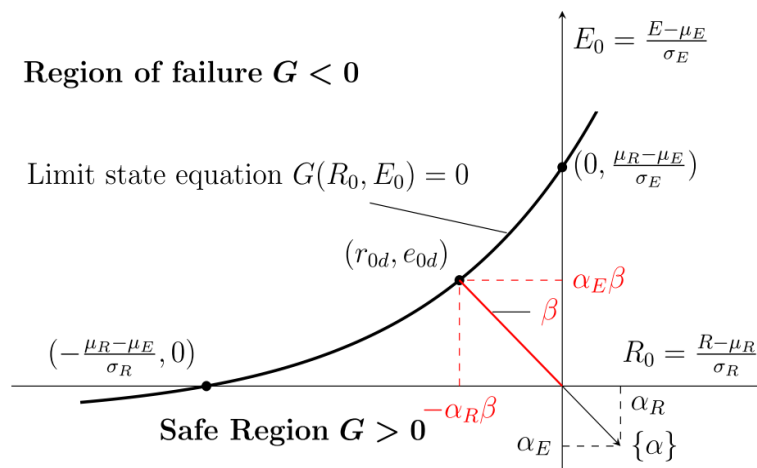


Figure 2.12: Reliability margin and sensitivity factors in a standardised space for a non-linear limit-state equation (Haldar and Mahadevan, 2000)

A simplified statistical approach in determining the reliability margin and the associated sensitivity factors has been presented in this section. Although the above explanation expressed the limit-state equation as a function of two variables, it is possible for the limit-state equation to be expressed as a function of more than two variables. This implies that the above procedure is not always possible to follow. Thus, in a more realistic multivariate case where there are n-number of random variables, a different form procedure is required (Nowak and Collins, 2000). A procedure in determining the reliability for such complex situations is subsequently discussed.

## 2.2.2 Reliability Simulation Methods

There exist many methods of reliability analysis for complex situations. The following reliability simulations were discussed as the most appropriate for the investigation of this thesis.

### 2.2.2.1 First Order Reliability Method

The First Order Reliability Method (from here on referred to as FORM) is a basic, yet efficient reliability method. Holický (2009) states that the EN 1990 design values are based on the FORM reliability method.

Initially developed by Hasofer and Lind, the FORM analysis aims to reduce a multivariate limit-state case to a normally distributed variable problem (Breitung, 2015). This procedure determines equivalent normal distribution statistical parameters of mean  $\mu^e$  and standard deviation  $\sigma^e$  at each design point, and iterates until convergence is reached at the design point corresponding to the smaller  $\beta$  value.

According to Holický (2009), the transformation of the non-normally distributed case to the normally distributed case is based on two conditions. The first is that the cumulative distribution functions and the equivalent standardised normal distribution variables should be equal. The second is that the probability density functions of the n-number of random variables should be equal to that of the equivalent normal density functions. Both of which must occur at the design point denoted as  $x^*$ . These conditions are described in Equation 2.33 and 2.34 respectively (Holický 2009).

$$\Phi_X(x^*) = \Phi_U\left(\frac{x^* - \mu_X^e}{\sigma_X^e}\right) \quad (2.33)$$

$$\varphi_X(x^*) = \frac{1}{\sigma_X^e} \varphi_U\left(\frac{x^* - \mu_X^e}{\sigma_X^e}\right) \quad (2.34)$$

Subsequently, the mean and the standard deviation of the equivalent normal distribution of variable  $X$  are determined in Equation 2.35 and 2.36 respectively.

$$\mu_X^e = x^* - \sigma_X^e \cdot [\Phi_U^{-1}(\Phi_X(x^*))] \quad (2.35)$$

$$\sigma_X^e = \frac{1}{\varphi_X(x^*)} \varphi_U\left(\frac{x^* - \mu_X^e}{\sigma_X^e}\right) = \frac{1}{\varphi_X(x^*)} \varphi_U[\Phi_U^{-1}(\Phi_X(x^*))] \quad (2.36)$$

The process to solve the reliability problem is an iterative process, since the limit-state equation is, in general, non-linear. The FORM analysis attempts to generate a tangent to the non-linear limit-state equation. With enough iterations, the generated tangent runs through the design point on the non-linear limit-state function. The distance perpendicular to the tangent from the design point to the origin of the standardised space is therefore the shortest. The number of iterations influence the accuracy of the outcome. With reference to Figure 2.10 and Figure 2.12, this is shown in Figure 2.13 (Holický, 2009).

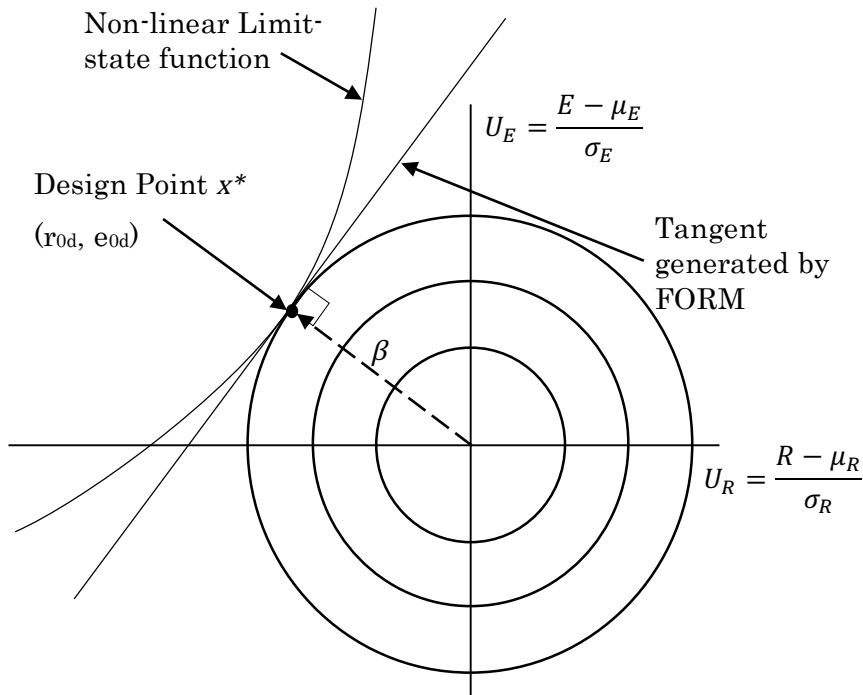


Figure 2.13: First order reliability method (Holický, 2009)

### 2.2.2.1.1 First Order Reliability Method Calculation Procedure

A summary of the iterative FORM procedure is presented in the following ten steps (Holicky, 2009):

1. Formulated as  $G(X) = 0$ , the limit-state function is expressed in terms of theoretical models of basic variables  $\{X\} = \{X_1, X_2, X_3, \dots, X_n\}$
2. An initial design point  $\{x^*\} = \{x_1^*, x_2^*, x_3^*, \dots, x_n^*\}$  is decided and assessed.
3. Equivalent normal distributions are found at the design point for all basic variables. This is done by using Equations 2.35 and 2.36.
4. From the standardised random variables  $\{U\} = \{U_1, U_2, U_3, \dots, U_n\}$  corresponding to the design point, the transformed standardised design point  $\{u^*\} = \{u_1^*, u_2^*, u_3^*, \dots, u_n^*\}$  is determined using Equation 2.37.

$$u_i^* = \frac{x_i^* - \mu_{X_i}^e}{\sigma_{X_i}^e} \quad (2.37)$$

5. Denoted as  $\{D\}$ , the vector of the partial derivatives for the limit-state function is evaluated at the design point. This is done in respect of the standardised variables and is shown in Equation 2.38.

$$\{D\} = \begin{Bmatrix} D_1 \\ D_2 \\ \vdots \\ D_n \end{Bmatrix} \quad \text{where} \quad D_i = \frac{\partial G}{\partial U_i} = \frac{\partial G}{\partial X_i} \cdot \frac{\partial X_i}{U_i} = \frac{\partial G}{\partial X_i} \cdot \sigma_{X_i}^e \quad (2.38)$$

6. From this, an estimation of reliability index  $\beta$  is calculated using Equation 2.39.

$$\beta = -\frac{\{D\}^T \{u^*\}}{\sqrt{\{D\}^T \{D\}}} \quad \text{where} \quad \{u^*\} = \begin{Bmatrix} u_1^* \\ u_2^* \\ \vdots \\ u_n^* \end{Bmatrix} \quad (2.39)$$

7. With reference to Equations 2.31 and 2.32, the sensitivity factors for each variable are then determined using Equation 2.40.

$$\{\alpha\} = \frac{\{D\}}{\sqrt{\{D\}^T \{D\}}} \quad (2.40)$$

8. A new design point is updated for  $n - 1$  standardised and original basic variables by using Equation 2.41 and 2.42 respectively.

$$u_i^* = \alpha_i \beta_i \quad (2.41)$$

$$x_i^* = \mu_{X_i}^e - u_i^* \sigma_{X_i}^e \quad (2.42)$$

9. From the limit-state function  $G(\{x^*\}) = 0$ , the design value of the remaining  $n$ -number of variables is recalculated.
10. Steps 3 to 9 are iteratively repeated until the reliability index converges to the design point with the required accuracy.

Depicted by Lopez and Beck (2012), Figure 2.14 shows a 3-dimensional graphical interpretation of the FORM analysis. It is to be noted that it regards the area under the hat-shaped curve that is past the tangent generated by the FORM analysis as the probability of failure. However, as the limit-state function in Figure 2.14 is non-linear and convex, the FORM analysis perceives a part of the area as unsafe, when in fact it is safe. This implies that the FORM analysis is slightly conservative, given that the limit-state function is convex as depicted in Figure 2.14. The closer the limit-state function is to a linear function, the less conservative it becomes.

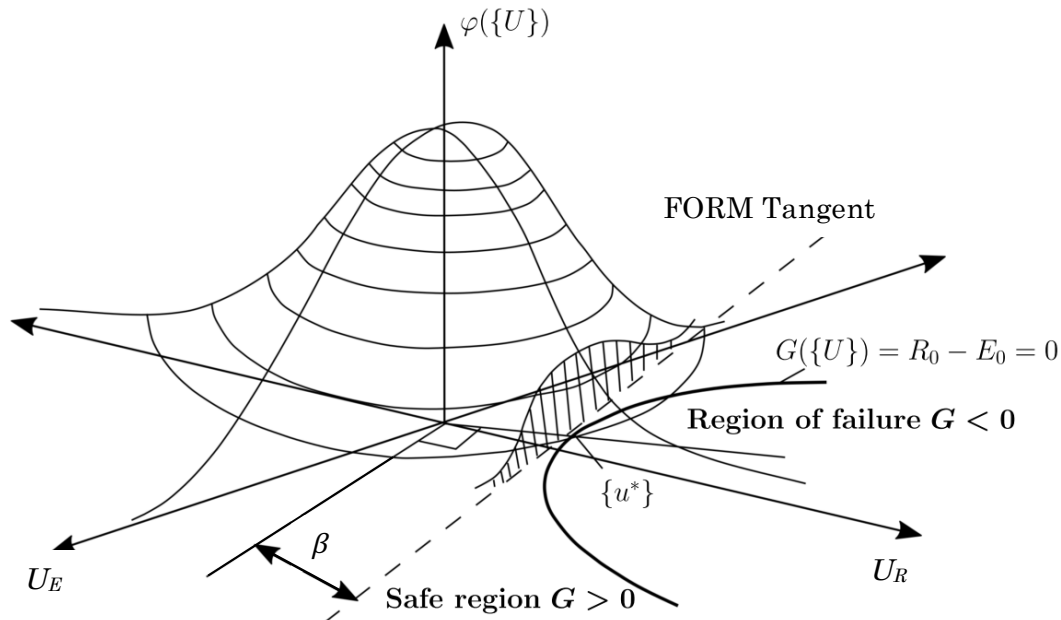


Figure 2.14: Graphical representation of the FORM analysis (Lopez and Beck, 2012)



For the case where the limit-state function is concave, the reliability margin that the FORM analysis determines may be under-conservative. This could prove to be problematic as the reliability margin generated by the FORM analysis may be higher than the true level of reliability. The Monte Carlo Simulation (from here on referred to as MCS) better predicts the level of reliability, provided that enough samples are generated. Comparing the results of the MCS and the FORM analysis, the general shape of the limit-state function could be estimated.

### 2.2.2.2 Monte Carlo Simulation Method

Cardoso *et al.* (2008) classifies three levels of reliability methods. Each level varies in accuracy and ease of calculation. Level 1 methods or semi-probabilistic methods approximates the probability of failure using partial factors. This method is most used in practice as it requires little calculation effort. However, the calibration of the partial factors in level 1 methods is based on level 2 or level 3 methods to achieve consistent performance. Level 2 methods, or approximate probabilistic methods, include the FORM analysis. This method is more accurate than the level 1 methods but require moderate computing efforts. Level 3 methods, or exact probabilistic methods, are where the probability of failure is determined from the joint probability of the random variables. Although these methods are the most accurate, they require the highest level of computing effort. The MCS is an example of a level 3 reliability method.

As accurate as the MCS may be, the method is not wide-spread in the analysis of structural reliability. This is because it is not as computationally efficient as the more common level 2 methods. For structural reliability applications, the tail-end of performance is evaluated, requiring large numbers of MCS samples to adequate accuracy. The use of the MCS in this investigation is purely to determine whether the shape of the limit-state function is concave or convex. Additionally, unlike the MCS analysis, the FORM analysis easily yields results for the sensitivity factors.

#### 2.2.2.2.1 Monte Carlo Simulation Calculation Procedure

With reference to Equation 2.28, a brief description of the MCS analysis for structural reliability is presented. It is to be understood that the probability of failure is expressed in Equation 2.43 (Cardoso *et al.*, 2008).  $X_1, X_2, X_3, \dots, X_n$  are the random variables associated with the limit-state. The term  $g(X_1, X_2, X_3, \dots, X_n) \leq 0$  is an expression of the violation of the limit-state equation. The term  $f_{X_1, X_2, X_3, \dots, X_n}(x_1, x_2, x_3, \dots, x_n)$  is the joint probability density function of realisations of all considered random variables.

$$p_f = P[g(X_1, X_2, X_3, \dots, X_n) \leq 0] \quad (2.43a)$$

$$= \iint_{g \leq 0} \dots \int f_{X_1, X_2, X_3, \dots, X_n}(x_1, x_2, x_3, \dots, x_n) dx_1 dx_2 dx_3, \dots, dx_n \quad (2.43b)$$

A descriptive interpretation of Equation 2.43 is that the area under the joint probability density function where the limit-state function is equal to or less than zero is the probability of failure. Depending on how many iterations are run, the MCS determines the probability of failure as expressed in Equation 2.44.

$$p_f = \frac{1}{N} \sum_{i=1}^N I(X_1, X_2, X_3, \dots, X_n) \quad (2.44)$$

$I(X_1, X_2, X_3, \dots, X_n)$  is a function that is defined by Equation 2.45.

$$I(X_1, X_2, X_3, \dots, X_n) = 1 \quad \text{for } g(X_1, X_2, X_3, \dots, X_n) \leq 0 \quad (2.45a)$$

$$I(X_1, X_2, X_3, \dots, X_n) = 0 \quad \text{for } g(X_1, X_2, X_3, \dots, X_n) > 0 \quad (2.45b)$$

The symbol  $N$  is the number of independent sets of values  $x_1, x_2, x_3, \dots, x_n$  obtained based on the probability distribution function of each random variable. Using Equation 2.29, the reliability level can be calculated once the probability of failure is determined.

Achintya & Mahadevan (2000) states that the accuracy of the probability of failure is dependent on the number of iterations. With more MC iterations, the probability of failure would approach the true value. A method to evaluate the accuracy of the MC results is to assess the coefficient of variation of the estimated probability of failure. This is depicted in Equation 2.46 (Achintya & Mahadevan, 2000).

$$COV = \frac{\sqrt{\frac{(1 - p_f) \cdot p_f}{N}}}{p_f} \quad (2.46)$$

$p_f$  is the probability of failure estimated from the MC simulation and  $N$  is the number of trials conducted. For the purposes of this study, the probability of failure relates to a reliability level of  $\beta = 3$  and 10 million trials were conducted for each MC simulation. The resulting coefficient of variance was 0.86%.

The point of departure of the discussion of the MCS is to convey the fact that, although it requires a greater computing effort, the MCS yields more accurate  $\beta$  values than the

FORM analysis. In this study, all  $\beta$  values presented in the results are from the FORM analysis. However, for each of the considered load combinations, a MCS was performed to estimate the shape of the limit-state function. If the  $\beta$  value determined from the MCS was greater than the  $\beta$  value from the FORM analysis, the limit-state function is convex, and the FORM analysis is conservative. If the  $\beta$  value determined from the MCS was less than the  $\beta$  value from the FORM analysis, the limit-state function is concave, and the FORM analysis is under-conservative.

## 2.3 Model Factor

The model factor or model uncertainty relates the test results to the predicted results of a model (Holický *et al.*, 2015). The model factor quantifies the epistemic level of uncertainty present in a prediction model. As in all models, it is rare for a prediction model to exactly predict test results. Sources of uncertainty stem from the inherent variability of materials, loads and member geometry, as well as epistemic uncertainty due to imperfect models with simplifications and statistical uncertainty. The model factor therefore plays a significant role in the reliability analysis. To account for the sources of uncertainty, the model factor for the DSM was introduced in this study.

Expresses in Equation 2.47, the model factor is the ratio of the test result to the predicted result of a prediction model. Model factors exist for the load effect and the structural resistance. The model factors associated with the load effect are dependent on the type of load. Each load type has a different model factor, as the difficulty of data collection and analysis may vary for the different types of loads. The model factors associated with the structural resistance are dependent on the level of approximation of the prediction model including test aspects such as section shape and buckling mode. The reliability margin investigated in this study covers the design procedure for the buckling modes of failure as discussed in Section 2.1.2.2.1. Therefore, a separate resistance model factor is used for each buckling mode.

$$\partial = \frac{F_{test}}{F_{model}} \quad (2.47)$$

It is to be noted that Equation 2.47 is the definition of a model factor for a single test. The model factors used in this study are considered as probability distribution functions, derived from a historic database of tests found in literature by Ganesan and Moen (2010). This is to say that the model factor statistically describes the predictive ability of the DSM model. **Error! Reference source not found.** shows the test-to-predicted ratios for all the CFS columns considered in the test database of Ganesan and Moen (2010) for the DSM. The test-to-predicted ratios are expressed as a function of global slenderness. Of the test database, 245 were of CFS lipped C members.

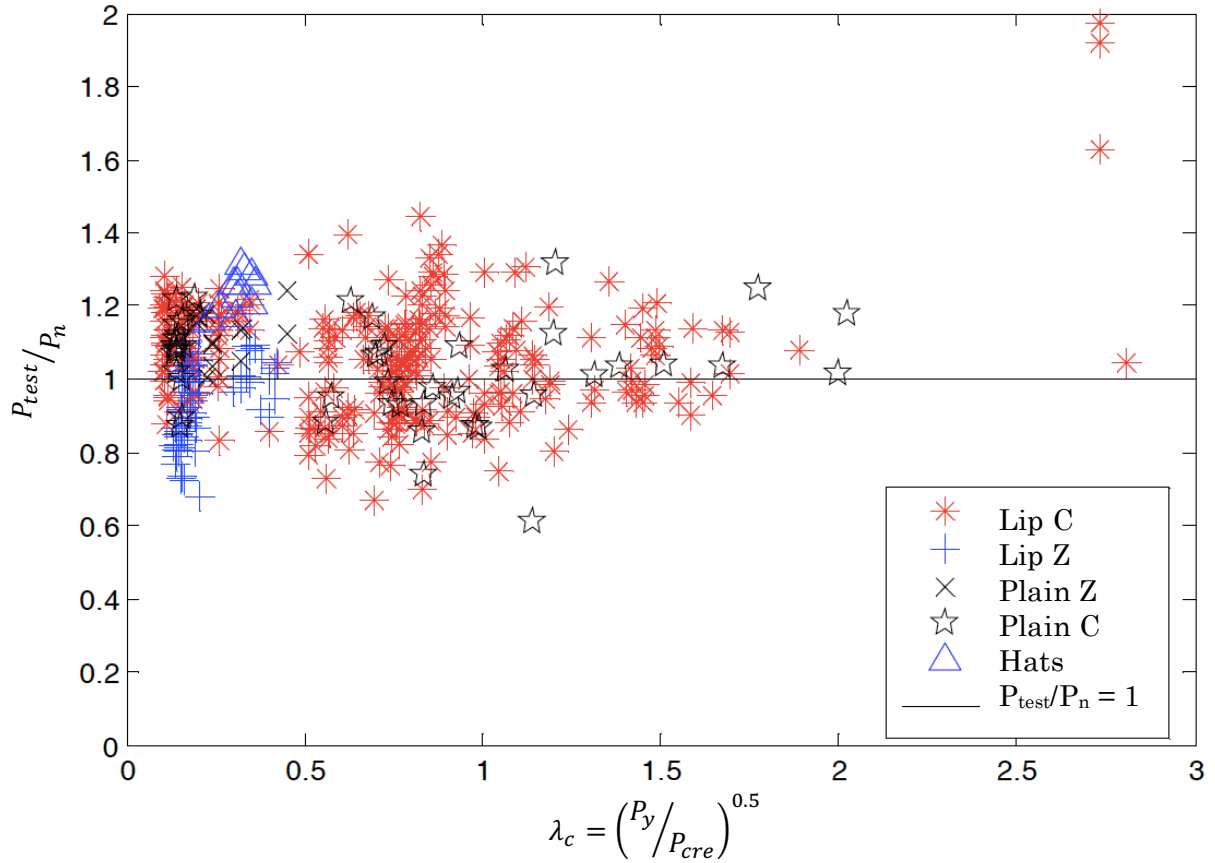


Figure 2.15: Test-to-predicted ratios of CFS columns as a function of global slenderness for the DSM (Ganesan and Moen, 2010)

Holický *et al.* (2015) categorises the effect that the model factor has on the level of uncertainty into three groups. The groups are dependent on the value of the sensitivity factors of the model factors obtained from a FORM analysis. Table 2.2 shows the characterisation of the model factors.

Table 2.2: Categorisation of the model factor (Holický, *et al.*, 2015)

Grouping	FORM Sensitivity Value
1 – Minor Effect	$\alpha_\partial < 0.32$
2 – Significant Effect	$0.32 < \alpha_\partial < 0.80$
3 – Dominating Effect	$0.80 < \alpha_\partial$

Holický, *et al.* (2015) states that by comparing physical test results with prediction model results, model uncertainty is obtained. Additionally, structural conditions should also be considered if needed. This concept is depicted in Figure 2.16. The significant factors that affect the test results, model results and structural-specific conditions are directly dependant on how the failure modes of a structural member are analysed. The following three aspects should be considered when quantifying model uncertainty (Holický, *et al.*, 2015).

1. *Test results:* well-calibrated test methods are typically unbiased with a test uncertainty mean of unity. The variability depends on external factors such as the skill level of staff and the type of tests conducted.
2. *Model results:* simplifications and other relevant computational options for numerical computer models should be reflected. Uncertainties in the input data should rather be reflected in the description of the basic variables.
3. *Structure-specific conditions:* Depending on the application of the structural member, it may be more desirable to quantify the differences between structure and specimens rather than to investigate the test uncertainty. Characters of the test uncertainty may represent the differences between structure and specimens.

The model factors used in the tests conducted in this thesis were quantitative representations only of the differences between the test results and the model results, which will include items 1 and 2 above. Structure-specific conditions were not considered.

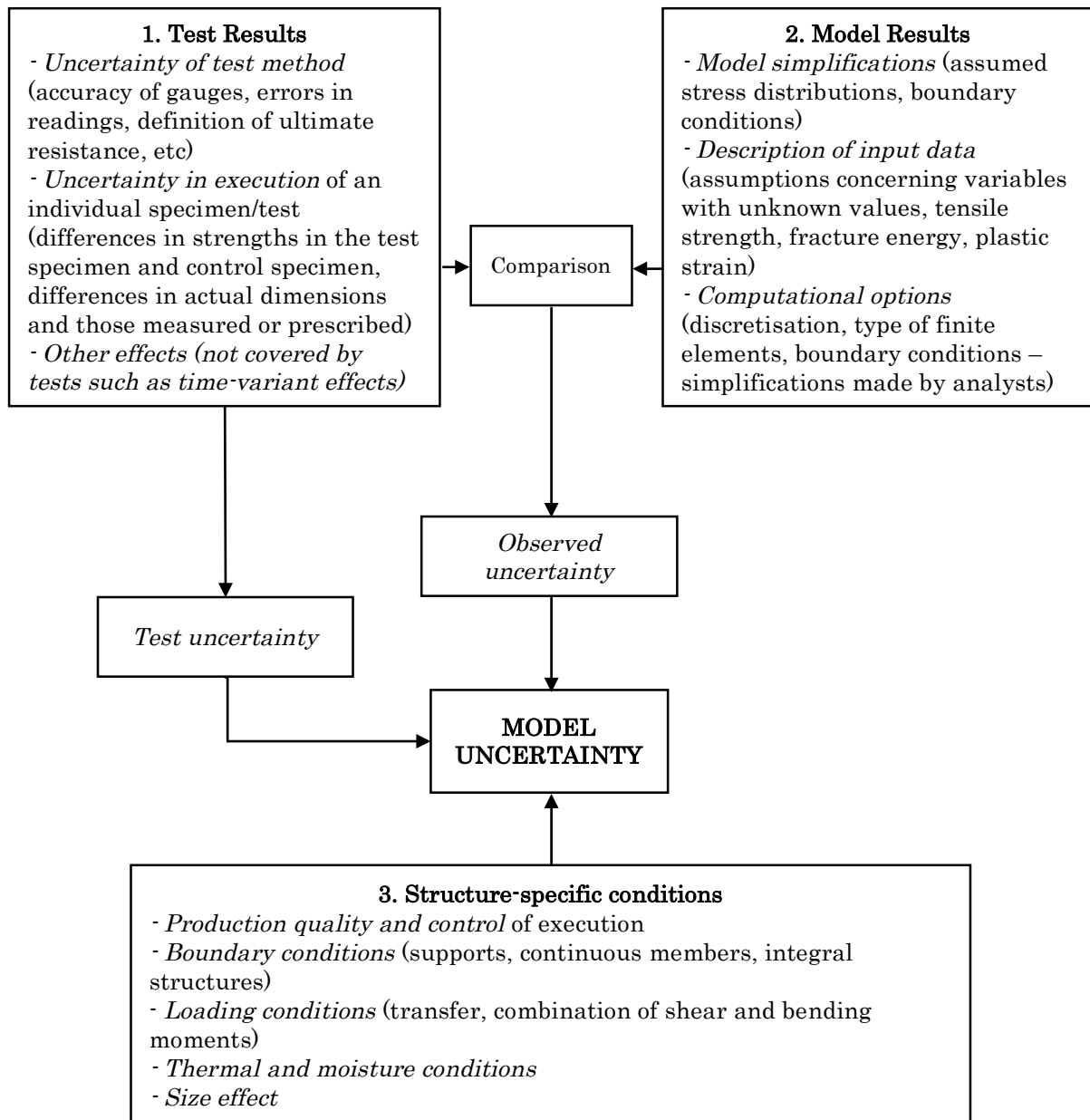


Figure 2.16: General concept of the model factor (Holický et al, 2015)

# CHAPTER 3:

## Assessment of Cold-Formed Steel Columns Designed with the Direct Strength Method

---

This chapter covers the processes that were followed to determine the reliability level of DSM designed CFS columns using the FORM analysis. To do this, a representative compression member was chosen. Load conditions were parametrically varied, and several member lengths were considered. To proceed with the DSM, the use of the CUFSM computer program, which incorporates the FSM, was required to distinguish the buckling modes and at which member lengths the different buckling modes govern design resistance.

### 3.1 Basis of Reliability Analysis

The basis of this study was to conduct a reliability analysis on a suitable limit-state equation formulation. Based on published literature and accepted published models, the random variables of the load effect and the structural resistance were chosen to represent a typical compression element in a structure.

The chosen member conforms to the prequalification criterion of SANS 10162-2 (2011) as summarised in Table 2.1. The member has two characteristic properties that describe the behaviour of the member under a given load. These properties are the material and the geometric properties. Each of these properties are to be considered as continuous random variables when conducting a reliability analysis. Typically, the yield stress of the material represents the material properties and the thickness of the member represents the geometric properties. However, based on research conducted by Bauer (2016), it was found that, when compared to the thickness and the yield stress, the resistance model factor governs uncertainty of the structural resistance. This is shown in Figure 3.1. Therefore, the thickness and the yield stress were taken as deterministic values.



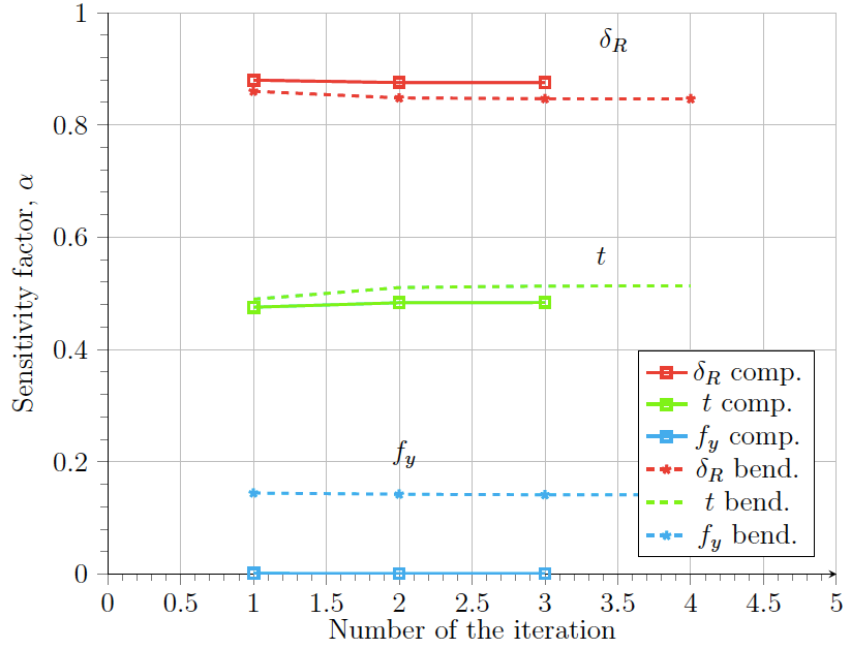


Figure 3.1: Sensitivity factors of structural resistance random variables (Bauer, 2016)

To proceed with the reliability analysis, however, the limit-state function was described in terms of the semi-probabilistic and full probabilistic formulations. The semi-probabilistic formulation of the limit-state equation is a representation of the limit-state in terms of codified values for the load effect and the structural resistance. To evaluate the inherent level of reliability achieved by the codified semi-probabilistic formulation of the limit-state, a full probabilistic formulation of the limit state is to be assessed. Here, the load effect and the structural resistance are represented by associated random variables. Each of the considered random variables are expressed as probability distribution functions.

This study assesses the inherent reliability level implied by the semi-probabilistic formulation of the limit-state. Specifically, the design structural resistance is based on the SANS 10162-2 (2011) formulation of the DSM using a prequalified column section. According to the DSM, the structural resistance is dependent on the buckling mode. In this study, the member length and profile varied to induce all the buckling modes. A range of load ratios were considered, based on SANS 10160-1 (2011).

### 3.1.1 Semi-Probabilistic Formulation of the Limit-State

The semi-probabilistic formulation of the limit-state expresses the design load and the design structural resistance as characteristic values multiplied by partial factors.

Therefore, the load effect and the structural resistance are deterministic values. The semi-probabilistic limit-state requirement is expressed in Equation 3.1.

$$R_d - E_d \geq 0 \quad (3.1)$$

$R_d$  is the codified design value for structural resistance and  $E_d$  is the codified design value of the load effect.

For the purposes of this study, the codified design value of the structural resistance prescribes to the DSM formulation presented in SANS 10162-2 (2011). This is to say that the design value of the structural resistance  $R_d$  in the semi-probabilistic formulation of the limit-state will equal the design compressive critical buckling load  $N_d$ .

The codified design value of the load prescribes to SANS 10160-1 (2011) for the various loads. For the purposes of this study, the considered load types were permanent, imposed and wind loads. The design values for each of the loads are represented in terms of their respective partial factors, combination factors and characteristic values. The partial and combination factors are dependent on the considered load combinations. The characteristic values of the loads were used as inputs to the full probabilistic formulation of the limit-state.

To obtain the design load of the semi-probabilistic formulation of the limit-state, the limit state requirement of Equation 3.1 was equated to zero. Hence, the total design load effect equated to the design value of the structural resistance.

### 3.1.2 Full Probabilistic Formulation of the Limit-State

To present the full probabilistic formulation of the limit-state, the basic variables of the limit-state were expressed as probability distribution functions. The statistical moment parameters of the basic random variables are expressed in terms of the characteristic values of the loads. The characteristic values of the loads were obtained from the semi-probabilistic formulation of the limit-state.

The full probabilistic formulation of the limit state can be expressed in Equation 2.20, where  $R$  and  $E$  are functions of associated random variables.

The structural resistance of the member in the full probabilistic formulation of the limit-state was calculated using the DSM described in Section 2.1.2.2.3. However, to attain a true, unconservative representation of the structural resistance, mean values of the material and geometric properties were used rather than the characteristic values.

Additionally, no partial factors or reduction factors were used in the calculation. The mean thickness was taken as the thickness given in the specification of the cross-sectional properties of the member. The overall structural resistance of the member in the full probabilistic formulation of the limit-state is represented by the symbol  $R$ . In this study, the structural resistance is comprised of the mean compressive critical buckling load  $N_{\mu}$  and the structural resistance model factor  $\partial_R$ .

The associated random variables are discussed and explained in subsequent sections. Essentially, the full probabilistic formulation of the limit-state was analysed to evaluate the inherent level of reliability of the semi-probabilistic formulation of the limit-state presented in SANS 10162-2 (2011).

### 3.1.3 Process of Reliability Analysis

The process of the reliability analysis is shown graphically in Figure 3.2. The geometric and material properties of a chosen compression member were initially defined. Using the CUFMS computer program, the design and mean yield capacities, represented by the symbols  $N_{y,d}$  and  $N_{y,\mu}$  respectively, were obtained. Subsequently, signature curves were generated for the design and mean capacities. For each signature curve, the buckling modes were identified in terms of their respective buckling half-wavelengths and load factors.

Using the design equations of the SANS 10162-2 (2011) formulation of the DSM, the semi-probabilistic formulation of the limit-state equation was established. Here, the design compressive capacity of the member  $N_d$  was calculated. The characteristic values of the loads were then determined from  $N_d$ , since Equation 3.1 was used and equated to zero. The codified combination factors and partial factors are dependent on the ratio of loads and the combination of these loads.

A FORM analysis of the full probabilistic limit-state equation was performed on the full probabilistic formulation of the limit-state. Each of the variables in the limit-state are expressed in terms of associated basic variables. The statistical parameters of the basic random variables of the load effect are based on the characteristic values of the considered loads. These were obtained from the semi-probabilistic formulation of the limit-state. The structural resistance considered the mean compressive capacity of the member  $N_{\mu}$ .

Model factors for the load effect and the structural resistance were included in the full probabilistic formulation of the limit-state. They were considered as continuous random

variables. The statistical parameters of the model factors were based on literature and historical tests.

The results of the full probabilistic formulation of the limit-state presented the reliability levels at the different load combinations for each buckling mode. At the corresponding load combinations for which the reliability level was determined, the sensitivity factors were also determined. Sensitivity factors reflect the influence each of the respective variables in the limit-state equation on the reliability level.

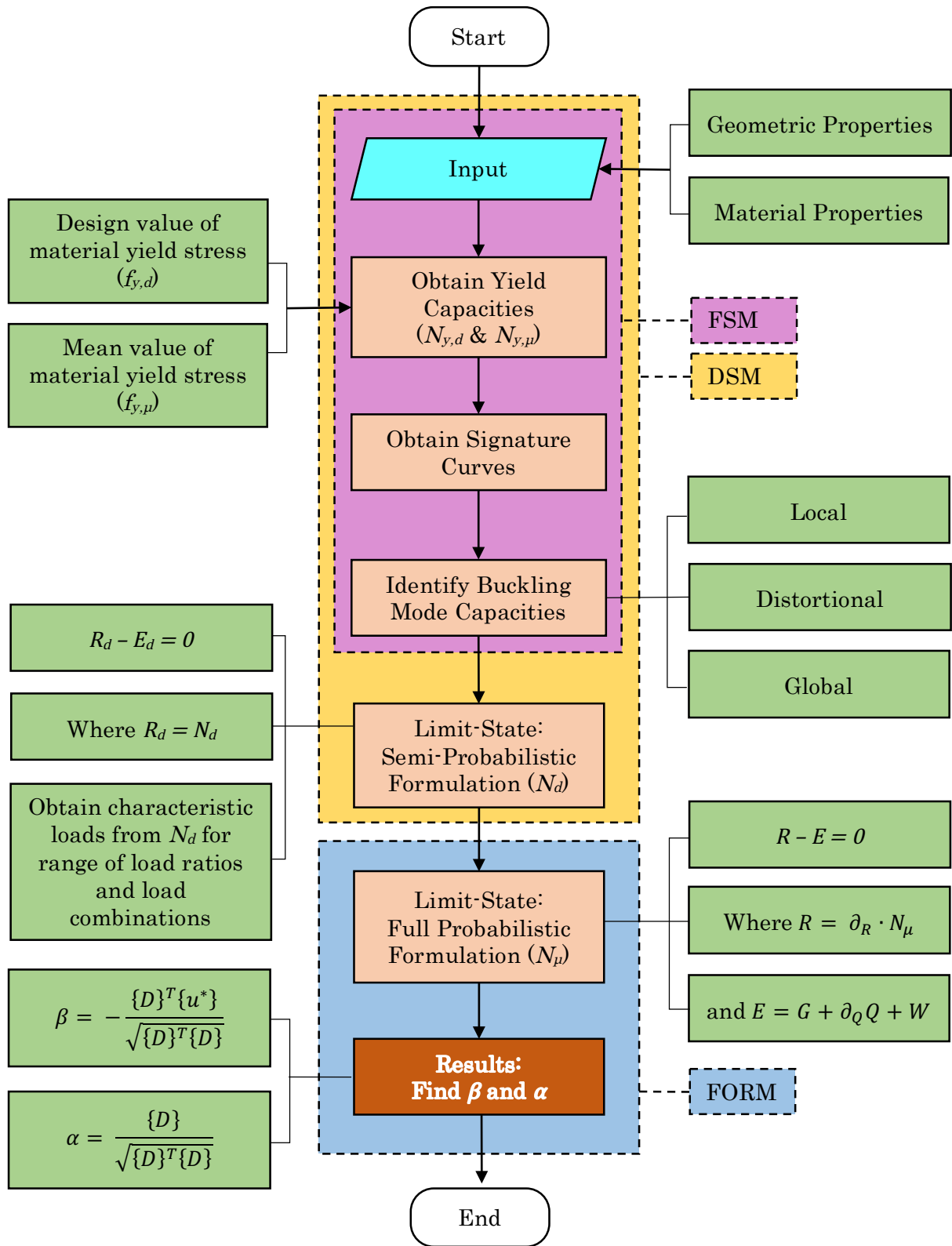


Figure 3.2: Flow diagram depicting the general procedure of the reliability analysis

The remainder of the chapter is to be read in conjunction with observing Figure 3.2. Herewith following, all steps shown in Figure 3.2 are explained as sub-headings in detail.

## 3.2 Analysis of Cold-Formed Steel Compression Member

The section geometry and profile of the chosen CFS compression member was obtained by a previous study conducted by Bauer (2016). In the study, the plain lipped C-section was chosen, shown in Figure 3.3. This is because it is considered as a common compression element in South African CFS design.

Furthermore, as only the local and global buckling modes were induced for the considered section, alterations were made to the section to induce distortional buckling. It was established that by adding a stiffener to the web of the member, the distortional and global buckling modes were induced. This is shown in Figure 3.4. Therefore, the local and global buckling analyses were performed on a plain lipped C-section and the distortional and global buckling analyses were performed on a stiffened lipped C-section with similar geometric and sectional properties.

### 3.2.1 Member Geometric Properties

The geometrical properties of the chosen plain lipped C-section and the stiffened lipped C-Section are shown in Table 3.1. The CUFSM computer program required the centreline dimensions as input parameters for modelling. These geometric properties of the sections were used for the calculation of  $N_d$  for the semi-probabilistic formulation of the limit-state and  $N_p$  for the full probabilistic formulation of the limit-state. Figure 3.3 and Figure 3.4 show the geometric detailing of the plain lipped C-section and the stiffened lipped C-section respectively.

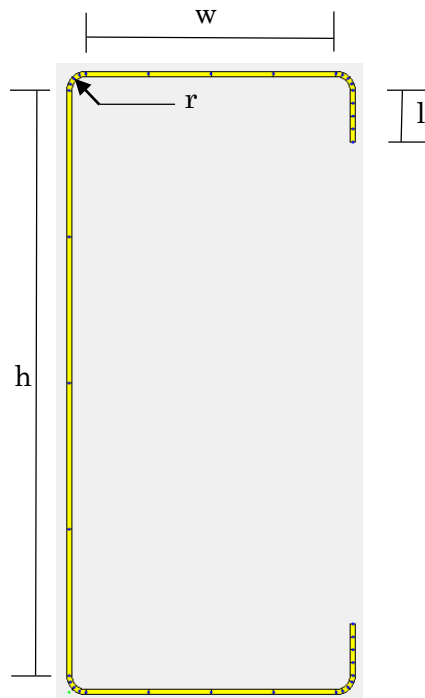


Figure 3.3: Plain lipped C-section with centreline dimensions

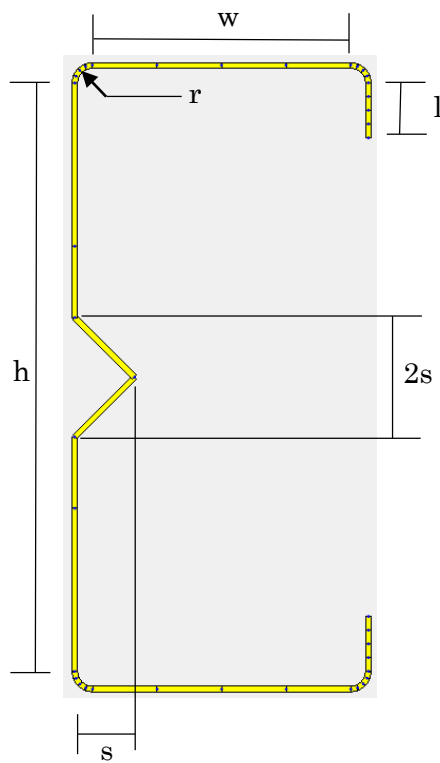


Figure 3.4: Stiffened lipped C-section with centreline dimensions

*Table 3.1: Geometrical properties of compression elements*

Section Property	Symbol	Plain Lipped C-Section		Stiffened Lipped C-Section	
		Dimension (mm)	Centreline Dimension (mm)	Dimension (mm)	Centreline Dimension (mm)
Web height	$h$	89	83.5	82.373	76.875
Flange width	$w$	41	35.5	41	35.5
Lip height	$l$	10.1	7.35	10.1	7.35
Angle radius	$r$	2	2.375	2	2.375
Thickness	$t$	0.75	0.75	0.75	0.75
Member length	$L$	4000	4000	4000	4000
Stiffener length	$s$	0	0	8.75	8

The sectional properties required to perform the calculations in Section 2.1.2.2.3 were obtained from the CUFSM computer program. For the cross-sections in Figure 3.3 and Figure 3.4, the section properties that were used in the codified DSM calculations are shown in Table 3.2. Observing Table 2.1, the analysed sections satisfy the prequalification limitations for the DSM design method.



Table 3.2: Sectional properties obtained from CUFSM

Geometric Property	Unit	Plain Lipped	Stiffened Lipped
		C-Section	C-Section
		Value	Value
$A$	mm <sup>2</sup>	138.0202	138.0213
$J$	mm <sup>4</sup>	25.8788	25.879
$x_{cg}$	mm	12.6011	12.5666
$y_{cg}$	mm	44.125	44.1247
$I_{xx}$	mm <sup>4</sup>	176897.216	154025.7559
$I_{yy}$	mm <sup>4</sup>	31731.8714	28810.2526
$x_o$	mm	-18.9829	-17.0042
$y_o$	mm	44.125	44.1247
$I_w$	mm <sup>6</sup>	51121114.09	43982030.78

$A$  is the gross area of the cross-section,  $J$  is the torsion constant for the cross-section,  $x_{cg}$  and  $y_{cg}$  are the coordinates of the centre of gravity of the section,  $I_{xx}$  and  $I_{yy}$  are the moments of inertia about the x- and y-axes respectively,  $x_o$  and  $y_o$  are the coordinates of the shear centre and  $I_w$  is the warping constant for the cross-section.

It is to be noted that the stiffened lipped C-section member shares the same cross-sectional area as the plain lipped C-section member. This is to say that the same amount of steel was used for each section.

### 3.2.2 Member Material Properties

The material properties of the members required for input values of the CUFSM computer program included the modulus of elasticity, Poisson's ratio, the shear modulus of elasticity and the yield stress. The same material properties were taken for the plain and lipped C-sections respectively. The material properties of grade G550 steel were used. These values are shown in Table 3.3.

*Table 3.3: Material properties of Grade G550 high strength steel*

Material Property	Symbol	Value	Unit
Modulus of elasticity	$E$	203,000	MPa
Shear modulus	$G$	78,077	MPa
Poisson's ratio	$\nu$	0.3	N/A

Grade G550 steel conforms to SANS 4998: Continuous hot-dip zinc-coated carbon steel sheet of structural quality (from here on referred to SANS 4998). As the yield stress of the steel was 550MPa, this conforms to the DSM pre-qualification limitations presented in Table 2.1 for the plain and stiffened lipped C-sections.

Clause 1.5.1.4(b) of SANS 10162-2 (2011) limits the yield stress of the steel based on the thickness of the element. The clause states that if the thickness of an element is between 0.6mm and 0.9mm, it should be assumed that the yield stress used in calculating  $N_d$  is taken as the lessor of 495MPa or 90% of the yield stress. The limitation of the yield stress was applied only to the calculation of  $N_d$  and not of  $N_\mu$ . This is because, as explained in Section 3.1.2, the mean compressive capacity of the column member is to be a true and unconservative representation of the steel resistance.

### 3.2.3 Design and Mean Yield Loads

The design and mean yield loads for the sections were calculated by multiplying the yield stress with the gross cross-sectional area of each section. The gross sectional areas used to calculate  $N_d$  and  $N_\mu$  are equivalent, however the yield stresses used to calculate  $N_d$  and  $N_\mu$  are different. This is because the yield stress to calculate  $N_d$  is the characteristic yield stress and the yield stress used to calculate  $N_\mu$  is the mean yield stress.

The calculation of the mean yield stress was determined by using Equation 3.2 from Holický (2009).

$$\mu_{f_y} = f_y + 2 \cdot \sigma_{f_y} \quad (3.2)$$

where

$$\sigma_{f_y} = 0.1 \cdot \mu_{f_y} \quad (3.3)$$

Observing Equations 3.2 and 3.3, the mean value and the standard deviation of the yield stress are co-dependant. Therefore, an iterative procedure is required to ensure convergence of the moment parameters of the yield stress. The design yield stress was assumed to be 495MPa due to the limiting clause 1.5.1.4(b) of SANS 10162-2 (2011). Satisfying Equations 3.2 and 3.3, the mean yield stress was calculated as 687.5MPa. The yield stresses were then multiplied by the cross-sectional area of the sections, found in Table 3.2. This resulted in mean and design yield loads as shown in Table 3.4.

*Table 3.4: Yield stresses and yield capacities for the plain and stiffened lipped C-sections*

	<b>Unit</b>	<b>Plain Lipped C-Section</b>	<b>Stiffened Lipped C-Section</b>
$f_{y,d}$	MPa	495	495
$f_{y,\mu}$	MPa	687.5	687.5
$N_{y,d}$	N	68,320	68,320
$N_{y,\mu}$	N	94,889	94,889

The study by Van Wyk (2014) investigated the tear-out resistance of screwed connections in CFS members. In the study, it was found that the mean yield stress of G550 grade CFS was 657.7MPa and the standard deviation was 70.5MPa. Therefore, by comparing the assumed value of the mean yield stress used in this study to that found by van Wyk (2014), an assumed mean yield stress of 687.5MPa is justified.

### 3.2.4 Signature Curves and Buckling Modes

The signature curves obtained by the CUFSM computer program for the calculation of  $N_d$  and  $N_\mu$  are shown in Figure 3.5 for the plain lipped C-section and in Figure 3.6 for the stiffened lipped C-section. The two signature curves of each section are similar in shape, however the signature curve used to calculate  $N_\mu$  is shifted lower than the signature curve used to calculate  $N_d$ . The load factors corresponding to the signature curve minima for the  $N_d$  and  $N_\mu$  signature curves are presented in Table 3.5 for the plain lipped C-section and Table 3.6 for the stiffened lipped C-section.

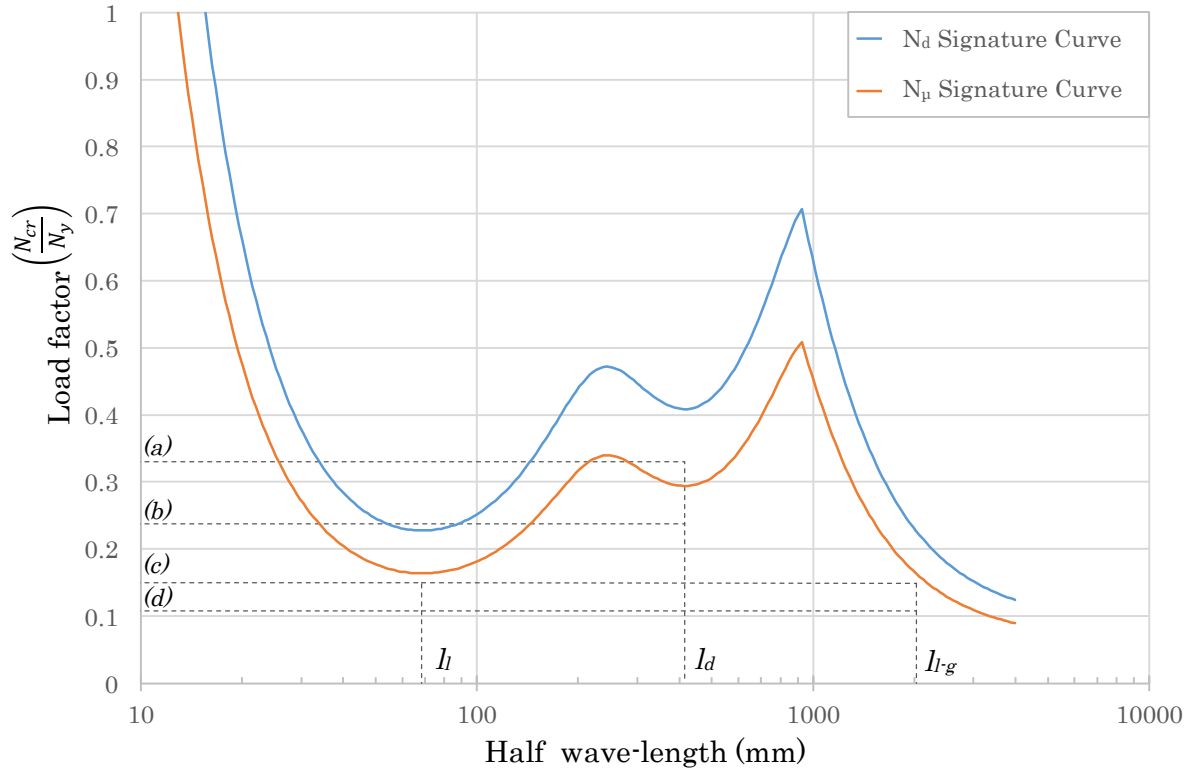


Figure 3.5: Signature curves of plain lipped C-section

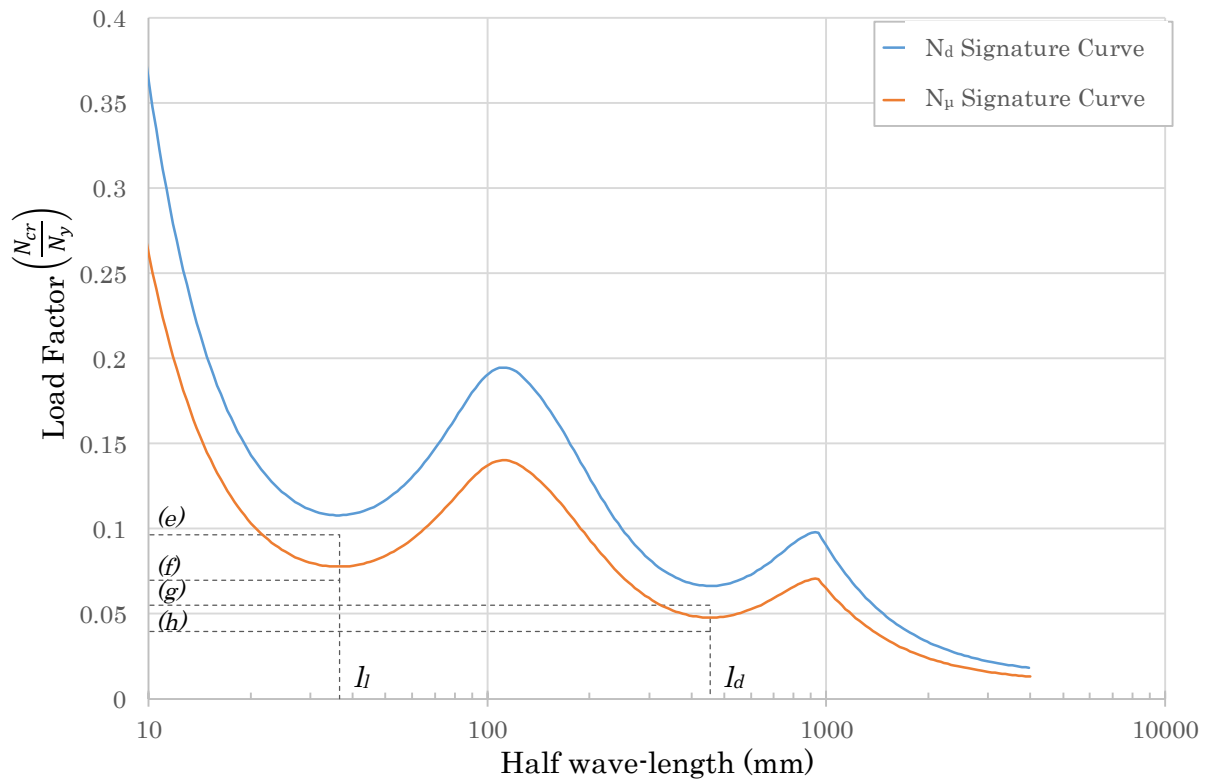


Figure 3.6: Signature curves of stiffened lipped C-section

Table 3.5: Load factors of  $N_d$  and  $N_\mu$  signature curves for plain lipped-C section

Signature Curve	Local buckling minima		Distortional buckling minima	
	Load factor $\frac{N_{cr,l}}{N_y}$	Half-wavelength $l_l$ (mm)	Load factor $\frac{N_{cr,d}}{N_y}$	Half-wavelength $l_d$ (mm)
$N_d$	(c) 0.14955	68.33	(a) 0.33068	413.56
$N_\mu$	(d) 0.10767	68.33	(b) 0.23806	413.56

Table 3.6: Load factors of  $N_d$  and  $N_\mu$  signature curves for stiffened lipped-C section

Signature Curve	Local buckling minima		Distortional buckling minima	
	Load factor $\frac{N_{cr,l}}{N_y}$	Half-wavelength $l_l$ (mm)	Load factor $\frac{N_{cr,d}}{N_y}$	Half-wavelength $l_d$ (mm)
$N_d$	(e) 0.096476	36.64	(g) 0.054979	453.57
$N_\mu$	(f) 0.069463	36.64	(h) 0.039585	453.57

The values in Table 3.5 and Table 3.6 correspond to those in Figure 3.5 and Figure 3.6 respectively. The load factors  $\frac{N_{cr,l}}{N_y}$  and  $\frac{N_{cr,d}}{N_y}$  in Table 3.5 and Table 3.6 are ratios of the local and distortional critical buckling loads respectively to the yield load. As seen in Figure 3.5 and Figure 3.6, these occur at the signature curve minima.

The DSM design equations suggest that, beyond a given buckling half-wavelength, a local-global buckling interaction occurs. This is to say that the calculated values of the local buckling capacity  $N_{cl}$  and the elastic buckling  $N_{ce}$  using the DSM are equal. Therefore, the reliability index at the local-global buckling interaction of the plain lipped C-section was also investigated. This was done by obtaining the buckling half-wavelength in the global buckling zone of the signature curve that shared an equal load factor at the local minimum on the signature curve, as shown in Figure 3.5. The symbol  $l_{-g}$  represents the local-global buckling half-wavelength as shown on Figure 3.5. The buckling half-wavelength of the local-global interaction was found to be 2024.61mm for the plain lipped C-section. No local-global buckling interaction was considered for the stiffened lipped C-section.

As observed for the plain lipped C-section, the local buckling load factor  $\frac{N_{cr,l}}{N_y}$  is less than the distortional buckling load factor  $\frac{N_{cr,d}}{N_y}$  for both signature curves of the plain lipped C-section. This is shown in Table 3.5. This implies that local buckling will occur at a lower load than distortional buckling for the plain lipped C-section. Additionally, observed for the stiffened lipped C-section, the distortional buckling load factor  $\frac{N_{cr,d}}{N_y}$  is less than the local buckling load factor  $\frac{N_{cr,l}}{N_y}$  for both signature curves of the stiffened lipped C-section. This is shown in Table 3.6. This suggests that distortional buckling will occur at a lower load than local buckling for the stiffened lipped C-Section.

Global buckling is induced in both sections at higher buckling half-wavelengths. This is to say that, irrespective of the section profile, the global buckling mode dominates the buckling capacity of the members at high member lengths.

### 3.2.5 Direct Strength Method Design of Members

Following the design procedures of the DSM presented in Section 2.1.2.2.3, the DSM calculations of the local buckling capacity  $N_{cl}$ , the distortional buckling capacity  $N_{cd}$  and elastic buckling capacity  $N_{ce}$  were calculated for different member lengths. This was done for the lipped and stiffened C-section members respectively, as shown in Figure 3.7 and Figure 3.8. For each member, the design, and the mean compressive loads to calculate  $N_d$  and  $N_{\mu}$  respectively are shown.

Additional to the figures, the buckling half-wavelengths for the curve minima in are also plotted in Figure 3.7 and Figure 3.8 respectively. The local and distortional buckling minima plots on Figure 3.5 and Figure 3.6 are with reference to Figure 3.5 and Figure 3.6 respectively.

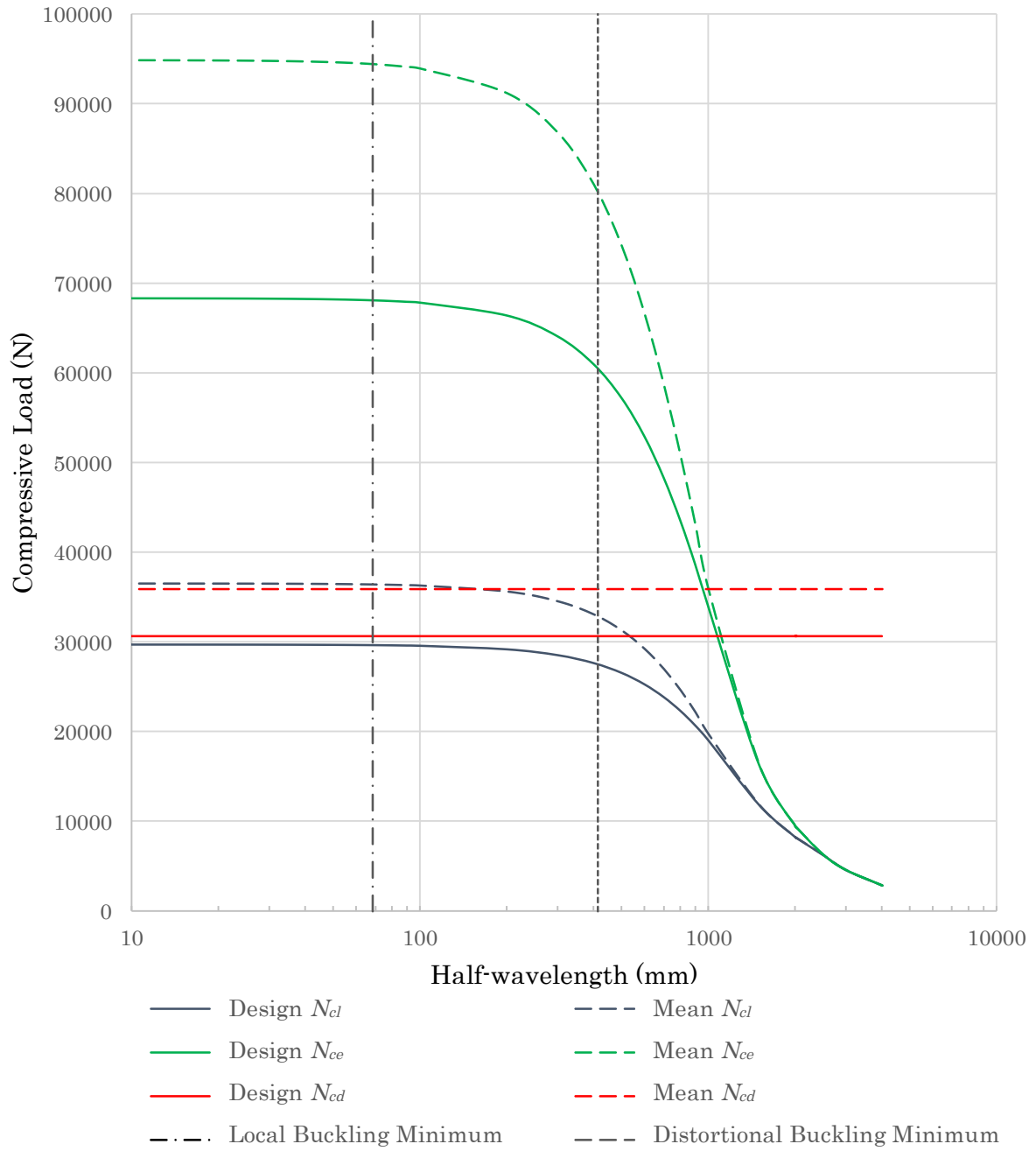


Figure 3.7: Direct strength method buckling loads for the plain lipped C-section

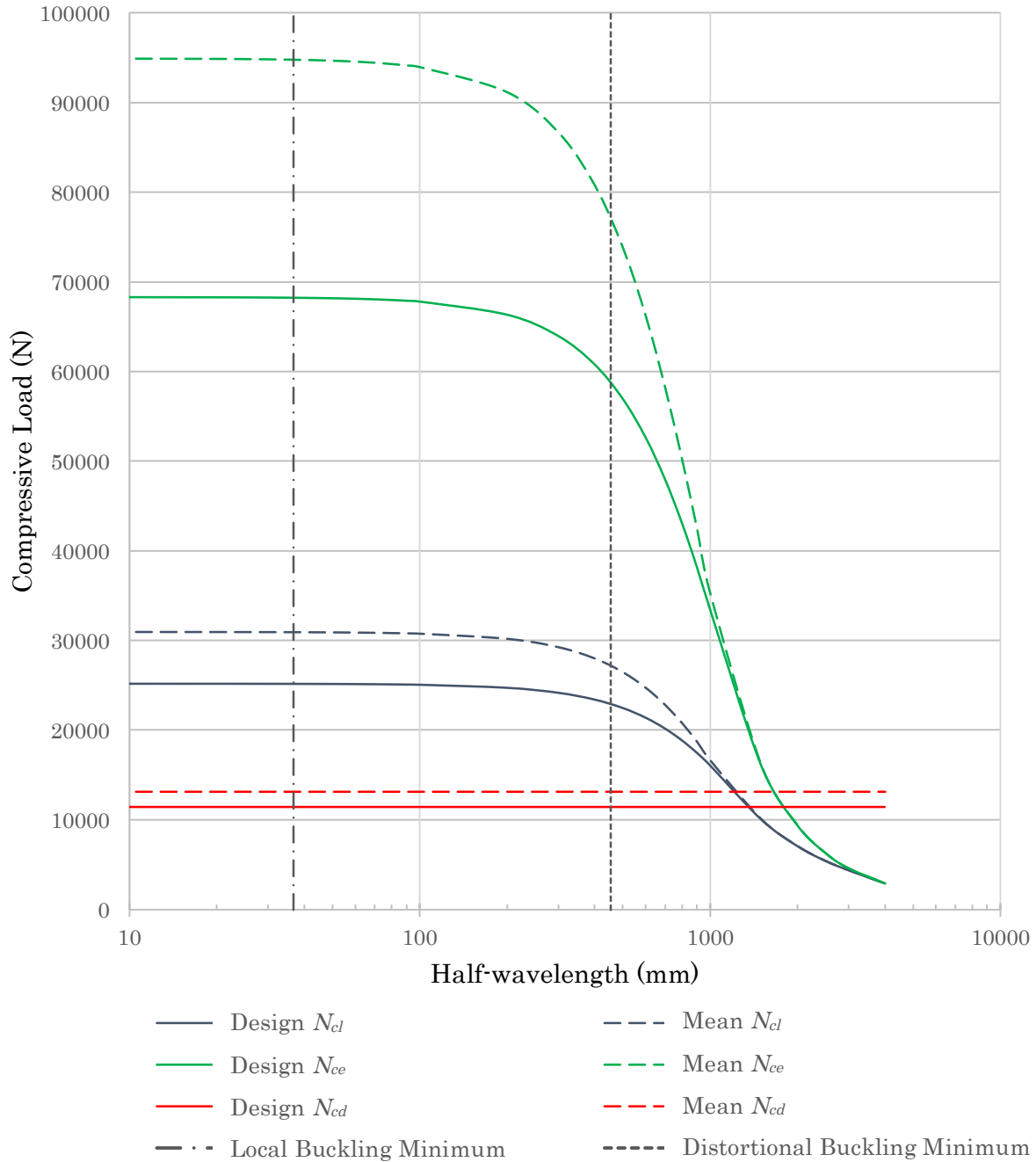


Figure 3.8: Direct strength method buckling loads for the stiffened lipped C-section

For the plain lipped C-section, it is observed that the local buckling minima of the signature curves in Figure 3.5 occurs at a buckling half-wavelength of 68.33mm. However, when calculating the local buckling load of  $N_{\mu}$  for the plain lipped C-section, the design equations of the DSM show that distortional buckling dominates at 68.33mm and not local buckling. This is shown in Figure 3.7, since the distortional buckling DSM plot is lower than the local buckling DSM plot at a length of 68.33mm. To avoid associating the local buckling minimum on the signature curve with the distortional buckling load



calculated with the DSM design equations, the local buckling load calculated from the DSM design equations was chosen for the local buckling analysis.

### 3.2.6 Reliability Analyses

As the main objective of this study was to determine the reliability index of the DSM, the reliability index was determined for each of the buckling modes presented in the DSM design method. To perform a reliability analyses for each buckling mode, six reliability analyses were performed. Four reliability analyses were performed on the plain lipped C-section and two reliability analyses were performed on the stiffened lipped C-section. The motivation for these tests are subsequently explained.

#### 3.2.6.1 Global Buckling Reliability Analysis

The reliability analysis of the global buckling mode was performed in three tests. Test one was performed on the plain lipped C-section member with a length of 4000mm. This is where the global buckling mode governs. Test two was performed on the plain lipped C-section member with a length of 2024.61mm. This is where the local-global buckling interaction occurs, as the load factor at this point on the signature curve matches that at the local buckling minimum. Test three was performed on the stiffened lipped C-section member with a length of 4000mm.

Comparing the results of test one and test two shows the significance of the length of the member on the reliability levels, given it is subject to global buckling. Comparing the results of test one and test three will show the significance of the shape of the section on the reliability levels, given that it is subject to global buckling. The global buckling model factor presented in Table 3.13 was used in each of these three tests.

#### 3.2.6.2 Local Buckling Reliability Analysis

The reliability analysis of the local buckling mode was performed in a single test. Test four was performed on the plain lipped C-section member with a length of 68.33mm. This is the length of the member where the local buckling load factor  $\frac{N_{cr,l}}{N_y}$  occurs on the signature curve. The local-global buckling interaction model factor presented in Table 3.13 was used for the local buckling mode.

#### 3.2.6.3 Local-Global Buckling Interaction Reliability Analysis

The reliability analysis of the local-global buckling interaction was performed in a single test. Test five again considers the plain lipped C-section member at a length of 2024.61mm like test 2. However, the local-global buckling interaction model factor presented in Table

3.13 was used for the reliability analysis for the buckling mode. This test assessed the local-global buckling interaction of the member by using the local-global buckling interaction model factor for when the member is subject to global buckling.

### 3.2.6.4 Distortional Buckling Reliability Analysis

The reliability analysis of the distortional buckling mode was performed in a single test. Test 6 was performed on the stiffened lipped C-section member with a length of 453.57mm. This is where the distortional buckling load factor  $\frac{N_{cr,d}}{N_y}$  occurs on the signature curve in Figure 3.6. The distortional buckling model factor presented in Table 3.13 for the reliability analysis for distortional buckling.

### 3.2.6.5 Buckling Analysis Summary

Table 3.7 summarises the six tests conducted to obtain the reliability analysis. It is to be noted that for each of the tests, the reliability index as well as the associated sensitivity factors of the variables was obtained for each considered load combination. An explanation of the model factors is presented in Section 3.4.2.

*Table 3.7: Test summary of reliability analysis*

Test Number	Buckling Mode	Section Type	Resistance Model Factor	Buckling half-wavelength (mm)
1	Global	Plain	$\partial_{R(g)}$	4000.00
2	Global	Plain	$\partial_{R(g)}$	2024.61
3	Global	Stiffened	$\partial_{R(g)}$	4000.00
4	Local	Plain	$\partial_{R(lg)}$	68.33
5	Local-Global	Plain	$\partial_{R(lg)}$	2024.61
6	Distortional	Stiffened	$\partial_{R(d)}$	453.57

It is to be noted that test five is conducted to assess the reliability levels for the local-global buckling interaction. The test uses a local-global buckling interaction resistance model factor for a member that is subject to global buckling. The reliability results of test one and test five are compared. This is to assess whether the local-global buckling interaction or the global buckling mode dominates uncertainty for a member that is subject to global buckling.

## 3.3 Semi-Probabilistic Formulation of the Limit-State

Discussed in Section 3.1.1, the semi-probabilistic formulation of the limit-state was used to obtain the characteristic values of the considered loads, for assumed load ratios, that would result in a column at its limit-state according to SANS 10162-2 (2011). This was done by obtaining the design compressive critical buckling capacity  $N_d$  and equating it to the total design load effect. The characteristic values of the considered loads would then be used in the full probabilistic formulation of the limit-state, as a basis to describe the loads probabilistically.

### 3.3.1 Obtaining Characteristic Values of the Loads

Once the design capacity of the member was calculated using the equations of the DSM, the considered loads were determined. Subsequently, the characteristic values of the considered loads were then calculated. Considering Equation 2.20, the limit-state is reached when the design structural resistance is equal to the design load effect. This is detailed in Equation 3.4, assuming load combinations of permanent, imposed and wind loading. Each design load may be expressed in terms of its characteristic loads and partial factors, as shown in Equation 3.5. The introduction of the combination factors is discussed once the dominating load case is identified.

$$N_d = G_d + Q_d + W_d \quad (3.4)$$

$$= (\gamma_G \cdot G_k) + (\gamma_Q \cdot Q_k) + (\gamma_W \cdot W_k) \quad (3.5)$$

The symbols  $\gamma_G$ ,  $\gamma_Q$  and  $\gamma_W$  are the partial factors of the permanent, imposed and the wind loads respectively. The partial factors are used to convert the characteristic values to the design values of each of the load conditions. The values of the partial factors depend on the limit-state and load combination scheme under consideration. Equation 3.5, however, does not consider action combination factors that are dependent on the dominating load combination.

For the purposes of this study, four load combinations were considered for the analysis, in accordance with the provisions of SANS 10160-1 (2011). Load combination 1 considers the STR limit-state with the imposed load as the leading load variable. Load combination 2 considers the STR limit-state with the wind load as the leading load variable. Load combination 3 considers the STR-P limit-state with the imposed load as the leading load

variable. Load combination 4 considers the STR-P limit-state with the wind load as the leading load variable. These are summarised in Table 3.8.

*Table 3.8: Summary of considered load combinations*

Load Combination	Denotation	Equation	
1	STR:Q	$N_d = \gamma_G G_k + \gamma_Q Q_k + \gamma_w \Psi_w W_k$	(3.6)
2	STR:W	$N_d = \gamma_G G_k + \gamma_Q \Psi_Q Q_k + \gamma_w W_k$	(3.7)
3	STR-P:Q	$N_d = \gamma_G G_k + \gamma_Q Q_k$	(3.8)
4	STR-P:W	$N_d = \gamma_G G_k + \gamma_w W_k$	(3.9)

Where  $\Psi_w$  and  $\Psi_Q$  are the action combination factors for the accompanying variable action of wind load in STR:Q and imposed load in STR:W respectively. The values of the partial factors and the combination factors are dependent on the load combination and are given in Table 3.9.

All partial factors and combination factors are obtained from SANS 10160-1 (2011) for unfavourable load cases, except for the wind load partial factor for an STR limit state. SANS 10160-1 (2011) suggests a wind load partial factor value of 1.3 be used in design. However, Botha (2016) recommends an update of the current wind load partial factor to a value of 1.6. Therefore, the recommended updated value is used in this study.

*Table 3.9: Values of partial and combination factors*

Variable	Limit State	
	STR	STR-P
$\gamma_G$	1.2	1.35
$\gamma_Q$	1.6	1.0
$\gamma_w$	1.6	1.0
$\Psi_Q$	0.3	0
$\Psi_w$	0	0

In SANS 10160-1 (2011), the values of the combination factors not only depend on the load case but also the specific use of the structure. For the purposes of this study, it was assumed that the structure type was of Category C: Public areas where people may congregate. The equations presented in Table 3.8 can be summarised as a conditional general expression. The conditional general expression is expressed in Equation 3.10.

$$N_d = \gamma_G G_k + \gamma_Q \Psi_Q Q_k + \gamma_W \Psi_W W_k \quad (3.10)$$

On the condition that

$$\Psi_Q = \begin{cases} 0.3 & \text{for load combination 2} \\ 0 & \text{for load combination 4} \\ 1 & \text{for other load combinations} \end{cases} \quad (3.11)$$

$$\Psi_W = \begin{cases} 0 & \text{for load combination 1} \\ 0 & \text{for load combination 3} \\ 1 & \text{for other load combinations} \end{cases} \quad (3.12)$$

Since it was unclear as to which load combination dominated the load effect, two load ratios were subsequently defined. The load ratios express the characteristic variable loads as a fraction of the total characteristic load. These are shown in Equations 3.13 and 3.14.

$$\chi_Q = \frac{Q_k}{G_k + Q_k + W_k} \quad (3.13)$$

$$\chi_W = \frac{W_k}{G_k + Q_k + W_k} \quad (3.14)$$

The symbol  $\chi_Q$  is the imposed load ratio and  $\chi_W$  is the wind load ratio. The values of the characteristic load ratios were parametrically varied from 0 to 1, in increments of 0.1. The reliability index was determined for each load combination of characteristic load ratios. Rearranging Equations 3.13 and 3.14 gives Equation 3.15 and 3.16 respectively.

$$\chi_Q \cdot G_k + (\chi_Q - 1) \cdot Q_k + \chi_Q \cdot W_k = 0 \quad (3.15)$$

$$\chi_W \cdot G_k + \chi_W \cdot Q_k + (\chi_W - 1) \cdot W_k = 0 \quad (3.16)$$

Equations 3.10, 3.15 and 3.16 can be solved simultaneously in matrix form, as shown in Equation 3.17 to Equation 3.19, to obtain the characteristic loads  $\{N_k\}$ . The matrix form expresses the characteristic loads as a vector and the associated factors as a 3 x 3 matrix. This is expressed in symbolic form.

$$\begin{bmatrix} \gamma_G & \gamma_Q \Psi_Q & \gamma_W \Psi_W \\ \chi_Q & \chi_Q - 1 & \chi_Q \\ \chi_W & \chi_W & \chi_W - 1 \end{bmatrix} \cdot \begin{Bmatrix} G_k \\ Q_k \\ W_k \end{Bmatrix} = \begin{Bmatrix} N_d \\ 0 \\ 0 \end{Bmatrix} \quad (3.17)$$

$$[A] \cdot \{N_k\} = \{N_d\} \quad (3.18)$$

$$\{N_k\} = inv[A] \cdot \{N_d\} \quad (3.19)$$

In Equations 3.18 and 3.19,  $[A]$  is the load factor matrix,  $\{N_k\}$  is the characteristic load vector and  $\{N_d\}$  is the design load vector.

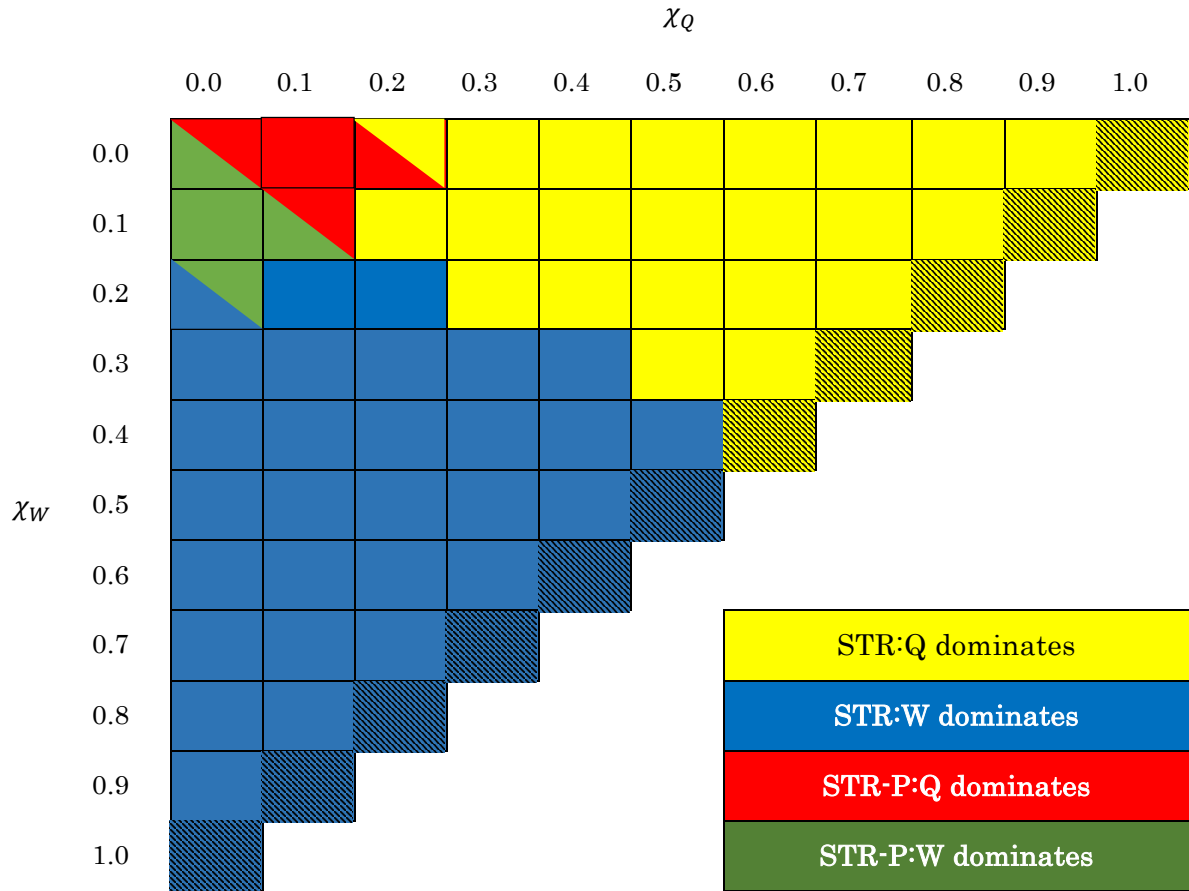
### 3.3.2 Load Combination Choice

Each of the considered load combinations presented in Table 3.8 had a dominating effect for a certain combination of  $\chi_Q$  and  $\chi_W$ . The dominating load combination was determined for each considered incremental value of  $\chi_Q$  and  $\chi_W$ .

Considering a total characteristic unit load, the respective design loads for each load combination and set of load ratios were calculated. The calculation process to identify the governing load combination for each value of  $\chi_Q$  and  $\chi_W$  is subsequently summarised.

1. Consider a characteristic unit load (i.e.:  $G_k + Q_k + W_k = 1$ )
  2. It follows from Equations 3.13 and 3.14 that:
    - a.  $Q_k = \chi_Q$
    - b.  $W_k = \chi_W$
    - c.  $G_k = 1 - \chi_Q - \chi_W$
  3. Initial conditions:
    - a. Set  $\chi_Q = 0$
    - b. Set  $\chi_W = 0$
  4. For  $0 \leq \chi_Q \leq 1$ :
    - a. For  $0 \leq \chi_W \leq 1$ :
      - i. If  $\chi_Q + \chi_W \leq 1$ :
        1. Compute corresponding total design load for each load case
        2. Dominating load case:  $\max[E_{d(LC1)}, E_{d(LC2)}, E_{d(LC3)}, E_{d(LC4)}]$
        3. Increment  $\chi_W$  by 0.1
        4. Repeat loop
      - ii. Else if  $\chi_Q + \chi_W > 1$ , end loop
    - b. Let  $\chi_W = 0$
    - c. Increment  $\chi_Q$  by 0.1
    - d. If  $\chi_Q + \chi_W \leq 1$ :
      - i. Repeat loop
    - e. Else if  $\chi_Q + \chi_W > 1$ :
      - i. End loop, all dominating load combinations are determined
5. The dominating load combinations are found over the range of considered load ratios and are shown in Table 3.10.

Table 3.10: Dominating load combinations for different values of  $\chi_Q$  and  $\chi_W$



It is to be noted, with reference to Table 3.10, the hatched diagonal from  $\chi_Q = 0.0$  and  $\chi_W = 1.0$  to  $\chi_Q = 1.0$  and  $\chi_W = 0.0$  constitutes a theoretical load case where there is no dead load. This is practically impossible, but it is still an important assessment at the theoretical outer range of the code application.



## 3.4 Full Probabilistic Formulation of the Limit-State

The full probabilistic formulation of the limit state expresses the variables of the load effect and of the structural resistance as random variables. Additionally, the associated model factors were also considered as random variables. The reliability analysis was conducted using a FORM analysis.

### 3.4.1 Variables of the Load Effect

Considered as separate continuous random variables, each of the load types were represented by probability density functions. Holický (2009) provides probabilistic descriptions of the load types as shown in Table 3.11, expressed in terms of characteristic values of each of the load types.

*Table 3.11: Statistical moment parameters of the considered loads (Holický, 2009)*

Load Variable	Symbol X	Distribution function	Mean Value $\mu_x$	Standard Deviation $\sigma_x$	Coefficient of Variation (%) V
Permanent	$G$	Normal	$G_k$	$0.07 G_k$	7
Imposed	$Q$	Gumbel	$0.6 Q_k$	$0.21 Q_k$	35
Wind	$W$	Gumbel	$0.65 W_k$	$0.32 W_k$	49

Holícký (2009) suggests that the standard deviation of the permanent load may be between  $0.03 G_k$  and  $0.10 G_k$ . The average of the range was used for this study.

When compared to the other loads, the permanent load has a significantly lower coefficient of variation. Additionally, the mean value of the permanent load is equal to the characteristic value of the permanent load. This shows that the permanent load is more accurately predicted than the other considered variable loads. Therefore, no model factor for the permanent load was considered in the full probabilistic formulation of the limit-state.

The imposed load considered in this study corresponds to a 50-year reference period. Unlike the permanent load, the imposed load has a relatively larger coefficient of variance and has a non-symmetrical Gumbel distribution. This implies that it may significantly

affect structural reliability, especially in cases with a high proportion of imposed load. A model factor is included for the imposed load. From Holický (2009), the model factor for the imposed load used in this study has a normal probability distribution. The mean of the model factor is 1.0 and the standard deviation may be between 0.05 to 0.10. In this study, the average of this range was used.

From the research of Botha (2016), the statistical moment parameters of the wind load used in this study are based on the updated Eurocode wind load prediction model. The statistical moment parameters of the wind load obtained from Botha (2016) accounts for the 50-year extremes of wind pressure, the pressure coefficient, the roughness factor and the model coefficient. Having the highest coefficient of variance of the three considered loads, the wind load may have the most significant effect on reliability. Table 3.12 shows the incorporated variables of the wind load model and their associated statistical moment parameters (Botha, 2016). The relatively high coefficient of variance of the design wind load model is partly due to the model factor being incorporated in the moment parameters of the wind load.

*Table 3.12: Updated Eurocode full probabilistic wind load model of the FORM analysis (Botha, 2016)*

<b>Variable</b>	<b>Distribution</b>	<b>Relative Mean</b> $[\mu_x/X_k]$	<b>Standard Deviation</b> $[\sigma_x/X_k]$	<b>Coefficient of Variation (%)</b> <b>V</b>
50-year extremes of wind pressure	Gumbel	0.92	0.31	34
Pressure coefficient	Normal	1.00	0.16	16
Roughness factor	Normal	0.84	0.10	12
Model Coefficient	Normal	0.80	0.16	20
Design wind load	Gumbel	0.65	0.32	49

### 3.4.2 Variables of the Structural Resistance

In this study, the overall structural resistance  $R$  in the full probabilistic formulation of the limit-state was composed of two variables; namely the mean critical buckling capacity  $N_\mu$  and the structural resistance model factor  $\partial_R$ . This is shown in Equation 3.20.

$$R = \partial_R \cdot N_\mu \quad (3.20)$$

In the calculation of the mean critical buckling capacity of the member, the mean values for member thickness material yield stress were used. This is to say that the material thickness and the yield stress were taken as deterministic values. Therefore, the mean critical buckling load was considered as a deterministic value. The element thickness and the material yield stress were not considered as random variables because the results of Bauer (2016). The study found that the model factor for the structural resistance had a dominating sensitivity contribution for the reliability index. Therefore, the structural resistance model factor was the only random variable in the calculation of the overall structural resistance.

Bauer (2016) recommended that different structural resistance model factors be used for different buckling modes. In a study by Ganesan and Moen (2010), the recorded data of 675 CFS column specimens were collected and analysed. The statistical moment parameters of the model factors for the variety of considered sections were determined in accordance to the DSM. Subsequently, the results for the appropriate sections were grouped in terms of the buckling modes considered in the DSM.

The shape of each of the distribution functions were not explicitly mentioned in Ganesan and Moen (2010) and were therefore considered to be normally distributed, based on Holický (2009).

From the research of Ganesan and Moen (2010), the statistical moment parameters of the model factors for each buckling mode are presented in Table 3.13.

Table 3.13: Statistical moment parameters of the structural resistance model factors for different buckling modes (Ganesan & Moen, 2010)

Model Factor Type	Symbol $\partial_R$	Distribution function	Mean Value $\mu_x$	Standard Deviation $\sigma_x$	Coefficient of Variation (%) V
Local-global buckling interaction	$\partial_{R(lg)}$	Normal	1.03	0.15	14
Distortional buckling	$\partial_{R(d)}$	Normal	1.07	0.10	9
Global buckling or yielding	$\partial_{R(g)}$	Normal	1.06	0.22	20

### 3.4.3 Reliability Analysis

The full probabilistic formulation of the limit-state equation for the reliability analysis conducted in this study is expressed in Equation 3.21. VaP, a computer program that implements the FORM algorithm was used in this study. VaP is distributed by Petschacher Software and Development (Petschacher, 1997) and is a well-established program. The program allows for the definition of an implicit limit-state as a function of probabilistic variables. The input parameters of the probabilistic variables are the distribution type and the statistical moment parameters.

$$G = \partial_R \cdot N_\mu - (G + \partial_Q \cdot Q + W) \quad (3.21)$$

Assessments were conducted on the reliability levels for each of the dominating load combinations. For all the reliability results, a check was done to assess whether they were greater than the target reliability level of  $\beta_t = 3$  presented in SANS 10160-1 (2011). Additional to the reliability levels, the sensitivity factors were obtained of each of the random variables for each dominating load combination. The sensitivity factors show the influence that each of the random variables have on the reliability level.

Tests that yielded reliability results below that of the target reliability were assessed and scrutinized. Reasons for the unsatisfactory levels of reliability are subsequently discussed.

Additionally, the reliability levels achieved by the FORM analysis are validated by comparing those that are achieved by the MC analysis.

### 3.4.4 Monte-Carlo Simulation

As mentioned in Section 2.2.2.2, a MCS was performed to determine whether the limit-state is concave or convex. The limit-state is concave if the reliability level achieved from the MCS is less than that achieved by the FORM analysis. Conversely, the limit-state is convex if the reliability level achieved from the MCS is greater than that achieved by the FORM analysis.

If the limit-state is concave, then the FORM analysis is an under-conservative. If the limit-state is convex, then the FORM analysis is conservative. A MCS was performed for each dominating load combination to estimate the shape of the limit-state for each load combination. Observing Table 3.10, four MC analyses were performed at the combinations of  $\chi_Q$  and  $\chi_W$  shown in Table 3.14.

*Table 3.14: MC analyses of dominating load combinations*

<b>Dominating Load Combination</b>	<b>Associated Leading Variable</b>	$\chi_Q$	$\chi_W$
STR	Q	1.0	0.0
STR	W	0.0	1.0
STR-P	Q	0.1	0.0
STR-P	W	0.0	0.1

### 3.4.5 Chapter Summary

This chapter covered the necessary processes that were conducted in this study to assess the inherent reliability of the SANS 10162-2 (2011) formulation of the DSM for compression members. Two representative cold-formed steel members were considered in this study. A plain lipped C-section and a stiffened lipped C-Section were considered. The local and global buckling modes were the dominating buckling modes for the plain lipped C-section. The distortional and global buckling modes were the dominating buckling modes for the stiffened lipped C-section. The geometric and material properties of the considered members adhered to the prequalification limitations of the DSM.

Signature curves for the mean and design compressive critical buckling loads were generated for each of the members. From the signature curves, the local, distortional, and global buckling load factors, as well as the corresponding buckling half-wavelengths were identified. The load factors and corresponding buckling half-wavelengths were used in the DSM design equations for each of the dominating critical buckling mode. The design and mean compressive critical buckling capacity of the members was determined. The design compressive critical buckling capacity was used in the semi-probabilistic formulation of the limit-state. The mean compressive buckling capacity was used in the full probabilistic formulation of the limit-state.

The design and mean compressive critical buckling capacity of the members were designed in accordance to the SANS 10162-2 (2011) formulation of the DSM. However, to achieve a true and unconservative representation of the member, the capacity reduction factor was not considered for the calculation of the mean compressive critical buckling load. Additionally, the mean yield stress was used in the calculations of the mean compressive critical buckling load.

Considering the semi-probabilistic formulation of the limit-state, the design compressive critical buckling capacity of the member was equated to the codified design load effect. The load effect consisted of permanent, imposed and wind loads. The characteristic values of the considered loads were obtained for a range of load ratios and load combinations in accordance with SANS 10160-1 (2011).

Of the full probabilistic formulation of the limit-state, each variable was considered as a random variable. The structural resistance consisted of the model factor and the mean compressive critical buckling load. The load effect consisted of permanent, imposed and wind loads. Only the model factor for the imposed load was considered.

A FORM analysis was conducted. The results of the form analysis included the reliability levels achieved for each buckling mode, as well as the sensitivity factors for each considered random variable. A MC analysis was conducted for each of the considered load combinations to check the validity of the results of the FORM analysis. If the resulting reliability levels of each conducted test were below the target reliability presented in SANS 10160-1 (2011) of  $\beta_t = 3$ , there may be cause for concern.

# CHAPTER 4:

## Results & Discussion

---

### 4.1 Results of Reliability Analysis

This section shows the results of the full probabilistic formulation of the limit-state. As discussed in Section 3.2.6.5, six tests were conducted. For each of the tests, the reliability level was assessed for all possible combinations of  $\chi_Q$  and  $\chi_W$ . Additionally, the sensitivity factors of each random variable in the full probabilistic formulation of the limit-state are shown. The sensitivity factors give an indication of which of the random variables in the full probabilistic formulation of the limit-state have the largest influence on the level of uncertainty for a given load combination.

For given load ratios of  $\chi_Q$  and  $\chi_W$  where the reliability level is low, an analysis was made to determine which of the random variables in the full probabilistic formulation of the limit state equation had the greatest effect on uncertainty. This was done by observing the sensitivity factors of each of the random variables for the given load ratios of  $\chi_Q$  and  $\chi_W$ .

As discussed in previous chapters, the sensitivity factors are either classified as having a minor, significant or a dominating effect, depending on its value. The reliability levels are characterised in increments of 0.5.

#### 4.1.1 Global Buckling

As discussed in Section 3.2.6.1, three tests were conducted to assess the reliability of the global buckling capacity of a member using the DSM. Test one was conducted on the plain lipped C-section at a length of 4000mm. Test two was also conducted on the plain lipped C-section but at a length of 2024.61mm. Test two was tested at the local-global interaction of the member, but the global buckling model factor was used. Test three was conducted on the stiffened lipped C-section at a length of 4000mm. The global buckling model factor was used for tests one to three.

#### 4.1.1.1 Test One

The following results are of the global buckling mode of the plain lipped C-section with a member length of 4000mm. Table 4.1 shows the reliability levels for the first test. Accompanying these results are the sensitivity factors for each of the random variables considered in the full probabilistic formulation of the limit-state equation. Table 4.2 to Table 4.6 show the sensitivity factors for the structural resistance model factor, the imposed load model factor, the permanent load, the imposed load, and the wind load respectively.

Table 4.1: Reliability levels for test one

		$\chi_Q$										
		0.0	0.1	0.2	0.3	0.4	0.5	0.6	0.7	0.8	0.9	1.0
$\chi_W$	0.0	1.92	1.97	2.02	2.21	2.38	2.53	2.64	2.73	2.80	2.84	2.87
	0.1	1.96	1.78	1.86	2.08	2.27	2.42	2.55	2.64	2.71	2.75	
	0.2	1.98	1.95	1.91	1.89	2.10	2.27	2.41	2.51	2.58		
	0.3	2.14	2.12	2.08	2.03	1.95	2.06	2.22	2.34			
	0.4	2.26	2.24	2.20	2.16	2.09	2.00	1.96			$\beta = 2.5 - 3.0$	
	0.5	2.34	2.31	2.28	2.23	2.17	2.09				$\beta = 2.0 - 2.5$	
	0.6	2.38	2.36	2.32	2.28	2.22					$\beta = 1.5 - 2.0$	
	0.7	2.40	2.38	2.34	2.29							
	0.8	2.41	2.38	2.34								
	0.9	2.41	2.38									
	1.0	2.40										



Table 4.2:  $\alpha_{DR}$  for test one

		$\chi_Q$										
		0.0	0.1	0.2	0.3	0.4	0.5	0.6	0.7	0.8	0.9	1.0
$\chi_W$	0.0	0.981	0.982	0.978	0.971	0.957	0.934	0.900	0.857	0.806	0.755	0.707
	0.1	0.979	0.977	0.973	0.964	0.947	0.919	0.880	0.830	0.775	0.723	
	0.2	0.968	0.965	0.957	0.940	0.921	0.890	0.847	0.796	0.741		
	0.3	0.944	0.938	0.926	0.905	0.872	0.839	0.800	0.753			
	0.4	0.903	0.891	0.874	0.851	0.819	0.777	0.730				
	0.5	0.845	0.827	0.806	0.780	0.751	0.715			Minor Effect		
	0.6	0.779	0.758	0.735	0.709	0.682			Significant Effect			
	0.7	0.715	0.694	0.671	0.647				Dominating Effect			
	0.8	0.660	0.639	0.617								
	0.9	0.613	0.593									
	1.0	0.574										

Table 4.3:  $\alpha_{DQ}$  for test one

		$\chi_Q$										
		0.0	0.1	0.2	0.3	0.4	0.5	0.6	0.7	0.8	0.9	1.0
$\chi_W$	0.0	0.000	0.014	0.029	0.044	0.060	0.078	0.095	0.113	0.128	0.142	0.152
	0.1	0.000	0.015	0.032	0.049	0.066	0.085	0.103	0.121	0.136	0.149	
	0.2	0.000	0.015	0.032	0.052	0.071	0.091	0.110	0.127	0.142		
	0.3	0.000	0.014	0.030	0.050	0.072	0.093	0.112	0.130			
	0.4	0.000	0.013	0.027	0.045	0.065	0.088	0.109				
	0.5	0.000	0.011	0.024	0.039	0.056	0.076			Minor Effect		
	0.6	0.000	0.010	0.021	0.034	0.048			Significant Effect			
	0.7	0.000	0.009	0.019	0.030				Dominating Effect			
	0.8	0.000	0.008	0.017								
	0.9	0.000	0.007									
	1.0	0.000										

Table 4.4:  $a_G$  for test one

		$\chi_Q$										
		0.0	0.1	0.2	0.3	0.4	0.5	0.6	0.7	0.8	0.9	1.0
$\chi_W$	0.0	0.196	0.182	0.165	0.139	0.114	0.090	0.068	0.047	0.029	0.013	0.000
	0.1	0.181	0.179	0.159	0.130	0.103	0.078	0.054	0.033	0.015	0.000	
	0.2	0.164	0.151	0.137	0.118	0.089	0.062	0.038	0.017	0.000		
	0.3	0.135	0.122	0.106	0.089	0.069	0.044	0.020	0.000			
	0.4	0.108	0.094	0.078	0.060	0.041	0.021	0.000				
	0.5	0.082	0.067	0.052	0.036	0.018	0.000			Minor Effect		
	0.6	0.059	0.045	0.031	0.016	0.000			Significant Effect			
	0.7	0.039	0.027	0.014	0.000				Dominating Effect			
	0.8	0.023	0.012	0.000								
	0.9	0.011	0.000									
	1.0	0.000										

Table 4.5:  $a_Q$  for test one

		$\chi_Q$										
		0.0	0.1	0.2	0.3	0.4	0.5	0.6	0.7	0.8	0.9	1.0
$\chi_W$	0.0	0.000	0.057	0.122	0.188	0.259	0.337	0.419	0.501	0.577	0.640	0.690
	0.1	0.000	0.063	0.134	0.206	0.284	0.368	0.454	0.539	0.613	0.672	
	0.2	0.000	0.061	0.135	0.223	0.306	0.394	0.484	0.568	0.640		
	0.3	0.000	0.057	0.127	0.211	0.310	0.404	0.494	0.579			
	0.4	0.000	0.053	0.115	0.190	0.278	0.378	0.477				
	0.5	0.000	0.047	0.102	0.166	0.240	0.326			Minor Effect		
	0.6	0.000	0.042	0.089	0.143	0.205			Significant Effect			
	0.7	0.000	0.037	0.078	0.125				Dominating Effect			
	0.8	0.000	0.033	0.069								
	0.9	0.000	0.030									
	1.0	0.000										

Table 4.6:  $\alpha_w$  for test one

		$\chi_Q$										
		0.0	0.1	0.2	0.3	0.4	0.5	0.6	0.7	0.8	0.9	1.0
$\chi_W$	0.0	0.000	0.000	0.000	0.000	0.000	0.000	0.000	0.000	0.000	0.000	0.000
	0.1	0.088	0.098	0.099	0.096	0.091	0.086	0.080	0.072	0.065	0.059	
	0.2	0.192	0.204	0.217	0.225	0.215	0.201	0.184	0.166	0.147		
	0.3	0.301	0.320	0.338	0.354	0.364	0.349	0.320	0.286			
	0.4	0.416	0.441	0.465	0.484	0.496	0.496	0.476				
	0.5	0.529	0.556	0.581	0.600	0.613	0.613					Minor Effect
	0.6	0.624	0.649	0.672	0.689	0.700						Significant Effect
	0.7	0.698	0.719	0.737	0.752							Dominating Effect
	0.8	0.751	0.768	0.783								
	0.9	0.790	0.804									
	1.0	0.819										

Observing Table 4.1, the reliability level for all possible combinations of  $\chi_Q$  and  $\chi_W$  are below the minimum allowable level of reliability of  $\beta_t = 3$ , presented in SANS 10160-1 (2011) for the RC2 reliability class. The lowest recorded level of reliability is  $\beta = 1.78$ , where  $\chi_Q = 0.1$  and  $\chi_W = 0.1$ . This is where the STR-P:Q and STR-P:W load combinations dominate. The highest recorded reliability level is  $\beta = 2.87$  where  $\chi_Q = 1.0$  and  $\chi_W = 0.0$ . This is where the STR:Q load combination dominates.

For the load ratio of  $\chi_Q$  and  $\chi_W$  where the reliability level is lowest, it is evident that the sensitivity factor for the structural resistance model factor in Table 4.2 has a dominating effect on the level of uncertainty. All the other random variables have a minor effect for this load combination.

#### 4.1.1.2 Test Two

The following results are of the global buckling mode of the plain lipped C-section with a member length of 2024.61mm. The reliability levels for the second test are shown in Table 4.7. The sensitivity factors for each of the random variables in the full probabilistic formulation of the limit-state equation are shown in Table 4.8 to Table 4.12 for the

structural resistance model factor, the imposed load model factor, the permanent load, the imposed load, and the wind load respectively.

Table 4.7: Reliability levels for test two

		$\chi_Q$										
		0.0	0.1	0.2	0.3	0.4	0.5	0.6	0.7	0.8	0.9	1.0
$\chi_W$	0.0	1.92	1.97	2.02	2.21	2.38	2.53	2.64	2.73	2.80	2.84	2.87
	0.1	1.96	1.78	1.86	2.08	2.26	2.42	2.54	2.64	2.71	2.75	
	0.2	1.98	1.95	1.91	1.89	2.10	2.27	2.41	2.51	2.58		
	0.3	2.14	2.12	2.08	2.03	1.95	2.06	2.22	2.34			
	0.4	2.26	2.24	2.20	2.15	2.09	2.00	1.96			$\beta = 2.5 - 3.0$	
	0.5	2.34	2.31	2.28	2.23	2.17	2.09				$\beta = 2.0 - 2.5$	
	0.6	2.38	2.36	2.32	2.28	2.22					$\beta = 1.5 - 2.0$	
	0.7	2.38	2.38	2.32	2.29							
	0.8	2.41	2.38	2.36								
	0.9	2.41	2.37									
	1.0	2.40										

Table 4.8:  $\alpha_{\partial R}$  for test two

		$\chi_Q$										
		0.0	0.1	0.2	0.3	0.4	0.5	0.6	0.7	0.8	0.9	1.0
$\chi_W$	0.0	0.981	0.982	0.978	0.971	0.957	0.934	0.900	0.856	0.806	0.755	0.707
	0.1	0.979	0.977	0.973	0.964	0.947	0.919	0.879	0.829	0.775	0.723	
	0.2	0.968	0.965	0.957	0.940	0.921	0.890	0.847	0.795	0.741		
	0.3	0.944	0.938	0.926	0.905	0.872	0.839	0.800	0.752			
	0.4	0.903	0.891	0.874	0.850	0.819	0.777	0.730				
	0.5	0.845	0.827	0.805	0.780	0.751	0.715			Minor Effect		
	0.6	0.779	0.758	0.734	0.709	0.682				Significant Effect		
	0.7	0.717	0.693	0.673	0.647					Dominating Effect		
	0.8	0.659	0.639	0.615								
	0.9	0.613	0.593									
	1.0	0.574										

Table 4.9:  $\alpha_{\partial Q}$  for test two

		$\chi_Q$										
		0.0	0.1	0.2	0.3	0.4	0.5	0.6	0.7	0.8	0.9	1.0
$\chi_W$	0.0	0.000	0.014	0.029	0.044	0.060	0.078	0.095	0.113	0.129	0.142	0.152
	0.1	0.000	0.015	0.032	0.049	0.066	0.085	0.103	0.121	0.136	0.149	
	0.2	0.000	0.015	0.032	0.052	0.071	0.091	0.110	0.128	0.142		
	0.3	0.000	0.014	0.030	0.050	0.072	0.093	0.113	0.130			
	0.4	0.000	0.013	0.027	0.045	0.065	0.088	0.109				
	0.5	0.000	0.011	0.024	0.039	0.056	0.076			Minor Effect		
	0.6	0.000	0.010	0.021	0.034	0.048				Significant Effect		
	0.7	0.000	0.009	0.020	0.030					Dominating Effect		
	0.8	0.000	0.008	0.016								
	0.9	0.000	0.007									
	1.0	0.000										

Table 4.10:  $\alpha_G$  for test two

		$X_Q$										
		0.0	0.1	0.2	0.3	0.4	0.5	0.6	0.7	0.8	0.9	1.0
$X_W$	0.0	0.196	0.182	0.165	0.139	0.114	0.090	0.068	0.047	0.029	0.013	0.000
	0.1	0.181	0.179	0.159	0.130	0.103	0.078	0.054	0.033	0.015	0.000	
	0.2	0.164	0.151	0.137	0.118	0.089	0.062	0.038	0.017	0.000		
	0.3	0.135	0.122	0.106	0.089	0.069	0.044	0.020	0.000			
	0.4	0.108	0.093	0.078	0.060	0.041	0.021	0.000				
	0.5	0.082	0.067	0.052	0.036	0.018	0.000			Minor Effect		
	0.6	0.059	0.045	0.031	0.016	0.000			Significant Effect			
	0.7	0.039	0.027	0.014	0.000				Dominating Effect			
	0.8	0.023	0.012	0.000								
	0.9	0.011	0.000									
	1.0	0.000										

Table 4.11:  $\alpha_Q$  for test two

		$X_Q$										
		0.0	0.1	0.2	0.3	0.4	0.5	0.6	0.7	0.8	0.9	1.0
$X_W$	0.0	0.000	0.057	0.122	0.188	0.259	0.337	0.420	0.502	0.578	0.640	0.690
	0.1	0.000	0.063	0.134	0.206	0.284	0.368	0.456	0.540	0.613	0.671	
	0.2	0.000	0.061	0.135	0.223	0.306	0.394	0.485	0.569	0.640		
	0.3	0.000	0.057	0.127	0.211	0.310	0.405	0.495	0.579			
	0.4	0.000	0.053	0.115	0.190	0.278	0.378	0.477				
	0.5	0.000	0.047	0.102	0.166	0.240	0.325			Minor Effect		
	0.6	0.000	0.042	0.089	0.143	0.205			Significant Effect			
	0.7	0.000	0.037	0.079	0.125				Dominating Effect			
	0.8	0.000	0.033	0.069								
	0.9	0.000	0.030									
	1.0	0.000										

Table 4.12:  $\alpha_w$  for test two

		$\chi_Q$										
		0.0	0.1	0.2	0.3	0.4	0.5	0.6	0.7	0.8	0.9	1.0
$\chi_W$	0.0	0.000	0.000	0.000	0.000	0.000	0.000	0.000	0.000	0.000	0.000	0.000
	0.1	0.088	0.098	0.099	0.096	0.091	0.086	0.079	0.072	0.065	0.061	
	0.2	0.192	0.206	0.217	0.225	0.215	0.201	0.184	0.165	0.147		
	0.3	0.301	0.320	0.339	0.355	0.365	0.349	0.320	0.285			
	0.4	0.416	0.442	0.465	0.485	0.497	0.496	0.476				
	0.5	0.529	0.556	0.581	0.601	0.613	0.614				Minor Effect	
	0.6	0.625	0.650	0.672	0.689	0.701					Significant Effect	
	0.7	0.696	0.719	0.735	0.752						Dominating Effect	
	0.8	0.751	0.768	0.785								
	0.9	0.790	0.805									
	1.0	0.819										

Comparing the results in Table 4.1 and Table 4.7, the reliability levels of test one and test two are similar. As in test one, the reliability levels for all possible combinations of  $\chi_Q$  and  $\chi_W$  are below the minimum allowable level of reliability of  $\beta_t = 3$  for test two. Comparing test one and test two, it is evident that the uncertainty levels of a member do not depend on the length of the member, given that the member is subject to global buckling.

#### 4.1.1.3 Test Three

The following results are of the global buckling mode of the stiffened lipped C-section with a member length of 4000mm. Table 4.13 shows the reliability levels for the third test. Table 4.14 to show the sensitivity factors for the structural resistance model factor, the imposed load model factor, the permanent load, imposed load, and the wind load respectively.

Table 4.13: Reliability levels for test three

		$\chi_Q$										
		0.0	0.1	0.2	0.3	0.4	0.5	0.6	0.7	0.8	0.9	1.0
$\chi_W$	0.0	1.92	1.97	2.02	2.21	2.38	2.53	2.64	2.73	2.80	2.84	2.87
	0.1	1.96	1.78	1.86	2.08	2.27	2.42	2.55	2.64	2.71	2.75	
	0.2	1.98	1.95	1.91	1.89	2.10	2.27	2.41	2.51	2.58		
	0.3	2.14	2.12	2.08	2.03	1.95	2.06	2.22	2.34			
	0.4	2.26	2.24	2.20	2.16	2.09	2.00	1.96			$\beta = 2.5 - 3.0$	
	0.5	2.34	2.32	2.28	2.23	2.17	2.09				$\beta = 2.0 - 2.5$	
	0.6	2.38	2.36	2.32	2.28	2.22					$\beta = 1.5 - 2.0$	
	0.7	2.40	2.38	2.34	2.29							
	0.8	2.41	2.38	2.34								
	0.9	2.41	2.38									
	1.0	2.40										

Table 4.14:  $\alpha_{\partial R}$  for test three

		$\chi_Q$										
		0.0	0.1	0.2	0.3	0.4	0.5	0.6	0.7	0.8	0.9	1.0
$\chi_W$	0.0	0.981	0.982	0.978	0.971	0.957	0.934	0.900	0.857	0.806	0.755	0.708
	0.1	0.979	0.977	0.973	0.964	0.947	0.919	0.879	0.830	0.775	0.723	
	0.2	0.968	0.965	0.957	0.940	0.921	0.890	0.847	0.796	0.741		
	0.3	0.944	0.938	0.926	0.905	0.872	0.839	0.800	0.753			
	0.4	0.903	0.891	0.874	0.851	0.819	0.777	0.730				
	0.5	0.845	0.827	0.806	0.781	0.751	0.715				Minor Effect	
	0.6	0.779	0.758	0.735	0.709	0.682					Significant Effect	
	0.7	0.715	0.694	0.671	0.647						Dominating Effect	
	0.8	0.660	0.639	0.617								
	0.9	0.613	0.593									
	1.0	0.574										



Table 4.15:  $\alpha_{\partial Q}$  for test three

		$\chi_w$										
		0.0	0.1	0.2	0.3	0.4	0.5	0.6	0.7	0.8	0.9	1.0
$\chi_w$	0.0	0.000	0.014	0.029	0.044	0.060	0.078	0.095	0.113	0.128	0.142	0.152
	0.1	0.000	0.015	0.032	0.049	0.066	0.085	0.103	0.121	0.136	0.149	
	0.2	0.000	0.015	0.032	0.052	0.071	0.091	0.110	0.127	0.142		
	0.3	0.000	0.014	0.030	0.050	0.072	0.093	0.112	0.130			
	0.4	0.000	0.013	0.027	0.045	0.065	0.088	0.109				
	0.5	0.000	0.011	0.024	0.039	0.056	0.076			Minor Effect		
	0.6	0.000	0.010	0.021	0.034	0.048			Significant Effect			
	0.7	0.000	0.009	0.019	0.030				Dominating Effect			
	0.8	0.000	0.008	0.017								
	0.9	0.000	0.007									
	1.0	0.000										

Table 4.16:  $\alpha_G$  for test three

		$\chi_w$										
		0.0	0.1	0.2	0.3	0.4	0.5	0.6	0.7	0.8	0.9	1.0
$\chi_w$	0.0	0.196	0.182	0.165	0.139	0.114	0.090	0.068	0.047	0.029	0.013	0.000
	0.1	0.181	0.179	0.159	0.130	0.103	0.078	0.054	0.033	0.015	0.000	
	0.2	0.163	0.151	0.137	0.118	0.089	0.062	0.038	0.017	0.000		
	0.3	0.135	0.122	0.106	0.089	0.069	0.044	0.020	0.000			
	0.4	0.108	0.094	0.078	0.060	0.041	0.021	0.000				
	0.5	0.082	0.067	0.052	0.036	0.018	0.000			Minor Effect		
	0.6	0.059	0.045	0.031	0.016	0.000			Significant Effect			
	0.7	0.039	0.027	0.014	0.000				Dominating Effect			
	0.8	0.023	0.012	0.000								
	0.9	0.011	0.000									
	1.0	0.000										

Table 4.17:  $\alpha_Q$  for test three

		$X_Q$										
		0.0	0.1	0.2	0.3	0.4	0.5	0.6	0.7	0.8	0.9	1.0
$X_W$	0.0	0.000	0.057	0.122	0.188	0.259	0.337	0.419	0.501	0.577	0.640	0.690
	0.1	0.000	0.063	0.134	0.206	0.284	0.368	0.456	0.539	0.613	0.672	
	0.2	0.000	0.061	0.135	0.223	0.306	0.394	0.484	0.568	0.640		
	0.3	0.000	0.057	0.127	0.211	0.310	0.404	0.494	0.578			
	0.4	0.000	0.053	0.115	0.190	0.278	0.378	0.477				
	0.5	0.000	0.047	0.102	0.166	0.240	0.326			Minor Effect		
	0.6	0.000	0.042	0.089	0.143	0.205			Significant Effect			
	0.7	0.000	0.037	0.078	0.125				Dominating Effect			
	0.8	0.000	0.033	0.069								
	0.9	0.000	0.030									
	1.0	0.000										

Table 4.18:  $a_W$  for test three

		$X_Q$										
		0.0	0.1	0.2	0.3	0.4	0.5	0.6	0.7	0.8	0.9	1.0
$X_W$	0.0	0.000	0.000	0.000	0.000	0.000	0.000	0.000	0.000	0.000	0.000	0.000
	0.1	0.088	0.098	0.099	0.096	0.091	0.086	0.079	0.072	0.065	0.059	
	0.2	0.192	0.204	0.217	0.225	0.215	0.201	0.184	0.166	0.147		
	0.3	0.300	0.320	0.338	0.354	0.364	0.349	0.320	0.286			
	0.4	0.416	0.441	0.464	0.484	0.496	0.496	0.477				
	0.5	0.528	0.556	0.581	0.600	0.613	0.613			Minor Effect		
	0.6	0.624	0.649	0.671	0.689	0.700			Significant Effect			
	0.7	0.698	0.719	0.737	0.752				Dominating Effect			
	0.8	0.751	0.768	0.784								
	0.9	0.790	0.804									
	1.0	0.819										

The results presented in Table 4.13 are once again like those presented in Table 4.1. The reliability levels are below the minimum allowable level of reliability of  $\beta_t = 3$  for all possible combinations of  $\chi_Q$  and  $\chi_W$ . Comparing the results of test three and test one, it is evident that the sectional shape of the member does not influence the reliability levels, given that the member is subject to global buckling and the cross-sectional area remains constant.

#### 4.1.1.4 Global Buckling Test Summary

For all the tests conducted for the global buckling failure mode, the reliability level was consistent. This is observed when comparing the values in Table 4.1, Table 4.7 and Table 4.13. From this, two observations are made. Firstly, the length of the member does not influence the levels of reliability or the sensitivity factors of the random variables, given the member is subject to global buckling. Secondly, the cross-sectional shape of the member does not influence the levels of reliability or the sensitivity factors of the random variables, given that the member is subject to global buckling.

Additionally, the sensitivity factors of the random variables in the full probabilistic formulation of the limit-state remained constant for different member lengths and section shapes, provided global buckling governed the design capacity. For all three tests, the structural resistance model factor had a dominating effect on the reliability level for the combination of load ratios that yielded the lowest reliability level. This is observed when comparing the values in Table 4.2, Table 4.8 and Table 4.14.

For all the global buckling analyses, the imposed load sensitivity factor and the permanent load sensitivity factor have a minor effect on the reliability level for all possible combinations of  $\chi_Q$  and  $\chi_W$ . This is observed when comparing the values in Table 4.4, Table 4.10 and Table 4.16. The sensitivity factors for the imposed load increase from a minor effect to a significant effect as the proportion of imposed load increases. The sensitivity factors for the wind load increase from a minor effect to a dominating effect as the proportion of wind load increases.

As mentioned in Section 3.4.3, MC analyses were conducted to determine whether the limit-state for each load combination is concave or convex. The results are shown in Table 4.19.

*Table 4.19: Reliability levels achieved through FORM and MCS for each load combination*

<b>Dominating Load Combination</b>	<b>Associated Leading Variable</b>	$\chi_Q$	$\chi_W$	<b>FORM <math>\beta</math></b>	<b>MCS <math>\beta</math></b>
STR	Q	1.0	0.0	2.87	2.80
STR	W	0.0	1.0	2.40	2.34
STR-P	Q	0.1	0.0	1.97	1.96
STR-P	W	0.0	0.1	1.96	1.95

Since none of the reliability levels achieved by the MCS analysis exceed those achieved by the FORM analysis, the shape of the limit-state for each load combination is convex. This implies that the FORM analysis is a conservative statistical analysis, specific to the tests conducted in this study.

## 4.1.2 Local Buckling and Local-Global Buckling Interaction

Test four was conducted to assess the reliability of the local buckling capacity of a member and test five was conducted to assess the reliability of the local-global buckling interaction buckling capacity of the member. Test four was conducted on the plain lipped C-section at a length of 68.33mm. Test five was also conducted on the plain lipped C-section but at a length of 2024.61mm. The local-global buckling interaction model factor was used for both tests.

### 4.1.2.1 Test Four

The following results are of the local buckling mode of the plain lipped C-section with a member length of 68.33mm. Table 4.20 shows the reliability levels for test four. The sensitivity factors for the structural resistance model factor, the imposed load model factor, the permanent load, the imposed load, and the wind load are shown in Table 4.21 to Table 4.25 respectively.

Table 4.20: Reliability levels for test four

		$\chi_Q$										
		0.0	0.1	0.2	0.3	0.4	0.5	0.6	0.7	0.8	0.9	1.0
$\chi_W$	0.0	3.35	3.42	3.46	3.67	3.80	3.86	3.86	3.82	3.78	3.73	3.69
	0.1	3.40	3.18	3.26	3.50	3.63	3.69	3.69	3.66	3.62	3.59	
	0.2	3.39	3.34	3.27	3.20	3.37	3.45	3.47	3.46	3.44		
	0.3	3.48	3.43	3.35	3.23	3.08	3.11	3.19	3.21			
	0.4	3.46	3.40	3.32	3.22	3.09	2.92	2.80				$\beta = 3.5 - 4.0$
	0.5	3.38	3.32	3.24	3.15	3.04	2.90					$\beta = 3.0 - 3.5$
	0.6	3.29	3.23	3.16	3.07	2.97						$\beta = 2.5 - 3.0$
	0.7	3.21	3.15	3.08	3.00							
	0.8	3.14	3.08	3.01								
	0.9	3.07	3.01									
	1.0	3.01										

Table 4.21:  $\alpha_{\beta R}$  for test four

		$\chi_W$										
		0.0	0.1	0.2	0.3	0.4	0.5	0.6	0.7	0.8	0.9	1.0
$\chi_W$	0.0	0.973	0.974	0.966	0.945	0.890	0.796	0.704	0.632	0.577	0.534	0.500
	0.1	0.970	0.966	0.957	0.930	0.864	0.764	0.674	0.605	0.553	0.512	
	0.2	0.943	0.936	0.919	0.883	0.823	0.731	0.646	0.580	0.530		
	0.3	0.862	0.843	0.820	0.790	0.744	0.686	0.617	0.556			
	0.4	0.740	0.717	0.693	0.669	0.643	0.611	0.569				
	0.5	0.640	0.619	0.599	0.578	0.558	0.537					Minor Effect
	0.6	0.568	0.550	0.532	0.514	0.496						Significant Effect
	0.7	0.515	0.499	0.483	0.467							Dominating Effect
	0.8	0.474	0.460	0.445								
	0.9	0.442	0.428									
	1.0	0.415										

Table 4.22:  $\alpha_{\partial Q}$  for test four

		$\chi_Q$										
		0.0	0.1	0.2	0.3	0.4	0.5	0.6	0.7	0.8	0.9	1.0
$\chi_W$	0.0	0.000	0.017	0.038	0.063	0.095	0.129	0.153	0.168	0.178	0.185	0.190
	0.1	0.000	0.019	0.042	0.070	0.104	0.137	0.159	0.172	0.181	0.187	
	0.2	0.000	0.018	0.041	0.072	0.106	0.138	0.160	0.173	0.182		
	0.3	0.000	0.015	0.034	0.060	0.092	0.126	0.153	0.169			
	0.4	0.000	0.012	0.027	0.045	0.068	0.098	0.130				
	0.5	0.000	0.010	0.022	0.036	0.053	0.074			Minor Effect		
	0.6	0.000	0.009	0.019	0.030	0.043			Significant Effect			
	0.7	0.000	0.008	0.016	0.026				Dominating Effect			
	0.8	0.000	0.007	0.014								
	0.9	0.000	0.006									
	1.0	0.000										

Table 4.23:  $\alpha_G$  for test four

		$\chi_Q$										
		0.0	0.1	0.2	0.3	0.4	0.5	0.6	0.7	0.8	0.9	1.0
$\chi_W$	0.0	0.233	0.215	0.195	0.162	0.127	0.092	0.063	0.041	0.025	0.011	0.000
	0.1	0.214	0.212	0.186	0.150	0.113	0.077	0.049	0.029	0.013	0.000	
	0.2	0.190	0.175	0.157	0.132	0.095	0.061	0.035	0.015	0.000		
	0.3	0.148	0.131	0.113	0.092	0.070	0.043	0.018	0.000			
	0.4	0.105	0.090	0.074	0.057	0.039	0.020	0.000				
	0.5	0.074	0.060	0.046	0.032	0.016	0.000			Minor Effect		
	0.6	0.051	0.039	0.027	0.014	0.000			Significant Effect			
	0.7	0.034	0.023	0.012	0.000				Dominating Effect			
	0.8	0.020	0.010	0.000								
	0.9	0.009	0.000									
	1.0	0.000										

Table 4.24:  $\alpha_Q$  for test four

		$\chi_Q$										
		0.0	0.1	0.2	0.3	0.4	0.5	0.6	0.7	0.8	0.9	1.0
$\chi_W$	0.0	0.000	0.070	0.163	0.277	0.427	0.584	0.691	0.755	0.796	0.825	0.845
	0.1	0.000	0.078	0.179	0.306	0.468	0.619	0.716	0.774	0.811	0.837	
	0.2	0.000	0.074	0.175	0.315	0.476	0.627	0.724	0.782	0.818		
	0.3	0.000	0.064	0.146	0.258	0.409	0.569	0.693	0.767			
	0.4	0.000	0.052	0.115	0.194	0.298	0.436	0.582				
	0.5	0.000	0.043	0.093	0.153	0.228	0.322			Minor Effect		
	0.6	0.000	0.037	0.078	0.127	0.185			Significant Effect			
	0.7	0.000	0.032	0.068	0.109				Dominating Effect			
	0.8	0.000	0.029	0.060								
	0.9	0.000	0.026									
	1.0	0.000										

Table 4.25:  $a_W$  for test four

		$\chi_Q$										
		0.0	0.1	0.2	0.3	0.4	0.5	0.6	0.7	0.8	0.9	1.0
$\chi_W$	0.0	0.000	0.000	0.000	0.000	0.000	0.000	0.000	0.000	0.000	0.000	0.000
	0.1	0.112	0.125	0.127	0.119	0.106	0.089	0.075	0.064	0.056	0.050	
	0.2	0.275	0.295	0.312	0.314	0.274	0.221	0.179	0.150	0.129		
	0.3	0.484	0.517	0.541	0.545	0.515	0.432	0.339	0.273			
	0.4	0.665	0.690	0.707	0.714	0.701	0.653	0.566				
	0.5	0.765	0.782	0.794	0.800	0.796	0.776			Minor Effect		
	0.6	0.821	0.834	0.843	0.848	0.847			Significant Effect			
	0.7	0.857	0.866	0.873	0.877				Dominating Effect			
	0.8	0.880	0.888	0.893								
	0.9	0.897	0.903									
	1.0	0.910										

The results presented in Table 4.20 show that most of the possible combinations of  $\chi_Q$  and  $\chi_W$  adhere to the minimum level of reliability of 3. However, the reliability levels are below the target reliability level of  $\beta_t = 3$ , where the wind and imposed loads are similar and dominate the load effect.

The lowest recorded reliability level is  $\beta = 2.80$ , where  $\chi_Q = 0.6$  and  $\chi_W = 0.4$ . This is where the STR:Q load combination dominates. The highest recorded level of reliability is  $\beta = 3.86$ , where  $\chi_Q = 0.5$  or  $0.6$  and  $\chi_W = 0.0$ . This is where the STR:Q load combination dominates. For the load ratio of  $\chi_Q$  and  $\chi_W$  where the reliability level is lowest, the structural resistance model factor, the imposed load and the wind load have a significant effect on the level of uncertainty.

#### 4.1.2.2 Test Five

The following results are of the local-global buckling interaction mode of the plain lipped C-section with a member length of 2024.61mm. The reliability levels for test five are shown in Table 4.26. The corresponding sensitivity factors for the structural resistance model factor, the imposed load model factor, the permanent load, the imposed load, and the wind load are shown in Table 4.27 to Table 4.31 respectively.

Table 4.26: Reliability levels for test five

		$\chi_Q$										
		0.0	0.1	0.2	0.3	0.4	0.5	0.6	0.7	0.8	0.9	1.0
$\chi_W$	0.0	2.56	2.64	2.70	2.95	3.12	3.20	3.23	3.23	3.21	3.19	3.17
	0.1	2.61	2.35	2.46	2.73	2.92	3.02	3.06	3.07	3.06	3.05	
	0.2	2.61	2.56	2.48	2.41	2.63	2.77	2.84	2.87	2.89		
	0.3	2.75	2.69	2.62	2.50	2.35	2.42	2.55	2.63			
	0.4	2.78	2.73	2.65	2.55	2.42	2.25	2.17				$\beta = 3.0 - 3.5$
	0.5	2.75	2.69	2.62	2.54	2.43	2.31					$\beta = 2.5 - 3.0$
	0.6	2.70	2.65	2.58	2.51	2.42						$\beta = 2.0 - 2.5$
	0.7	2.66	2.60	2.54	2.48							
	0.8	2.61	2.56	2.51								
	0.9	2.57	2.52									
	1.0	2.61										



Table 4.27:  $\alpha_{\partial R}$  for test five

		$\chi_Q$										
		0.0	0.1	0.2	0.3	0.4	0.5	0.6	0.7	0.8	0.9	1.0
$\chi_W$	0.0	0.959	0.961	0.951	0.923	0.857	0.759	0.668	0.598	0.543	0.501	0.467
	0.1	0.956	0.950	0.938	0.905	0.832	0.732	0.643	0.575	0.522	0.481	
	0.2	0.921	0.913	0.892	0.852	0.790	0.702	0.619	0.553	0.502		
	0.3	0.833	0.815	0.791	0.759	0.711	0.654	0.590	0.532			
	0.4	0.756	0.736	0.713	0.683	0.646	0.596	0.544				
	0.5	0.614	0.594	0.575	0.555	0.534	0.511			Minor Effect		
	0.6	0.542	0.525	0.507	0.490	0.472			Significant Effect			
	0.7	0.488	0.473	0.458	0.442				Dominating Effect			
	0.8	0.447	0.433	0.419								
	0.9	0.415	0.402									
	1.0	0.392										

Table 4.28:  $\alpha_{\partial Q}$  for test five

		$\chi_Q$										
		0.0	0.1	0.2	0.3	0.4	0.5	0.6	0.7	0.8	0.9	1.0
$\chi_W$	0.0	0.000	0.020	0.045	0.074	0.108	0.138	0.159	0.173	0.181	0.187	0.192
	0.1	0.000	0.022	0.049	0.080	0.114	0.144	0.163	0.176	0.184	0.189	
	0.2	0.000	0.021	0.048	0.080	0.114	0.143	0.163	0.175	0.184		
	0.3	0.000	0.018	0.040	0.068	0.100	0.130	0.154	0.170			
	0.4	0.000	0.016	0.034	0.057	0.083	0.111	0.136				
	0.5	0.000	0.012	0.026	0.042	0.061	0.084			Minor Effect		
	0.6	0.000	0.010	0.022	0.035	0.050			Significant Effect			
	0.7	0.000	0.009	0.019	0.030				Dominating Effect			
	0.8	0.000	0.008	0.017								
	0.9	0.000	0.007									
	1.0	0.000										

Table 4.29:  $\alpha_G$  for test five

		$\chi_Q$										
		0.0	0.1	0.2	0.3	0.4	0.5	0.6	0.7	0.8	0.9	1.0
$\chi_W$	0.0	0.282	0.261	0.236	0.194	0.150	0.108	0.074	0.048	0.028	0.013	0.000
	0.1	0.260	0.256	0.225	0.180	0.133	0.091	0.058	0.034	0.015	0.000	
	0.2	0.228	0.210	0.187	0.156	0.112	0.072	0.041	0.018	0.000		
	0.3	0.175	0.155	0.133	0.109	0.082	0.050	0.022	0.000			
	0.4	0.132	0.113	0.093	0.071	0.048	0.024	0.000				
	0.5	0.087	0.071	0.054	0.037	0.019	0.000			Minor Effect		
	0.6	0.060	0.046	0.031	0.016	0.000			Significant Effect			
	0.7	0.039	0.027	0.014	0.000				Dominating Effect			
	0.8	0.023	0.012	0.000								
	0.9	0.011	0.000									
	1.0	0.000										

Table 4.30:  $\alpha_Q$  for test five

		$\chi_Q$										
		0.0	0.1	0.2	0.3	0.4	0.5	0.6	0.7	0.8	0.9	1.0
$\chi_W$	0.0	0.000	0.085	0.194	0.323	0.482	0.627	0.723	0.781	0.819	0.845	0.863
	0.1	0.000	0.093	0.209	0.349	0.511	0.651	0.741	0.795	0.830	0.854	
	0.2	0.000	0.088	0.208	0.349	0.504	0.645	0.738	0.796	0.832		
	0.3	0.000	0.075	0.170	0.292	0.438	0.579	0.694	0.768			
	0.4	0.000	0.065	0.145	0.243	0.361	0.487	0.603				
	0.5	0.000	0.050	0.109	0.179	0.262	0.363			Minor Effect		
	0.6	0.000	0.043	0.091	0.148	0.214			Significant Effect			
	0.7	0.000	0.037	0.079	0.126				Dominating Effect			
	0.8	0.000	0.033	0.070								
	0.9	0.000	0.030									
	1.0	0.000										

Table 4.31:  $\alpha_w$  for test five

		$\chi_w$										
		0.0	0.1	0.2	0.3	0.4	0.5	0.6	0.7	0.8	0.9	1.0
$\chi_w$	0.0	0.000	0.000	0.000	0.000	0.000	0.000	0.000	0.000	0.000	0.000	0.000
	0.1	0.134	0.148	0.150	0.141	0.125	0.104	0.087	0.075	0.065	0.058	
	0.2	0.317	0.338	0.352	0.349	0.310	0.255	0.208	0.174	0.149		
	0.3	0.525	0.553	0.571	0.568	0.535	0.467	0.382	0.314			
	0.4	0.641	0.664	0.679	0.682	0.666	0.628	0.568				
	0.5	0.784	0.799	0.809	0.810	0.801	0.775			Minor Effect		
	0.6	0.838	0.849	0.856	0.858	0.854				Significant Effect		
	0.7	0.872	0.880	0.885	0.888					Dominating Effect		
	0.8	0.894	0.901	0.905								
	0.9	0.910	0.915									
	1.0	0.920										

The results presented in Table 4.26 show that most of the possible combinations of  $\chi_Q$  and  $\chi_w$  do not achieve the minimum level of reliability  $\beta_t = 3$ . Scenarios where there is a higher portion of imposed load meets the target level of reliability.

The lowest assessed level of reliability is 2.17, at  $\chi_Q = 0.6$  and  $\chi_w = 0.4$ , where the STR:Q load combination dominates. The highest recorded level of reliability is  $\beta = 3.23$ , at  $\chi_Q = 0.6$  or  $0.7$  and  $\chi_w = 0.0$ , where the STR:Q load combination dominates. For the load ratio of  $\chi_Q$  and  $\chi_w$  where the reliability level is lowest, the structural resistance model factor, the imposed load, and the wind load each have significant effects on the level of uncertainty. However, this is at the theoretical limit where there is no imposed load and the scenario is practically impossible.

#### 4.1.2.3 Local Buckling and Local-Global Buckling Interaction Test Summary

When comparing the reliability results of test four and test five, it is evident that the lowest level of reliability is reached for both tests at the same load ratio of  $\chi_Q = 0.6$  and  $\chi_w = 0.4$ . This is observed in Table 4.20 and Table 4.26. For both tests, the sensitivity factors of the structural resistance model factor, the imposed load and the wind load have significant effects on the level of reliability where the reliability level is at its lowest. This

is observed in Table 4.21 and Table 4.27. It is to be noted that the STR:Q load combination yielded the lowest levels of reliability for both tests.

The reliability levels achieved from the local-global buckling mode are higher than those of the global buckling mode and lower than the local buckling mode. This is expected because, as mentioned in Section 2.1.2.2.1, an interaction of buckling modes reduces the section capacity.

For all the local buckling analyses, the sensitivity factors for the imposed load model factor and the permanent load have a minor effect on uncertainty for all possible combinations of  $\chi_Q$  and  $\chi_W$ . This is observed in Table 4.22 and Table 4.23 respectively. The sensitivity factors for the imposed load increases from a minor effect to a dominating effect as the proportion of imposed load increases. The sensitivity factors for the wind load increase from a minor effect to a dominating effect as the proportion of wind load increases. This is observed in Table 4.25.

### 4.1.3 Distortional Buckling

As discussed in Section 3.2.6.4, one test was conducted to assess the reliability of the distortional buckling capacity of a member using the DSM. Test six was conducted on the stiffened lipped C-section at a length of 453.57mm. The distortional buckling modal factor was used for this test

#### 4.1.3.1 Test Six

The following results are of the distortional buckling mode of the stiffened lipped C-section with a member length of 453.57mm. The reliability levels for test six are shown in Table 4.32. The corresponding sensitivity factors for the structural resistance model factor, the imposed load model factor, the permanent load, the imposed load, and the wind load are shown in Table 4.33 to Table 4.37 respectively.

Table 4.32: Reliability levels for test six

		$\chi_Q$										
		0.0	0.1	0.2	0.3	0.4	0.5	0.6	0.7	0.8	0.9	1.0
$\chi_W$	0.0	4.88	4.99	4.95	4.88	4.67	4.47	4.30	4.16	4.05	3.95	3.87
	0.1	4.92	4.55	4.58	4.55	4.38	4.21	4.07	3.95	3.86	3.77	
	0.2	4.55	4.43	4.25	4.01	3.99	3.89	3.79	3.71	3.63		
	0.3	4.21	4.09	3.95	3.76	3.51	3.46	3.45	3.41			
	0.4	3.92	3.81	3.69	3.54	3.37	3.15	2.99				$\beta = 4.5 - 5.0$
	0.5	3.69	3.59	3.49	3.36	3.22	3.06					$\beta = 4.0 - 4.5$
	0.6	3.51	3.43	3.33	3.22	3.10						$\beta = 3.5 - 4.0$
	0.7	3.38	3.29	3.21	3.11							$\beta = 3.0 - 3.5$
	0.8	3.26	3.19	3.11								$\beta = 2.5 - 3.0$
	0.9	3.17	3.10									
	1.0	3.09										

Table 4.33:  $\alpha_{AR}$  for test six

		$\chi_Q$										
		0.0	0.1	0.2	0.3	0.4	0.5	0.6	0.7	0.8	0.9	1.0
$\chi_W$	0.0	0.934	0.935	0.864	0.653	0.529	0.455	0.406	0.369	0.341	0.318	0.300
	0.1	0.919	0.905	0.835	0.635	0.514	0.442	0.392	0.357	0.329	0.307	
	0.2	0.700	0.679	0.659	0.615	0.505	0.431	0.381	0.345	0.318		
	0.3	0.529	0.514	0.499	0.486	0.470	0.423	0.373	0.336			
	0.4	0.439	0.427	0.415	0.403	0.392	0.380	0.356				
	0.5	0.383	0.371	0.361	0.351	0.340	0.331					Minor Effect
	0.6	0.343	0.333	0.324	0.314	0.305						Significant Effect
	0.7	0.313	0.304	0.296	0.287							Dominating Effect
	0.8	0.290	0.282	0.274								
	0.9	0.272	0.264									
	1.0	0.256										

Table 4.34:  $\alpha_{\partial Q}$  for test six

		$\chi_Q$										
		0.0	0.1	0.2	0.3	0.4	0.5	0.6	0.7	0.8	0.9	1.0
$\chi_W$	0.0	0.000	0.029	0.090	0.164	0.191	0.202	0.208	0.211	0.213	0.214	0.214
	0.1	0.000	0.032	0.093	0.164	0.190	0.201	0.206	0.209	0.211	0.212	
	0.2	0.000	0.022	0.055	0.124	0.177	0.194	0.202	0.206	0.208		
	0.3	0.000	0.015	0.035	0.063	0.111	0.166	0.188	0.198			
	0.4	0.000	0.012	0.026	0.044	0.069	0.105	0.148				
	0.5	0.000	0.010	0.021	0.035	0.052	0.075			Minor Effect		
	0.6	0.000	0.008	0.018	0.029	0.043				Significant Effect		
	0.7	0.000	0.007	0.016	0.025					Dominating Effect		
	0.8	0.000	0.007	0.014								
	0.9	0.000	0.006									
	1.0	0.000										

Table 4.35:  $\alpha_G$  for test six

		$\chi_Q$										
		0.0	0.1	0.2	0.3	0.4	0.5	0.6	0.7	0.8	0.9	1.0
$\chi_W$	0.0	0.358	0.331	0.279	0.179	0.121	0.084	0.058	0.039	0.023	0.011	0.000
	0.1	0.325	0.318	0.261	0.164	0.107	0.071	0.046	0.027	0.012	0.000	
	0.2	0.226	0.203	0.180	0.147	0.093	0.058	0.033	0.014	0.000		
	0.3	0.145	0.128	0.110	0.091	0.071	0.042	0.018	0.000			
	0.4	0.100	0.086	0.071	0.055	0.038	0.020	0.000				
	0.5	0.071	0.058	0.045	0.031	0.016	0.000			Minor Effect		
	0.6	0.049	0.038	0.026	0.013	0.000				Significant Effect		
	0.7	0.033	0.022	0.011	0.000					Dominating Effect		
	0.8	0.020	0.010	0.000								
	0.9	0.009	0.000									
	1.0	0.000										

Table 4.36:  $\alpha_Q$  for test six

		$\chi_Q$										
		0.0	0.1	0.2	0.3	0.4	0.5	0.6	0.7	0.8	0.9	1.0
$\chi_W$	0.0	0.000	0.126	0.410	0.717	0.818	0.863	0.888	0.904	0.916	0.924	0.930
	0.1	0.000	0.135	0.421	0.723	0.823	0.868	0.892	0.908	0.919	0.926	
	0.2	0.000	0.091	0.240	0.562	0.785	0.853	0.885	0.904	0.917		
	0.3	0.000	0.063	0.148	0.275	0.502	0.750	0.843	0.882			
	0.4	0.000	0.050	0.111	0.191	0.303	0.471	0.670				
	0.5	0.000	0.041	0.090	0.150	0.226	0.326			Minor Effect		
	0.6	0.000	0.036	0.077	0.125	0.183				Significant Effect		
	0.7	0.000	0.031	0.067	0.108					Dominating Effect		
	0.8	0.000	0.028	0.059								
	0.9	0.000	0.025									
	1.0	0.000										

Table 4.37:  $a_W$  for test six

		$\chi_Q$										
		0.0	0.1	0.2	0.3	0.4	0.5	0.6	0.7	0.8	0.9	1.0
$\chi_W$	0.0	0.000	0.000	0.000	0.000	0.000	0.000	0.000	0.000	0.000	0.000	0.000
	0.1	0.222	0.246	0.223	0.142	0.104	0.083	0.070	0.061	0.054	0.048	
	0.2	0.677	0.700	0.688	0.519	0.297	0.215	0.171	0.144	0.124		
	0.3	0.836	0.846	0.846	0.822	0.714	0.478	0.339	0.267			
	0.4	0.893	0.899	0.900	0.892	0.865	0.789	0.634				
	0.5	0.921	0.926	0.927	0.923	0.911	0.883			Minor Effect		
	0.6	0.938	0.941	0.943	0.941	0.934				Significant Effect		
	0.7	0.949	0.952	0.953	0.952					Dominating Effect		
	0.8	0.957	0.959	0.960								
	0.9	0.962	0.964									
	1.0	0.967										

The results presented in Table 4.32 show that all but one of the possible combinations of  $\chi_Q$  and  $\chi_W$  meets the target level of reliability of  $\beta_t = 3$ . Of all the tests conducted, test six yielded the highest reliability levels for all possible combinations of  $\chi_Q$  and  $\chi_W$ .

The lowest recorded level of reliability was  $\beta = 2.99$ , where  $\chi_Q = 0.6$  and  $\chi_W = 0.4$ . This is where the STR:Q load combination dominates. The highest recorded level of reliability was  $\beta = 4.99$ , where  $\chi_Q = 0.1$  and  $\chi_W = 0.0$ . This is where the STR-P:Q load combination dominates. For the load ratio of  $\chi_Q$  and  $\chi_W$  where the reliability level is lowest, the structural resistance model factor, the imposed load and the wind load have a significant effect on the level of uncertainty.

#### **4.1.3.2 Distortional Buckling Test Summary**

The distortional buckling analysis yielded the highest reliability levels of the six tests. This is observed in Table 4.32. Only one combination of load ratios, where  $\chi_Q = 0.6$  and  $\chi_W = 0.4$ , yielded a reliability level below the target reliability level. Since this is a theoretical case where there is no permanent load, the case is practically impossible. Therefore, the reliability levels of the distortional buckling capacity are generally acceptable.



## 4.2 Discussion of Reliability Results

### 4.2.1 Overview

The results of this study show the reliability levels of the local, distortional, and global buckling modes. A total of six tests were conducted. Three tests were conducted to assess the reliability levels of the global buckling mode. Two tests were conducted to assess that reliability levels of the local buckling mode; one of which assessed the reliability of the local-global buckling mode interaction. One test was conducted to assess the reliability levels of the distortional buckling mode.

Of each test, the sensitivity factors of each of the associated random variables were also determined. This was to assess the influence each of the random variables had on the level of uncertainty.

### 4.2.2 Discussion of Reliability Levels of Buckling Modes

#### 4.2.2.1 Distortional Buckling Mode

Almost all the reliability levels for the distortional buckling mode were greater than the target reliability of  $\beta_t = 3$ . Only one load ratio yielded a reliability level below 3. At the point of lowest reliability, the imposed and wind load ratios were  $\chi_Q = 0.6$  and  $\chi_W = 0.4$  respectively, as seen in Table 4.32. However, this combination of the load ratios implies that there is no permanent load. Since this scenario is impossible as permanent load is always present, there is no cause for concern of the reliability levels for the distortional buckling capacity.

#### 4.2.2.2 Local Buckling Mode

Like the reliability levels of the distortional buckling mode, most of the reliability levels of the local buckling mode were greater than the target reliability of  $\beta_t = 3$ . The load ratios that yielded unsatisfactory reliability levels were at low proportions of permanent load, and where  $\chi_Q$  and  $\chi_W$  are similar as seen in Table 4.20. The same sentiment of the assessment of the reliability levels for distortional buckling mode applies to those of the local buckling mode.

#### 4.2.2.3 Local-Global Buckling Interaction

The local-global buckling mode interaction yielded most reliability levels that were below the target reliability level of  $\beta_t = 3$ . As stated by Kwon *et al.* (2009), the interaction of buckling modes significantly reduces the compressive capacity of the section. Although

the reliability levels of the local-global buckling interaction are higher than those of the global buckling mode, they are lower than those of the local buckling mode.

#### 4.2.2.4 Global Buckling Mode

For the global buckling mode, the reliability levels generally prove to be significantly too low. None of the load ratios yielded a reliability level greater than the target reliability level of  $\beta_t = 3$ . The lowest reliability level occurred where there was a significantly higher proportion of permanent load with low proportions of imposed and wind loads. Of all the buckling modes, the global buckling mode yielded the lowest reliability levels.

#### 4.2.3 Detailed Discussion

Unlike the global buckling mode, the results of the local and distortional buckling modes show that the lowest levels of reliability occur with load cases of a low permanent load and similar imposed and wind load factors. The sensitivity factors that have the largest effect on the reliability levels for these load cases are those of the structural resistance model factor, the imposed load, and the wind load. However, the lowest reliability level occurs for the practically impossible load case where there is little to no permanent load.

The reliability results of the local-global interaction show that there are several load combinations that yield unsatisfactory results. However, the results of the global buckling mode yielded lower reliability levels. Therefore, the global buckling mode dominates uncertainty for members subjected to global buckling

It is cause for concern that, of all the considered buckling modes, the results of the global buckling mode yielded unsatisfactory reliability levels for all the considered load combinations. Observing the sensitivity factors, the global buckling model factor has a predominant effect on the level of reliability, especially for load combinations with high permanent loads. Therefore, the predictive model for the global buckling capacity is poor.

These results suggest that the predictive capacity of the distortional and local buckling modes better predict their associated modes of failure than that of the global buckling mode. Additionally, for the global buckling mode, the sensitivity factors of the considered load effects are lower than those of the structural resistance model factor for load combinations that yielded low reliability levels. This is to say that the safety margin inherent of SANS 10160-1 does not compensate enough to achieve an overall acceptable level of reliability.

The considered column was unbraced along the length of the member. However, this study did not consider the case where a slender column member is braced at points along its length. For example, cladding may be fastened to the flange or web along the length of the member with a bolt spacing. This supplies the member with braced or lateral stability.

Lateral stability along the length of a CFS column will affect the buckling modes and their respective load factors when compared to an unbraced CFS column. Depending on the bolt spacing, global buckling is less likely to govern the failure mode, since the effective length of the member about the one axis is decreased. In this case, distortional buckling may not be induced, since rotation of the top flange is restricted. Local buckling is therefore more likely to govern. This may result in an increased reliability of the member.

# CHAPTER 5:

## Conclusion & Recommendations

---

### 5.1 Conclusion

The reliability analysis conducted in this thesis investigated whether the inherent reliability of the SANS 10162-2 (2011) formulation of the DSM for compression members adhered to the target level of reliability required by SANS 10160-1 (2011). The target level of reliability is  $\beta_t = 3$  for a RC2 reliability classification. A full probabilistic formulation of the limit-state was used to evaluate the reliability of the semi-probabilistic formulation of the limit-state as per SANS 10160-1 (2011) for the load effect and SANS 10162-2 (2011) for structural resistance.

A FORM analysis was used to determine the reliability level of each buckling mode. A plain lipped C-section was considered as a codified representative member adhering to the geometric and material property limitations of the DSM. The global and local buckling capacities of the considered member were assessed. A lipped C-section with a web stiffener was used to assess the distortional and global buckling capacities. The four load combinations of SANS 10160-1 (2011) for STR and STR-P, respectively with wind or variable loads as leading actions were considered in the analysis. The total load was distributed into permanent, imposed and wind loads according to load ratios which was parametrically varied to cover the range of application.

The distortional buckling mode yielded the highest reliability levels for all combinations of the imposed and wind load ratios. All but one combination of the load ratios was above the target reliability level of  $\beta_t = 3$ . The reliability levels for the distortional buckling mode ranged from  $\beta = 2.99$  to  $\beta = 4.99$ .

Most of the reliability levels for the local buckling mode were above the target reliability level of  $\beta_t = 3$ . Load conditions with a low ratio of permanent load to the total load, and similar levels of imposed and wind loads yielded the lowest reliability levels. The reliability levels for the local buckling mode ranged from  $\beta = 2.80$  to  $\beta = 3.86$ .

Few of the reliability levels of the local-global buckling interaction were above that of the target reliability level of  $\beta_t = 3$ . Load conditions with higher proportions of imposed load yielded reliability levels above the target reliability of  $\beta_t = 3$ . The reliability levels of the local-global buckling interaction ranged from  $\beta = 2.17$  to  $\beta = 3.23$ .

Of all buckling modes, it was found that the global buckling mode yielded the lowest reliability levels. The reliability levels for all combinations of the imposed and wind load ratios were below the target reliability level. The reliability levels for the global buckling mode ranged from  $\beta = 1.78$  to  $\beta = 2.87$ . For a member subject to global buckling at a length of 2024.61mm, the global buckling mode dominates uncertainty over the local-global buckling interaction.

The length of the member and shape of the cross section influences the capacity of the member. This is because ranges of member lengths are subjected to different buckling modes. However, for a given cross-sectional area, it was found that the shape of the cross section does not influence the reliability level of the global buckling mode. Additionally, the length of the member does not influence the reliability level given that the member length is within the global buckling range.

It was found that, for all possible combinations of the imposed and wind load ratios where the reliability was below the minimum level of reliability, the structural resistance model factor governed uncertainty.

The study conducted by Bauer (2016) found that the safety margin supplied by the resistance standard SANS 10162-2 (2011) is not enough to achieve acceptable levels of reliability. In the conclusion of Bauer (2016), it was assumed that, by incorporating the loading standard, overall acceptable levels of reliability could be achieved. The main conclusion of this study is that the safety margin provided by the loading standard of SANS 10160-1 (2011) is not sufficient to make up for the lack of safety margin provided by SANS 10162-2 (2011) and to ensure an overall acceptable level of reliability. Thus, the capacity reduction factor used in the DSM of SANS 10162-2 (2011) needs to be decreased to achieve an overall acceptable level of reliability, particularly for cases where global buckling is the critical failure mode.

## 5.2 Recommendations

This study only considered the analysis of pure compression members. As part of a structural system, most columns are subject to compression and bending stresses simultaneously. Therefore, the work presented in this study is limited. A further study may need to be conducted, assessing the reliability levels of CFS beam-column members. Literature by Ganesan and Moen (2010) presents model factors for the buckling modes of only pure compression members. Therefore, model factors for the buckling modes of members subject to bending needs to be developed in order to analyse the reliability levels of the interaction of bending and compressive stresses in CFS members.

Additionally, incorporating the combination of bending and compressive stresses in CFS member design using the DSM has not been entirely investigated. Currently, it is recommended that the interaction of bending and compression forces for the DSM is to follow the basic methodology of the EWM through interaction equations. However, studies are being conducted to investigate the true behaviour of members subject to the interaction. A more thorough stability analysis of beam-columns may lead to a behaviour different to that assumed by the interaction equations. (Schafer, 2006b).

In this study, one capacity reduction factor as per SANS 10162-2 (2011) was used for all buckling modes, as the considered cross sections adhered to the geometric and material limitations of the DSM. Therefore, since it was found that the assessed reliability levels differed systematically for each buckling mode, it is recommended that the capacity reduction factor for compression members  $\phi_c$  proposed in SANS 10162-2 (2011) be re-evaluated. Specifically, it is recommended that a capacity reduction factor be assigned for each buckling mode.

A further reliability analysis was conducted for the global buckling mode, since it yielded the lowest reliability levels of the buckling modes. The capacity reduction factor  $\phi_c$  was decreased from a value of 0.85 accordingly until the lowest level of reliability of  $\beta_t = 3$  was achieved. It was found that, by using a capacity reduction of 0.58, the reliability analysis yielded satisfactory reliability levels. The results show that the global buckling prediction model is poor.

Of all the buckling mode interactions, this study only considered the local-global buckling interaction. Further research may need to be conducted to assess the influence that other

buckling mode interactions have on the reliability levels. Additionally, the buckling interactions are not defined in the DSM.

# References

- Achintya, H. & Mahadevan, S. 2000. *Probability, Reliability and Statistical Methods in Engineering Design*. John Wiley & Sons.
- Allen, D. 2006. History of Cold Formed Steel. *Structure Magazine*. November Edition: 28-32.
- American Iron and Steel Institute, Canadian Standards Association and Camara Nacional de la Industria del Hierro y del Acero. 2016. *North American Specification for the design of cold-formed steel structural members*.
- Bauer, A. 2016. The Reliability Margin of the Direct Strength Method Prediction Model for Cold-Formed Steel Members. Unpublished master's thesis. Stellenbosch: University of Stellenbosch.
- Botha, J. 2016. Probabilistic Models of Design Wind Loads in South Africa. Unpublished doctoral dissertation. Stellenbosch: University of Stellenbosch
- Breitung, K. 2015. 40 years FORM: Some new aspects? *Probabilistic Engineering Mechanics*, 42:71-77.
- Cardoso, J. B., de Almeida, J. R., Dias, J. M. & Coelho, P. G. 2008. Structural reliability analysis using Monte Carlo simulation and neural networks. *Advances in Engineering Software*, 39(6): 505-513.
- Freitas, M.S., Brandão, A.L. and Freitas, A. 2013. Resistance factor calibration for cold-formed steel compression members. Rem: Revista Escola de Minas, vol. 66, no. 2, pp. 233-238.
- Ganesan, K. & Moen, C. D. 2010. Evaluating the LEFD Factor for Cold-Formed Steel Compression Members, in *International Speciality Conference on Cold-Formed Steel Structures*. Missouri: Missouri University of Science and Technology: 33-48
- Haldar, A. & Mahadevan, S. 2000. *Reliability assessment using stochastic finite element analysis*. John Wiley & Sons.
- Holický, M. 2009. *Reliability analysis for structural design*. AFRICAN SUN MEDIA.



- Holický, M., Retief, J. V. & Sýkora, M. 2015. Assessment of model uncertainties for structural resistance. *Probabilistic Engineering Mechanics*.
- Kwon, Y. B., Kim, B. S. & Hancock, G. J. 2009. Compression tests of high strength cold-formed steel channels with buckling interaction. *Journal of Constructional Steel research*. Elsevier Ltd, 65(2): 278-289.
- Li, Z. & Schafer, B. W. 2010. Buckling analysis of cold-formed steel members with general boundary conditions using CUFSM: Conventional and constrained finite strip methods. *20<sup>th</sup> International Speciality Conference on Cold-Formed Steel Structures*. Missouri: University of Missouri.
- Lopez, R. H. & Beck, A. T. 2012. Reliability-based design optimisation strategies based on FORM: a review. *Journal of the Brazilian Society of Mechanical Sciences and Engineering*. 34(4):506-514.
- Nowak, A. S. & Collins, K. R. 2000. *Reliability of structures*. CRC Pres.
- Petschader, M. 1997. VaP variable processor, version 1.6. *ETH Zurich*.
- Schafer, B. W. 2002. Progress on the Direct Strength Method. *Sixteenth International Speciality Conference on Cold-Formed Steel Structures*: 647-662.
- Schafer, B. W. 2006a. Direct Strength Method (DSM) Design Guide. *American Iron and Steel Institute*.
- Schafer, B. W., 2006b. Designing cold-formed steel using the direct strength method, in: *Eighteenth International Specialty Conference on Cold-Formed Steel Structures*: 475-488.
- South African Bureau of Standards. *South African National Standard 4998: Continuous hot-dip zinc-coated carbon steel sheet of structural quality*.
- South African Bureau of Standards. 2011. *South African National Standard 10160-1 Basis of structural design and actions for buildings and industrial structures Part 1: Basis of structural design*. SABS Standards Division, Pretoria.
- South African Bureau of Standards. 2011. *South African National Standard 10162-1 The structural use of steel Part 1: Limit-states design of hot-rolled steelwork*. SABS Standards Division, Pretoria.

South African Bureau of Standards. 2011. *South African National Standard 10162-2 The structural use of steel Part 2: Cold-formed steel structures*. SABS Standards Division, Pretoria.

Ungermann, D., Lübke, S. & Burne, B. 2014. Tests and design approach for plain channels in local and coupled local-flexural buckling based on Eurocode 3. *Thin-Walled Structures*. Elsevier, 81: 108-120.

Van Wyk, R. 2014. Reliability of cold-formed steel screwed connections in tilt-and bearing. Master's thesis, Civil Engineering, University of Stellenbosch, Stellenbosch, South Africa

Yu, C. & Schafer, B. W. 2005. Distortional buckling of cold-formed steel members in bending.

Yu, W. -W. & LaBoube, R. A. 2010. *Cold-Formed Steel Design: Fourth Edition*. John Wiley & Sons.

Zieman, R.D. 2010. *Guide to stability design criteria for metal structures*. John Wiley & Sons.